environment types) of hitherto unknown high pressure and high temperature modifications (see sec. 8.4.).

8. Semi-empirical approaches to the prediction of (intermetallic) compound formation

8.1. General remarks on procedures of prediction of compound and structure formation in alloy systems

In the previous sections a brief sampling of some correlations has been given which relate crystallochemical characteristics of the phase to the properties of the component elements. This group of correlations may be considered as a first reference point for a number of methods of predicting the formation, in a given system, of a compound and/or of a certain structure. It is well known that, in scientific literature, more and more space is dedicated to the question of the forecast of chemical equilibria in simple and complex systems. A clear indication of this interest, both from a general and a technological point of view, may be seen in the development and success of a number of monographs and periodic publications and proceedings on this subject. Several approaches to this problem have been considered: we may mention, with special attention to metal systems, the explicit over-all summary already presented by KAUFMAN *et al.* (see KAUFMAN and BERNSTEIN [1970]) and the more recent discussion by MASSALSKI [1989].

The role of a thermodynamic approach is well known: a thermodynamic control, optimization and prediction of the phase diagram may be carried out by using methods such as those envisaged by KUBASCHEWSKI and EVANS [1958], described by KAUFMAN and NESOR [1973], ANSARA *et al.* [1978], HILLERT [1981] and very successfully implemented by LUKAS *et al.* [1977, 1982], SUNDMAN *et al.* [1985]. The integration of phase diagram calculations into the design of multicomponent alloys, and performance prediction, has been discussed by MIODOWNIK [1993]. The knowledge (or the prediction) of the intermediate phases which are formed in a certain alloy system may be considered as a preliminary step in the more general, and complex, problem of assessment and prediction of all the features of phase equilibria and phase diagrams. (See also ALDINGER and SEIFERT [1993]).

Evidence has to be given to the phase stability problem (MASSALSKI [1989]). The significant progress and the limits, of the first principles calculations may be mentioned (HAFNER [1989], PETTIFOR, chapter 2), the usefulness, however, of a number of semiempirical approaches has to be pointed out. Several schemes and criteria have been suggested to forecast and/or optimize the data concerning certain properties. In the following a short outline will be reported on some prediction methods based on selected correlations between elemental properties and structure formation.

8.2. Stability diagrams, structure maps

Several authors have tried to classify and order the numerous data concerning the different intermetallic substances by using two (or three) dimensional structure maps (*stability, existence diagrams*).

References: p. 363.

These maps were prepared by selecting coordinates based on those parameters (generally properties of the component elements) which were considered to be determinant factors of the structural stability and phase formation control.

As an introductory example to this subject we may remember the well known diagrams developed by DARKEN and GURRY [1953] for *solid solution prediction*. In such diagrams (as shown in fig. 57) all elements may be included. The two coordinates represent the atomic size (generally the radius corresponding to CN 12) and the electronegativity of the elements. It is well known that the first table of electronegativity values was introduced by PAULING [1932]. Several alternative definitions have since been proposed. A reliable compilation extensively used in discussing the metallurgical behaviour is that by TEATUM *et al.* [1968]. References to other scales will be reported later.

To determine the solid solubility of the different elements in a given metal, in the Darken and Gurry map, the region with the selected metal (Mg, for instance, in fig. 57) in the center can be considered. Generally we observe that elements which have high solubility lie inside a small region around the selected metal. As a rule of thumb an ellipse may be drawn in the diagram (with the selected metal in the center), for instance, with ± 0.3 electronegativity unity difference in one axis and $\pm 15\%$ atomic radius difference on the other axis. For those elements for which there is a low (or a negligible) solubility a larger region has to be considered.

For a review of the application of the Darken and Gurry method to predict solid solubilities see GSCHNEIDNER [1980]. An improvement of the method by means of simultaneous use of rules based on the electronic and crystal structures of the metals involved, is also presented.

The diagrams reported in figs. 50 and 58 are examples of other structure stability maps which have been suggested and successfully used in order to obtain a good separation (classification) of typical alloying behaviours (compound formation, crystallization in a certain structure type, etc.).

As an outline of more general approaches along these lines we may mention a selection of a few methods proposed by several researchers.

8.3. Savitskii–Gribulya–Kiselyova method (cybernetic computer-learning prediction system)

Cybernetic computer-learning methods have been proposed by SAVITSKII *et al.* [1980] for predicting the existence of intermetallic phases with a given structure and/or with certain properties. The computer learning, in this case, is a process of collecting experimental evidence on the presence (or absence) of a property of interest in various physicochemical systems (defined by means of a convenient selection of the properties of the components).

As a result of machine learning a model is produced of characteristic exhibition of a property (for instance, the formation of a particular type of chemical compound) which corresponds to a distribution "pattern" of this property in the multidimensional representative space of the properties of the elements. The subsequent pattern recognition corresponds to a criterium for the classification of the known compounds and for the

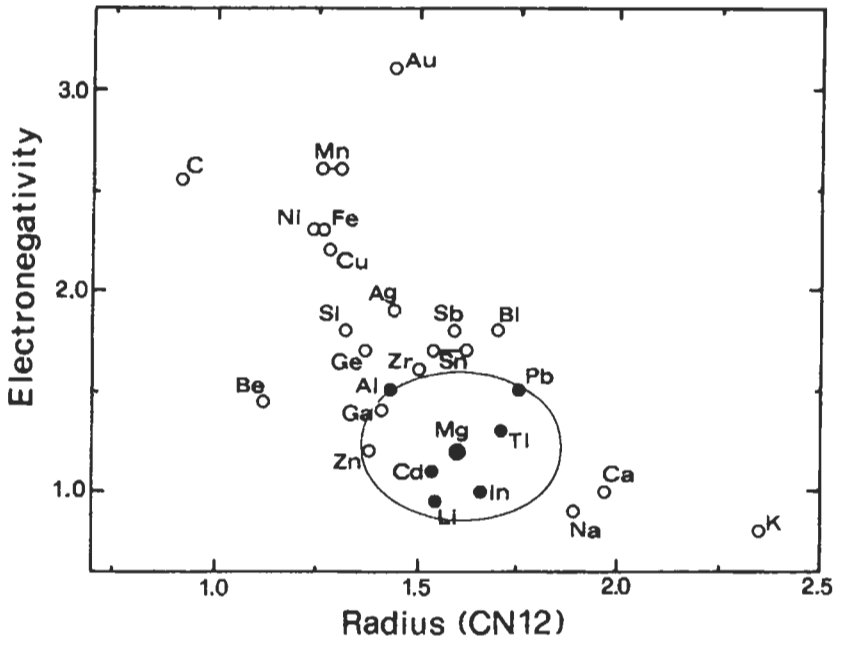

Fig. 57. Darken and Gurry diagram for the element Mg. (Solubility in Mg greater (•) or less (○) than 5 atom % is indicated.)

prediction of those still unknown.

Examples of this approach reported by Savitskii are the prediction of the formation of Laves phases, of $CaCu_5$ type phases, of compounds XY_2Z_4 (X, Y any of the elements, Z = O, S, Se, Te), etc. (Data on the electronic structures of the components were selected as input).

The main principles and applications for the cybernetic prediction of inorganic substances which would have pre-defined properties have been summarized and discusssed by KISELYOVA [1993].

8.4. Villars, Villars and Girgis approaches (analysis of the dependence of the behaviour of alloy systems on the properties of the component elements)

In an examination of the binary structure types (containing more than five representatives, VILLARS and GIRGIS [1982] observed that 85% exihibited the following regularities:

a) linear dependence of interatomic distances on concentration weighted radii;
b) narrow ranges of the space-filling parameter and of the unit cell edge ratio c/a (and b/a) for the representatives of a given structure types;
c) dependence between the position of the elements in the Periodic Table (in the s, p, d, f blocks) and their equipoint occupation in the structure;

References: p. 363.

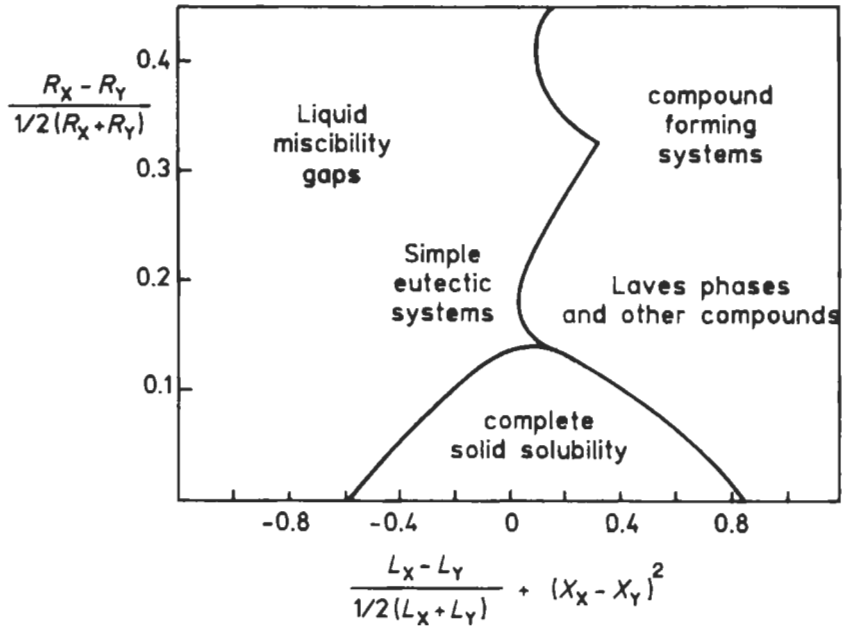

Fig. 58. Kubaschewski's plot of the regions of preference for formation of certain type of binary equilibrium diagrams (R_i, L_i and X_i are atomic radius, heat of sublimation and electronegativity of element i).

d) narrow grouping of the phases pertaining to a given structure type, in isostoichiometric diagrams based on the positions of the components in the Periodic Table.

These relationships have been used to predict the existence and/or the structure type (and the unit cell characteristics) of binary intermetallic compounds.

By using a systematic procedure to find the relevant element properties representing the alloying behaviour of binary systems VILLARS [1983, 1985] defined three expressions for atomic properties which enable systems that form compounds to be separated from those that do not.

A systematic elimination procedure was also used by VILLARS [1982] to find atomic property expressions which could be used to distinguish the crystal structures of intermetallic compounds. 182 sets of tabulated physical properties and calculated atomic properties were considered. These were combined, for binary phases, according to the modulus sums, differences and ratios. The best separations were obtained by using three-dimensional maps, which, for a binary A_xB_y, $x<y$ compound, were based on the following variables (VILLARS and HULLIGER [1987], VILLARS *et al.* [1989]):

ΣVE, averaged sum of the valence electrons of the elements A and B, defined by

$$\Sigma VE = \left(x\,VE_A + y\,VE_B\right)/\left(x + y\right), \tag{24}$$

ΔX, electronegativity difference, according to the MARTYNOV–BATSANOV [1980] scale defined by

$$\Delta X = \left[2x / (x + y)\right](X_A - X_B) \tag{25}$$

$\Delta (r_s + r_p)_Z$, difference of Zunger's pseudo-potential radii sum (ZUNGER [1981]), defined by

$$\Delta\left(r_s + r_p\right)_Z = \left[2x / (x + y)\right]\left[\left(r_s + r_p\right)_{Z,A} - \left(r_s + r_p\right)_{Z,B}\right] \tag{26}$$

The relevant data concerning the different elements have been reported in table 9 (from VILLARS [1983]).

Several structural types, corresponding to about 5500 binary compounds and alloys, were considered. 147 structure types were classified as 97 coordination types. The applications of these maps (which, in the most favorable cases, make it possible to predict not only the coordination number and polyhedron but also the structure type or a limited number of possibilities) were discussed. The possible extension to ternary and quaternary phases was also considered.

As an example of an investigation of a selected group of ternary alloys we may mention a paper by HOVESTREYDT [1988]. In analogy with the work of Villars a three-dimensional structure stability diagram was constructed. For the equiatomic RETX compounds formed by the rare earth metal (RE) with transition metal (T) and Ga, Si or Ge (X) the variables considered were: the difference in atomic radii $r_X - r_{RE}$, the Martynov–Batsanov electronegativity of the T metal and the expression $G_T + G_X + P_X$, related to the position in the Periodic Table of the T and X elements, where G is the group and P the period number. A good separation was obtained for the 8 structural types considered (corresponding to 202 compounds).

Special, modified, structure stability diagrams have been used for the elements by VILLARS and DAAMS [1993]. Maps were built by using the variables valence electron number and Zunger pseudopotential radius and reporting the atomic environment types (see sec. 7.2.7) found in the element structures. A simple separation into different stability domains was observed. By including the high temperature, high pressure crystal structure data, a prediction was made of the atomic environment modifications, hitherto unknown for several elements, to be found under high pressure, high temperature conditions. (See sec. 7.2.7.).

An empirical relation between band gap and Zunger's orbital electronegativity in sp-bonded compounds has been determined by MAKINO [1994a] using a formula derived from the bond orbital model. Based on the bond orbital model and Zunger's orbital electronegativity, new structural maps of AB, AB_2 and AB_3 compounds between transition metals have been successfully constructed (MAKINO [1994b]).

8.5. Miedema's theory and structural information

The model for energy effects in alloys suggested by Miedema and coworkers is well known. By assigning two coordinates (Φ and n_{WS}) to each transition element it was possible to separate all those binary alloys with positive heats of formation from those with negative values (MIEDEMA [1973]).

Successive steps in the formulation of the model have been described, for instance,

Table 9
Valence Electron Number (VE), Martynov–Batsanov electronegativity (X_{MB}) and Zunger's pseudo potential sum R_Z (from VILLARS [1983]).

H 1																
2.10																
1.25																
Li 1	Be 2					El	VE					B 3	C 4	N 5	O 6	F 7
0.90	1.45						X_{MB}					1.90	2.37	2.85	3.32	3.78
1.61	1.08						R_Z					0.795	0.64	0.54	0.465	0.405
Na 1	Mg 2											Al 3	Si 4	P 5	S 6	Cl 7
0.89	1.31											1.64	1.98	2.32	2.65	2.98
2.65	2.03											1.675	1.42	1.24	1.10	1.01
K 1	Ca 2	Sc 3	Ti 4	V 5	Cr 6	Mn 7	Fe 8	Co 9	Ni 10	Cu 11	Zn 12	Ga 3	Ge 4	As 5	Se 6	Br 7
0.80	1.17	1.50	1.86	2.22	2.00	2.04	1.67	1.72	1.76	1.08	1.44	1.70	1.99	2.27	2.54	2.83
3.69	3.00	2.75	2.58	2.43	2.44	2.22	2.11	2.02	2.18	2.04	1.88	1.695	1.56	1.415	1.285	1.20
Rb 1	Sr 2	Y 3	Zr 4	Nb 5	Mo 6	Tc 7	Ru 8	Rh 9	Pd 10	Ag 11	Cd 12	In 3	Sn 4	Sb 5	Te 6	I 7
0.80	1.13	1.41	1.70	2.03	1.94	2.18	1.97	1.99	2.08	1.07	1.40	1.63	1.88	2.14	2.38	2.76
4.10	3.21	2.94	2.825	2.76	2.72	2.65	2.605	2.52	2.45	2.375	2.215	2.05	1.88	1.765	1.67	1.585
Cs 1	Ba 2	La 3	Hf 4	Ta 5	W 6	Re 7	Os 8	Ir 9	Pt 10	Au 11	Hg 12	Tl 3	Pb 4	Bi 5	Po 6	At 7
0.77	1.08	1.35	1.73	1.94	1.79	2.06	1.85	1.87	1.91	1.19	1.49	1.69	1.92	2.14	2.40	2.64
4.31	3.402	3.08	2.91	2.79	2.735	2.68	2.65	2.628	2.70	2.66	2.41	2.235	2.09	1.997	1.90	1.83
Fr 1	Ra 2	Ac 3														
0.70	0.90	1.10														
4.37	3.53	3.12														
		Ce 3	Pr 3	Nd 3	Pm 3	Sm 3	Eu 3	Gd 3	Tb 3	Dy 3	Ho 3	Er 3	Tm 3	Yb 3	Lu 3	
		1.1	1.1	1.2	1.15	1.2	1.15	1.1	1.2	1.15	1.2	1.2	1.2	1.1	1.2	
		4.50	4.48	3.99	3.99	4.14	3.94	3.91	3.89	3.67	3.65	3.63	3.60	3.59	3.37	
		Th 3	Pa 3	U 3	Np 3	Pu 3	Am 3									
		1.3	1.5	1.7	1.3	1.3	1.3									
		4.98	4.96	4.72	4.93	4.91	4.89									

For a few elements, such as the rare earths, the Martynov–Batsanov electronegativity was not available, Pauling values were reported.

by NIESSEN *et al.* [1983] and by DE BOER *et al.* [1988].

The enthalpy of formation of solid and liquid binary alloys was described as proportional to the expression:

$$f\left[-P\left(\Delta\Phi^*\right)^2 + Q\left(\Delta n_{WS}^{1/3}\right)^2 - R\right] \tag{27}$$

where f is a concentration (and molar volumes) dependent function, $\Delta\Phi^* = \Phi_A^* - \Phi_B^*$ where $\Phi i*$ is the work function of each element, closely related to its electronegativity, (the values tabulated by Miedema, however, have been slightly readjusted by amounts comparable to the experimental uncertainty of work function values), n_{WS} is the electron density at the boundary of the Wigner–Seitz cell for each element. P, Q and R are constants for specific groups of elements (their values are related to the position in the Periodic Table of the elements involved). In the same model (MIEDEMA and NIESSEN [1982]) the volume variation in the formation of the intermetallic compound is evaluated as proportional to $(\Delta\Phi^*)[(\Delta(n_{WS})^{-1}])$.

Although the way to predict formation enthalpies of alloys was introduced as an empirical one it is important to observe that the model incorporates basic physics. A quantum-mechanical interpretation of Miedema's parameters has already been proposed by CHELIKOWSKY and PHILLIPS [1977, 1978].

Extensions of the model to complex alloy systems have been considered. As an interesting application we may mention the discussion on the stabilities of ternary compounds presented by DE BOER *et al.* [1988]. In the case of the Heusler type alloys XY_2Z, for instance, the stability conditions with respect to mechanical mixtures of the same nominal composition ($XY_2 + Z$, $X + Y_2Z$, $XY + YZ$, etc.) have been systematically examined and presented by means of diagrams.

The Miedema's parameters, $\Delta\Phi^*$, $\Delta n_{WS}^{1/3}$, moreover, have been used as variables for the construction of structural plots of intermetallic phases (ZUNGER [1981]), RAJASEKHARAN and GIRGIS [1983]). According to Rajasekharan and Girgis on a $\Delta\Phi^*$, $\Delta n_{WS}^{1/3}$ map, considerable resolution is obtained among the binary systems in which different structure types occur. The points corresponding to the systems in which the Laves phases (or the phases of types as Cr_3Si, $TiAl_3$, etc.) occur show linear relationships on the map. (The good separation, moreover, between the line connecting the Cr_3Si type phase points and that of the Laves phase points, can be related to the almost total exclusion of the Cr_3Si type phases from the 250 binary systems containing Laves phases and that of the Laves phases from the about 90 binary systems in which a Cr_3Si type phase occur). (See also ch. 2, § 7).

8.6. Prediction of the properties of selected families of alloys: Gschneidner's relations as an example

Stability maps and/or correlation diagrams may be especially simple and easy to handle for selected groups of similar alloys. (For instance, alloys of the elements of the same group of the Periodic Table).

As an example we may mention the alloys of the rare earth metals (especially the

"trivalent ones"). It is well known that, within this family of elements, several properties change according to well-recognized and systematic patterns. The atomic number itself can be used in this case as a simple and convenient chemical parameter). In several instances it has been pointed out that a systematic consideration of the crystal structures (and of the phase diagrams) of alloys formed by analogous elements (as those of the trivalent rare earth family) enables a number of empirical regularities to be deduced and theoretical statements to be made. (See a general discussion on this subject by GSCHNEIDNER [1969, 1971], the comments by YATSENKO *et al.* [1979, 1983], COLINET *et al.* [1984a, 1984b], VASSILIEV *et al.* [1993], FERRO *et al.* [1994] and SOMMER *et al.* [1995] on alloys thermodynamics, the papers by MASSALSKI [1989] on the applications of this behaviour to phase diagram assessment, by PARTHE and CHABOT [1984], ROGL [1984] and by IANDELLI and PALENZONA [1979] for a systematic crystallochemical description. See SERENI [1984] for examples and a discussion of the properties of the rare earth metals themselves. See also some comments of this point in sec. 7.2.4.a). Criteria based on the mentioned characteristics have been used in assessment procedures and in the prediction of phase diagrams and of phase (and structure type) formation. Fig. 59 may be considered as an example of such typical trends and of their correlations. Special applications (prediction of Pm-alloys) have been described by SACCONE *et al.* [1990] and (forecast of selected phase diagrams) by BORZONE *et al.* [1990], FERRO *et al.* [1993] and SACCONE *et al.* [1995]. The applicability of similar criteria to the assessment and prediction of phase equilibria in selected groups of ternary rare earth alloys (containing two different RE metals) has been exemplified by GIOVANNINI et al. [1994, 1995a, 1995b] in the description of complex Mg–RE alloy systems.

Considering other families of similar compounds we may mention as an other example of systematic descriptions of selected groups of phases and of the use of special interpolation and extrapolation procedures to predict specific properties, the contributions given by GUILLERMET *et al.* [1991, 1992] (cohesive and thermodynamic properties, atomic average volumes, etc. of nitrides, borides, etc. of transition metals).

8.7. Pettifor's chemical scale and structure maps

We have seen that in a phenomenological approach to the systematics of the crystal structures (and of other phase properties) several types of coordinates, derived from physical atomic properties, have been used for the preparation of (two, three-dimensional) stability maps. Differences, sums, ratios of properties such as electronegativities, atomic radii, valence electron numbers have been used. These variables, however, as stressed, for instance, by VILLARS *et al.* [1989] do not always clearly differentiate between chemically different atoms.

As already mentioned in sec. 1 of this chapter, PETTIFOR [1984, 1985a, 1986a] *created a chemical scale* (χ) which orders the elements along a single axis. This scale (and the progressive order number of the elements in this scale: the so-called *Mendeleev number*, M) starts with the least electronegativity element and ends with the most electronegative one (see table 1).

For binary compounds (and alloys) X_nY_m (with a given n:m ratio) two-dimensional

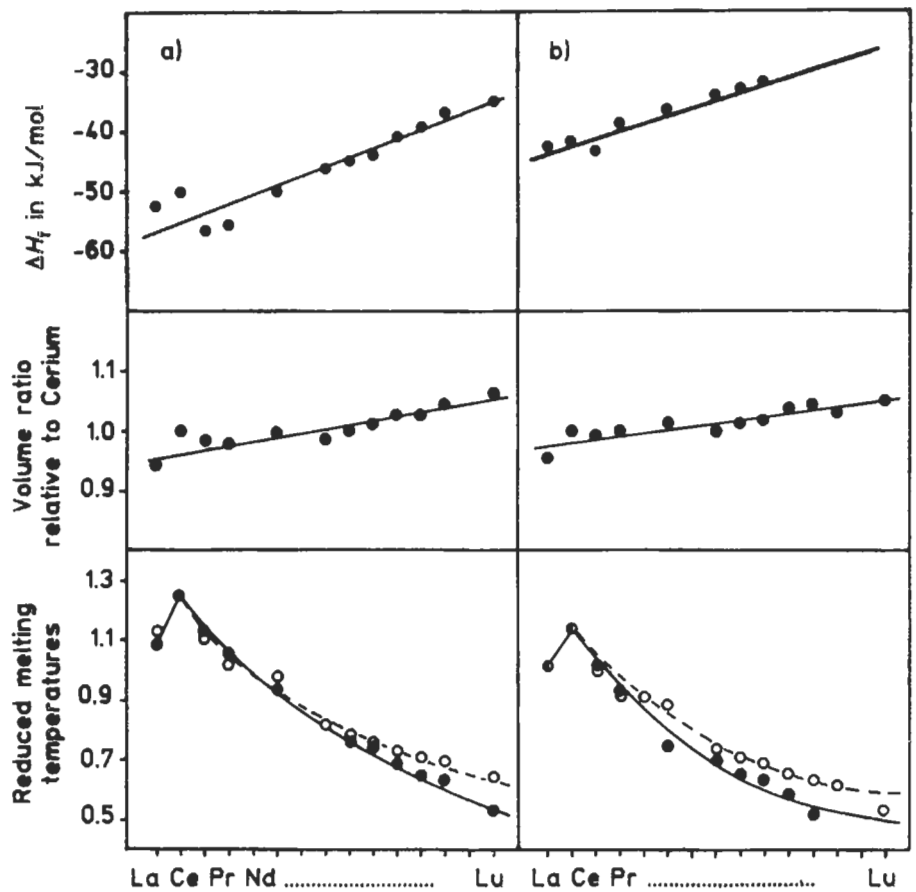

Fig. 59. Gschneidner's plots for some rare earth (RE) alloys.

a) $REIn_3$ compounds

b) $RETl_3$ compounds

Following data are reported as a function of RE atomic number: Formation enthalpy, volume ratio relative to cerium (see sec. 7.2.4.a) and reduced melting temperature T_R. This is the ratio (Kelvin/Kelvin) of the melting point of the phase and of the melting point of the involved earth metal. (•) experimental values; (◦) hypothetical values (reference values) of T_R computed for compounds assumed to have a constant melting point. The difference between the experimental and computed slopes of T_R curves is considered to be an indication of the variation of the thermal stability of the phases along the series).

In these cases, all the diagrams show a decreasing phase stability for an increase of the atomic number.

χ_X, χ_Y (or M_X, M_Y) maps may be prepared. See chapter 2, § 6.2 and the simplified version reported in fig. 60 for the reader's convenience. It has been proved that by using this ordering of the elements an excellent structural separation may be obtained of the binary compounds of various stoichiometries (n:m = 1:1, 1:2, 1:3, 1:4, ..., 1:13, 2:3, 2:5, ..., 2:17, 3:4, ..., etc.) (PETTIFOR [1986a]). See also VILLARS *et al.* [1989] who have

References: p. 363.

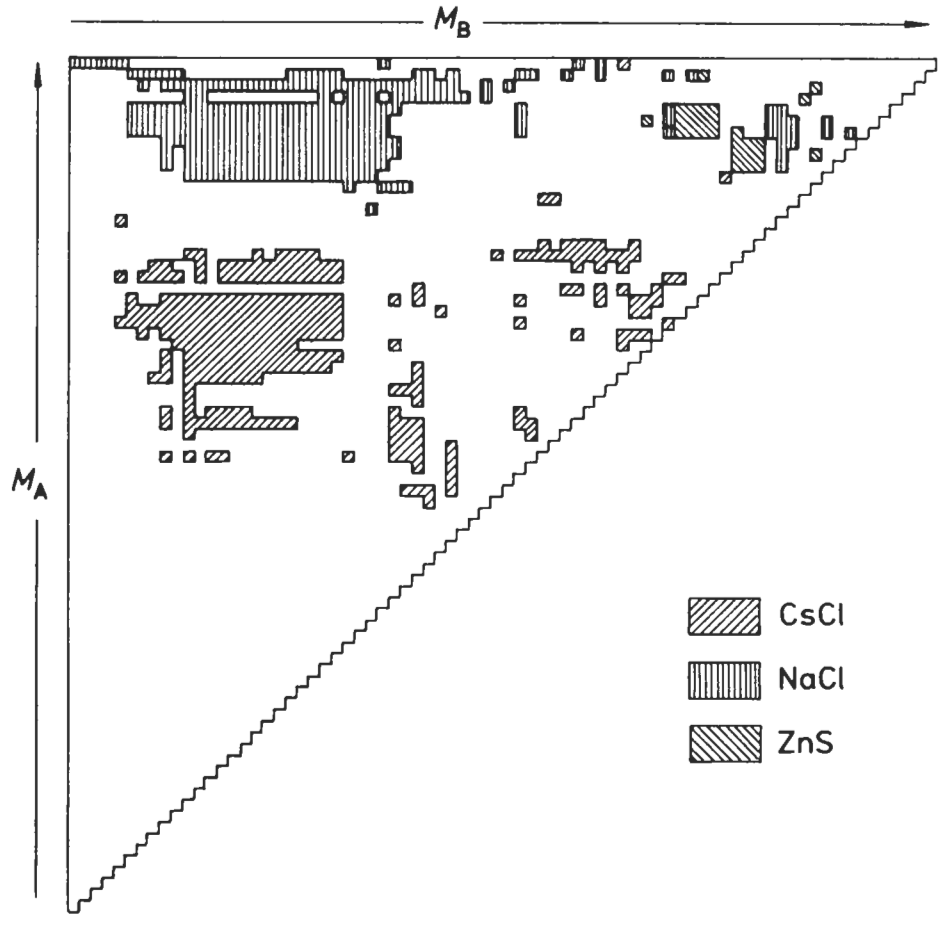

Fig. 60. Simplified version of the Pettifor's map for AB compounds. The elements are arranged along the axes according to their M_t, Mendeleev number. As an example the existence regions of the NaCl, CsCl and cubic ZnS type phases are evidenced. For more details see chapter 2, § 6.2.

updated the Pettifor maps for several stoichiometries.

An extension of the application of these maps to the systematic description of certain groups of ternary alloys has been presented also by PETTIFOR [1988a, 1988b]. Composition averaged Mendeleev numbers can be used, for instance, in the description of pseudobinary, ternary or quaternary alloys. All these maps show well defined domains of structural stability for a given stoichiometry, thus making the search easier for new ternary or quaternary alloys with a particular structure type and which, as a consequence, have the potential of interesting properties and applications (PETTIFOR [1988a, 1988b]; see also ch. 2, § 6.2).

9. *Acknowledgments*

This is a revised and somewhat extended version of a chapter by the same authors, published in 1993 in Volume 1, edited by V. Gerold, of the *Materials Science and Technology* series. We, and the Editors of *Physical Metallurgy*, are grateful to VCH Publishers, Weinheim, for permission to use this material.

Appendix 1. Gazetteer, in alphabetic order, of intermetallic phases cited in this chapter.

(In the formulae of the phases in the 1st column the element symbols are in alphabetical order, in the prototype formulae they are in the Pettifor's order (see sec. 2). Heavy-faced characters have been used for the phases corresponding to the prototypes)

Phase and Prototype	Corresponding Prototype	Section of this chapter
A1, A_2,...B_1, B_2,..., etc.:	Strukturberichte Symbols	3.4
Ag	cF4–Cu	6.2.1
Ag_3Al	cP20–Mn	7.2.2
Ag_5Al_3	hP2–Mg	7.2.2
AgAsBa	hP6–Ni_2In	6.5.3
AgAsMg	**cF12–AgMgAs**	6.4.3
Ag_5Cd_8	cI52–Cu_5Zn_8	6.1.5, 7.2.2
AgI	hP4–ZnO	6.3.3
Ag_9In_4	cP52–Cu_9Al_4	6.1.5, 7.2.2
Ag_5Li_7	cI52–Cu_5Zn_8	6.1.5, 7.2.2
AgSe	cF8–ZnS (sphalerite)	6.3.3
$AgTe_2Tl$	**tI8–$AgTlTe_2$**	6.5.9
$AgZn_3$	hP2–Mg	7.2.2
Ag_5Zn_8	cI52–Cu_5Zn_8	6.1.5, 7.2.2
Al	cF4–Cu	6.2.1
AlAs	cF8–ZnS (sphalerite)	6.3.3
Al_2Au	cF12–CaF_2	6.4.2
AlB_2	**hP3–AlB_2**	6.5.6, 6.5.10
Al_4Ba	**tI10–$BaAl_4$**	6.5.9
$Al_{1-x}Co_x$	cP2–CsCl	6.1.2
$AlCr_6Si$	cP8–Cr_3Si	6.6.2
β-Al-Cu	cI2–W	6.1.1
$AlCu_3$	cI2–W	7.2.2
Al_2Cu	**tI12–$CuAl_2$**	**5**
Al_4Cu_9	**cP52–Cu_9Al_4**	6.1.5, 7.2.2
$AlCu_2Mn$	**cF16–$MnCu_2Al$**	3.4, 6.1.3
$Al_5(Cu,Ni)_3$		6.1.5
$Al_6(Cu,Ni)_4$		6.1.5
$Al_7(Cu,Ni)_5$		6.1.5
$Al_8(Cu,Ni)_6$		6.1.5
$Al_{11}(Cu,Ni)_6$		6.1.5
$Al_{13}(Cu,Ni)_8$		6.1.5

References: p. 363.

$Al_{15}(Cu,Ni)_{10}$		6.1.5
$Al_{17}(Cu,Ni)_{12}$		6.1.5
$AlCuS_2$	tI16–$CuFeS_2$	7.2.1, 6.3.3
Al_3Er	cP4–$AuCu_3$	6.2.7
AlFe	cP2–CsCl	6.1.2
$AlFe_3$	cF16–$BiLi_3$	4.1.1(a)
Al_3Gd	hP8–Ni_3Sn	6.2.7
$Al_{23}Gd_4Ni_6$		3.2.
Al_3La	hP8–Ni_3Sn	6.2.7
Al_3Mg_2	**cF1832–Mg_2Al_3**	6.6.5, 5
$Al_{12}Mg_{17}$	**cI58–$Mg_{17}Al_{12}$**	6.6.5
$AlMo_3$	cP8–Cr_3Si	6.6.2
AlN	hP4–ZnO	6.3.3
$AlNb_3$	cP8–Cr_3Si	6.6.2
$AlNi_3$	cP4–$AuCu_3$	3.5.5
$Al_{1-x}Ni_x$	cP2–CsCl	6.1.2
$Al_{23}Ni_6Y_4$		3.2.
Al_3OsU_2	**hP12–U_2OsAl_3**	6.6.4
AlP	cF8–ZnS (sphalerite)	6.3.3
$AlPd_2$	oP12–Co_2Si	6.5.4
$AlPt_3$	cP4–$AuCu_3$	3.5.5
Al_2Pt	cF12–CaF_2	6.4.2
AlSb	cF8–ZnS (sphalerite)	6.3.3, 7.2.1
Al_3Sc	cP4–$AuCu_3$	6.2.7
$AlSnV_6$	cP8–Cr_3Si	6.6.2
Al_3Th	hP8–Ni_3Sn	6.2.7
$AlTi_3$	hP8–Ni_3Sn	6.2.7
Al_3Ti	**tI8–$TiAl_3$**	4.1.1(a)
Al_3Tm	cP4–$AuCu_3$	6.2.7
AlV_3	cP8–Cr_3Si	6.6.2
Al_8V_5	cI52–Cu_5Zn_8	6.1.5, 7.2.2
AlY_3	cP4–$AuCu_3$	3.5.5
Al_3Y	hP8–Ni_3Sn	6.2.7
Al_3Y	cP4–$AuCu_3$	3.5.5
Al_3Yb	cP4–$AuCu_3$	6.2.7
$AlZr_2$	hP6–Ni_2In	6.5.3
Al_2Zr	hP12–$MgZn_2$	6.6.4
Al_3Zr	**tI16–Al_3Zr**	4.1.1(a)
Al_3Zr_4	**hP7–Zr_4Al_3**	Table 6
Ar	cF4–Cu	6.2.1
AsB	cF8–ZnS (sphalerite)	6.3.3
AsCaCu	hP6–Ni_2In	6.5.3
AsCuS	**oP12–CuAsS**	5
AsGa	cF8–ZnS (sphalerite)	6.3.3
AsIn	cF8–ZnS (sphalerite)	6.3.3
$AsNa_3$	**hP8–$NaAs_3$**	3.4.
AsNb	**tI8–NbAs**	6.5.9
AsNi	**hP4–NiAs**	4.1, 6.5.1
As_2Zn	mP24–ZnP_2	7.2.1
Au	cF4–Cu	6.2.1
$AuBe_5$	**cF24–$AuBe_5$**	6.6.4
Au_5Cd_8	cI52–Cu_5Zn_8	6.1.5, 7.2.2
AuCu (I)	**tP2–AuCu**	4.1.1,.6.2.4

AuCu (II)	**oI40–AuCu**	4.1.1, 4.2, 6.2.4
$AuCu_3$	**cP4–$AuCu_3$**	3.5.5, 4.1, 4,1,1, 6.2.3.
Au_3Ge	hP2–Mg	7.2.2
Au_5Hg_8	cI52–Cu_5Zn_8	6.1.5, 7.2.2
Au_9In_4	cP52–Cu_9Al_4	6.1.5, 7.2.2
Au_5K	hP6–$CaCu_5$	6.2.8
$AuNb_3$	cP8–Cr_3Si	6.6.2
AuSiTh	hP3–BaPtSi	6.5.6
$AuSn_2$	**oP24–$AuSn_2$**	5
$AuTa_3$	cP8–Cr_3Si	6.6.2
$AuTi_3$	cP8–Cr_3Si	6.6.2
$B_3C_xPd_5Y$		6.6.2
$BCeCo_4$	**hP12–$CeCo_4B$**	4.5
B_2CeCo_3	**hP6–$CeCo_3B_2$**	4.5, 6.2.8
$B_3Ce_2Co_7$	**hP24–$Ce_2Co_7B_3$**	4.5
$B_4Ce_3Co_{11}$	**hP18–$Ce_3Co_{11}B_4$**	4.5
B_2CoW_2	**oI10–W_2CoB_2**	4.5
B_3CoW_3	**oC28–W_3CoB_3**	4.5
BCr	**oC8–CrB**	4.5
B_3Cr_5	**tI32–Cr_5B_3**	3.4
BIr	hP2–WC	6.5.5
$B_6Lu_5Ni_{19}$	**hP30–$Lu_5Ni_{19}B_6$**	4.5
B_4LuRh_4		6.6.2
$B_2Nd_3Ni_{13}$	**hP18–$Nd_3Ni_{13}B_2$**	4.5
BNi	oC8–BCr	3.2
BOs	hP2–WC	6.5.5
BRu	hP2–WC	6.5.5
Ba	cI2–W	6.1.1
$BaCd_{11}$	**tI48–$BaCd_{11}$**	5
$Ba_2Cu_3O_{7-x}Y$		6.6.2
BaH_2(h)	oP12–Co_2Si	6.5.4
$BaHg_{11}$	**cP36–$BaHg_{11}$**	5
$BaPb_3$	**hR36–$BaPb_3$**	6.2.3
BaPtSb	**hP3–BaPtSb**	6.5.6
α-Be	hP2–Mg	6.2.6
Be	cI2–W	6.1.1
$Be_{1-x}Co_x$	cP2–CsCl	6.1.2
$Be_{1-x}Cu_x$	cP2–CsCl	6.1.2
BeN_2Si	**oP16–$BeSiN_2$**	6.3.3
$Be_{1-x}Ni_x$	cP2–CsCl	6.1.2
BeO	hP4–ZnO	6.3.3
BePd	cP2–CsCl	6.1.2
BePo	cF8–ZnS (sphalerite)	6.3.3
BeS	cF8–ZnS (sphalerite)	6.3.3
BeSe	cF8–ZnS (sphalerite)	6.3.3
BeTe	cF8–ZnS (sphalerite)	6.3.3
$Bi_2(Ca,Sr)_3Cu_2O_{9-x}$		6.6.2
BiF_3	**cF16–BiF_3**	3.5.1, 6.1.4
$BiLi_3$	**cF16–Li_3Bi**	4.1.1, 6.1.4, 6.2.2
BrCs	cP2–CsCl	6.1.2
BrCu	hP4–ZnO	6.3.3, 7.2.1
BrTl	cP2–CsCl	6.1.2
C(diamond)	**cF8–C**	6.3.1

References: p. 363.

C(graphite)	**hP4–C**	6.3.4
C(lonsdaleite)	**hP4–C**	6.3.3
C_2Ca	tI6–CaC_2	3.2
$C_{1-x}Hf$	cF8–NaCl	6.4.1
CMo	hP2–WC	6.5.5
$C_{1-x}Nb$	cF8–NaCl	6.4.1
C_5Nb_6	mC22–Nb_6C_5	6.4.1
CSi polytypes		4.3, 6.3.3, 7.2.1
$C_{1-x}Th$	cF8–NaCl	6.4.1
$C_{1-x}Ti$	cF8–NaCl	6.4.1
$C_{1-x}V$	cF8–NaCl	6.4.1
C_5V_6	m??44–V_6C_5	6.4.1
C_7V_8	cP60–V_8C_7	6.4.1
CW	**hP2–WC**	6.4.1, 6.5.5, 5
$C_{1-x}W$	cF8–NaCl	6.4.1
$C_{1-x}Zr$	cF8–NaCl	6.4.1
α-Ca	cF4–Cu	6.2.1
β-Ca	cI2–W	6.1.1
$CaCu_5$	**hP6–$CaCu_5$**	4.5, 6.2.8
CaF_2	**cF12–CaF_2**	3.2, 6.2.2, 6.4.2
$CaIn_2$	**hP6–$CaIn_2$**	6.4.3, 6.5.7
Ca_2Pb	oP12–Co_2Si	6.5.4
$CaSi_2$	**hR18–$CaSi_2$**	3.4
Ca_2Si	oP12–Co_2Si	6.5.4
$Ca_{31}Sn_{20}$	tI204–$Pu_{31}Rh_{20}$	3.2
Cd	hP2–Mg	6.2.6
Cd_3Cu_4	**cF1124–Cu_4Cd_3**	5, 6.6.5
CdI_2	**hP3–CdI_2**	3.2, 4.1, 6.5.2
Cd_2Na	**cF1192–$NaCd_2$**	5, 6.6.5
$Cd_{43}Pd_8$	cP52–Cu_9Al_4	6.1, 7.2.2
CdPo	cF8–ZnS (sphalerite)	6.3.3
CdS	cF8–ZnS (sphalerite)	6.3.3
CdS	hP4–ZnO	6.3.3
CdSe	cF8–ZnS (sphalerite)	6.3.3
CdSe	hP4–ZnO	6.3.3
CdTe	cF8–ZnS (sphalerite)	6.3.3
α-Ce	cF4–Cu	6.2.1
γ-Ce	cF4–Cu	6.2.1
Ce_5Mg_{41}	**tI92–Ce_5Mg_{41}**	5
Ce_2Ni_{17}	**hP36–Ce_2Ni_{17}**	4.5
$\approx Ce_2NiSi_3$	hP3–AlB_2	6.5.6, Table 3
$Ce_6Ni_2Si_3$	**hP22–$Ce_6Ni_2Si_3$**	4.1, 6.5.6
$Ce_5Ni_2Si_3$	**hP40–$Ce_5Ni_2Si_3$**	4.1, 6.5.6
CeO_2	cF12–CaF_2	6.4.2
ClCu	hP4–ZnO	6.3.3
ClNa	**cF8–NaCl**	6.2,2, 6.4.1
Cl_2Pb	**oP12–$PbCl_2$**	3.4, 6.5.4
ClCs	**cP2–CsCl**	4.1.1, 6.1.2, Table 3
ClTl	cP2–CsCl	6.1.2
Co	hP2–Mg	6.2.6
α-Co	cF4–Cu	6.2.1
Co–Cr–Mo (R phases)	3.4	
Co_2EuP_2	tI10–$ThCr_2Si_2$	4.4, 6.5.9

CoFeSn	hP6–Ni_2In	6.5.3
Co_3GaY_3	oC28–W_3CoB_3	4.5
Co_4GaY_4	**mC18–Y_4Co_4Ga**	4.5
Co_5GaY_5	**oC44–Y_5Co_5Ga**	4.5
Co_2Ge	hP6–Ni_2In	6.5.3
Co_2Ge_2RE	tI10–$ThCr_2Si_2$	6.5.9
Co_5La	hP6–$CaCu_5$	6.2.8
CoO	**tI4–CoO**	6.1.5
Co_2RESi_2	tI10–$ThCr_2Si_2$	6.5.9
Co_2Si	**oP12–Co_2Si**	6.5.4
Co_5Sm	hP6–$CaCu_5$	6.2.8
$CoTe_2$	hP3–CdI_2	6.5.2
Co_3V	**hP24–VCo_3**	6.2.3
Co_5Zn_{21}	cP52–Cu_9Al_4	6.1.5
Cr	cI2–W	6.1.1
σCr–Fe	**tP30–σCr–Fe**	6.6.3, Table 6
Cr–Mo-Ni (P phases)		3.4, Table 6
Cr_3Os	cP8–Cr_3Si	6.6.2
$Cr_{12}P_7$	hP19–26–$Cr_{12}P_7$	Table 3
Cr_3Si	cP8–Cr_3Si	6.6.2, Table 6
Cr_2Si_2Th	**tI10–$ThCr_2Si_2$**	6.5.9
Cr_3Pt	cP8–Cr_3Si	6.6.2
ω-Cr–Ti phase	**hP3–Cr–Ti**	6.5.6
α-Cr_2Ti	cF24–Cu_2Mg	6.6.4
β-Cr_2Ti	hP12–$MgZn_2$	6.6.4
γ-Cr_2Ti	hP12–Ni_2Mg	6.6.4
Cu	**cF4–Cu**	6.2.1
$CuFeS_2$	**tI16–$FeCuS_2$**	5, 6.3.1, 6.3.3
Cu_9Ga_4	**cP52–Cu_9Al_4**	6.1.5
Cu_2Ge_2RE	tI10–$ThCr_2Si_2$	6.5.9
CuI	hP4–ZnO	6.3.3
Cu_5La	hP6–$CaCu_5$	6.2.8
CuLaSi	hP6–Ni_2In	6.5.3
Cu_2Mg	**cF24–Cu_2Mg**	3.4, 4.3, 6.6.4, Table 6
$Cu_{16}Mg_6Si_7$	cF116–Th_6Mn_{23}	3.4
Cu_4MgSn	**cF24–Cu_4MgSn**	6.6.4
CuPt(I)	**hR96–CuPt(I)**	4.1.1a
Cu_2RESi_2	tI10–$ThCr_2Si_2$	6.5.9
CuS_2Sb	**oP16–$CuSbS_2$**	5
Cu_5Si	t**	7.2.2
Cu_5Sn		7.2.2
$CuTi_3$	**tP4–Ti_3Cu**	4,1,1 a, 6.2.5
(β-)Cu–Zn	cI2–W	4.1.1, 6.1.1, 7.2.2
(β'-)Cu–Zn	cP2–CsCl	4.1.1, 6.1.2
Cu_5Zn_8	**cI52–Cu_5Zn_8**	6.1.5
Diamond: see C (diamond)		
α-Dy	hP2–Mg	6.2.6
E phases: see oP12–TiNiSi		
Er	hP2–Mg	6.2.6
Er_2RhSi_3	**hP24–Er_2RhSi_3**	6.5.6
Eu	cI2–W	6.1.1
α-Fe (δ)	cI2–W	6.1.1
γ-Fe	cF4–Cu	6.2.1

References: p. 363.

Fe_3Ga	hP8–Ni_3Sn	6.2.7
Fe_3Ge	hP8–Ni_3Sn	6.2.7
Fe_2Ge_2RE	tI10–$ThCr_2Si_2$	6.5.9
Fe_4N	**cP5–Fe_4N**	4.1, 4.1.1 b
Fe_8N	**tI8–Fe_8N**	4.1.1 b
FeNNi	**tP3–FeNiN**	4.1.1 b
Fe_2P	**hP9–Fe_2P**	6.5.8
Fe_2RESi_2	tI10–$ThCr_2Si_2$	6.5.9
FeS_2 (pyrite)	**cP12–FeS_2**	4.1
FeSbV	hP6–Ni_2In	6.5.3
Fe_3Sn	hP8–Ni_3Sn	6.2.7
Fe_7W_6	**hR39–W_6Fe_7**	3.4,5, 6.6.3, Table 6
Fe_3Zn_{10}	cI52–Cu_5Zn_8	6.1.5
Frank–Kasper phases		3.4, 6.6
G phases: see cF116–$Mn_{23}Th_6$		
$GaGeNb_6$	cP8–Cr_3Si	6.6.2
Ga_5Ir_3	**tP32–Ir_3Ga_5**	4.4
GaN	hP4–ZnO	6.3.3
$GaNb_3$	cP8–Cr_3Si	6.6.2
Ga_4Ni	cI52–Cu_5Zn_8	6.1.5
GaV_3	cP8–Cr_3Si	6.6.2
Ga_7V_6	cI52–Cu_5Zn_8	6.1.5
GdNi	oC8–CrB	3.2.
$GdSe_2$	oP12–Co_2Si	6.5.4
Ge	cF8–C (diamond)	6.3.1
Ge_5Ir_4	**tP36–Ir_4Ge_5**	4.4
$GeMg_2$	cF12–CaF_2	6.4.2, Table 3
Ge_2Mn_2RE	tI10–$ThCr_2Si_2$	6.5.9
GeNa	**mP32–NaGe**	3.4
$GeNb_3$	cP8–Cr_3Si	6.6.2
Ge_2Ni_2RE	tI10–$ThCr_2Si_2$	6.5.9, 7.2.5 b
$GeRh_2$	oP12–Co_2Si	6.5.4
$Ge_{31}V_{17}$	**tP192–$V_{17}Ge_{31}$**	4.4
Graphite: see C (graphite)		
Hägg phases		3.4
Heusler phases		3.4, 6.1.3
HfS_2	hP3–CdI_2	6.5.2
HgS	cF8–ZnS (sphalerite)	6.3.3
HgSe	cF8–ZnS (sphalerite)	6.3.3
HgTe	cF8–ZnS (sphalerite)	6.3.3
$HgTi_3$	cP4–$AuCu_3$	3.5.5
$HfPt_3$	cP4–$AuCu_3$	3.5.5
Ho	hP2–Mg	6.2.6
Hume–Rothery phases		3.4, 6.1.5, 7.2.2
$InLa_2$	hP6–Ni_2In	6.5.3
$InLa_3$	cP4–$AuCu_3$	3.5.5
In_3La	cP4–$AuCu_3$	3.5.5
InN	hP4–ZnO	6.3.3
$InNi_2$	**hP6–Ni_2In**	6.5.3
ITl	cP2–CsCl	6.1.2
Ir	cF4–Cu	6.2.1
$IrMo_3$	cP8–Cr_3Si	6.6.2
K	cI2–W	6.1.1

K_2O	cF12–CaF_2	6.4.2
Kr	cF4–Cu	6.2.1
K_2S	cF12–CaF_2	6.4.2
KSbZn	hP6–Ni_2In	6.5.3
K_2Se	cF12–CaF_2	6.4.2
K_2Te	cF12–CaF_2	6.4.2
α-La	**hP4–La**	6.2.6
β-La	cF4–Cu	6.2.1
$LaNi_5$	hP6–$CaCu_5$	6.2.8
$LaPt_5$	hP6–$CaCu_5$	6.2.8
LaPtSi	**tI12–LaPtSi**	6.5.10
Laves phases		3.4, 4.3, 6.6.4, Table 6
$LaZn_5$	hP6–$CaCu_5$	6.2.8
Li	cI2–W	6.1.1
Li–Mg–Zn Laves polytypes		6.6.4
Li_2O	cF12–CaF_2	6.4.2
Li_2O_3Si		3.2.
LiN_3Si_2		3.2.
$Li_{10}Pb_3$	cP52–Cu_9Al_4	6.1.5
Li_2S	cF12–CaF_2	6.4.2
Li_2Se	cF12–CaF_2	6.4.2
Li_2Te	cF12–CaF_2	6.4.2
Lonsdaleite: see C (lonsdaleite)		
Lu	hP2–Mg	6.2.6
M phases		Table 6
Martensite (Fe/C)		6.1.5
Mg	**hP2–Mg**	6.2.6
$MgNi_2$	**hP24–Ni_2Mg**	3.4, 6.6.4, 4.3, Table 6
Mg_2Pb	cF12–CaF_2	6.4.2
Mg_2Si	cF12–CaF_2	6.4.2
Mg_2Sn	cF12–CaF_2	3.4, 6.4.2
$MgZn_2$	**hP12–$MgZn_2$**	3.4, 6.6.4, 4.3, Table 6
α-Mn	**cI58 α-Mn**	6.6.5
Mn_2RESi_2	tI10–$ThCr_2Si_2$	6.5.9
MnS	hP4–ZnO	6.3.3
MnSe	hP4–ZnO	6.3.3
Mn_2Sn	hP6–Ni_2In	6.5.3
MnTe	hP4–ZnO	6.3.3
$Mn_{12}Th$	**tI26–$ThMn_{12}$**	6.2.8
$Mn_{23}Th_6$	**cF116–Th_6Mn_{23}**	3.4
$MnZn_3$	cP4–$AuCu_3$	3.5.5
Mo	cI2–W	6.1.1
$MoNi_4$	**tI10–$MoNi_4$**	4.1.1a
MoP	hP2–WC	6.5.5
$MoPt_2$	**oI6–$MoPt_2$**	4.1.1a
$MoSi_2$	**tI6–$MoSi_2$**	3.2, Table 3
NNb	hP4–ZnO	6.3.3
NNb	hP2–WC	6.5.5
$N_{1-x}V$	cF8–NaCl	6.4.1
$N_{1-x}W$	cF8–NaCl	6.4.1
NW	hP2–WC	6.4.1, 6.5.5
Na	cI2–W	6.1.1
Na_2O	cF12–CaF_2	6.4.2

References: p. 363.

Na_2S	cF12–CaF_2	6.4.2
Na_2Se	cF12–CaF_2	6.4.2
NaSi	**mC32–NaSi**	3.4
Na_2Te	cF12–CaF_2	6.4.2
NaTl	**cF16–NaTl**	3.4, 6.1.4
$NaZn_{13}$	**cF112–$NaZn_{13}$**	5
Nb_3Sn	cP8–Cr_3Si	6.6.2
Nb_3Pt	cP8–Cr_3Si	6.6.2
Ne	cF4–Cu	6.2.1
$Ni_7Pr_{15}Si_{10}$	**hP64–$Pr_{15}Ni_7Si_{10}$**	4.1,6.5.6
Ni_2Si_2RE	tI10–$ThCr_2Si_2$	6.5.9
NiSiTi	**oP12–TiNiSi**	6.5.4
Ni_3Sn	**hP8–Ni_3Sn**	6.2.7, 4.1.1a
$Ni_{17}Th_2$	**hP38–Th_2Ni_{17}**	6.2.8
Ni_3Ti	**hP16–$TiNi_3$**	6.2.3
Ni_2Zn_{11}	cI52–Cu_5Zn_8	6.1.5, 7.2.2
Ni_3Zr	hP8–Ni_3Sn	6.2.7
Nowotny phases		4.4
Os	hP2–Mg	6.2.6
OTa_4	**oP5–Ta_4O**	4.1.1b
O_2Th	cF12–CaF_2	6.4.2
$O_{1\pm x}Ti$	cF8–NaCl	6.4.1
OTi_2	hP3–CdI_2	6.5.2
O_2U	cF12–CaF_2	6.4.2
$O_{1\pm x}V$	cF8–NaCl	6.4.1
OW_3	cP8–Cr_3Si	6.6.2
OZn	**hP4–ZnO**	6.3.2
P phases	oP56–(Cr-Mo-Ni)	Table 6
Pb	cF4–Cu	6.2.1
Pb_3U	cP4–$AuCu_3$	3.5.5
Pd	cF4–Cu	6.2.1
Pd_2Sn	oP12–Co_2Si	6.5.4
$Pd_{1-x}Ti_x$ (r)	oP4–AuCd	6.1.2
$Pd_{1-x}Ti_x$ (h)	cP2–CsCl	6.1.2
α-Po	cP1–Po	3.5.2
Pt	cF4–Cu	6.2.1
$PtMn_3$	cP4–$AuCu_3$	3.5.5
PtS_2	hP3–CdI_2	6.5.2
Pt_2RESn_2	tI10–$ThCr_2Si_2$	6.5.9
$Pt_{1-x}Ti_x$ (r)	oP4–AuCd	6.1.2
$Pt_{1-x}Ti_x$ (h)	cP2–CsCl	6.1.2
Pt_2U	**oC12–UPt_2**	4.5
$Pu_{31}Rh_{20}$	**tI204–$Pu_{31}Rh_{20}$**	3.2.
Pyrite: see FeS_2		
$\mathfrak{R}$ phases	hR159 Co-Cr-Mo	Table 6
RE (rare earth) alloys		8.6
RE (metals)		6.1.1, 6.2.6
Rb	cI2–W	6.1.1
Re	hP2–Mg	6.2.6
$Re_{24}Ti_5$(χ-phase)	**cI58–Ti_5Re_{24}**	6.6.5
Rh	cF4–Cu	6.2.1
Rh_2Sn	oP12–Co_2Si	6.5.4
Ru	hP2–Mg	6.2.6

Ru_2Sn_3	**tP20–Ru_2Sn_3**	4.4
Samson phases		6.6.5
SZn(sphalerite)	**cF8–ZnS**	6.3.1, 6.3.2
SZn(wurtzite)	**hP4–ZnO**	6.3.2
S_2Th	oP12–Co_2Si	6.5.4
SeZn	hP4–ZnO	6.3.3
Si	cF8–C (diamond)	6.3.1
α-Si_2Th	**tI12–α-$ThSi_2$**	6.5.10
β-Si_2Th	hP3–AlB_2	6.5.10
≈Si_5Th_3	hP3–AlB_2	6.5.10
Si_2Ti	**oF24–$TiSi_2$**	4.4
Si_2U_3	**tP10–U_3Si_2**	5
SiV_3	cP8–Cr_3Si	6.6.2
Si_3W_5	**tI32–W_5Si_3**	3.4
Sm	**hR9–Sm**	6.2.6
α-Sn	cF8–C (diamond)	6.3.1
β-Sn	**tI4–β-Sn**	6.3.1
$SnTi_2$	hP6–Ni_2In	6.5.3
α-Sr	cF4–Cu	6.2.1
Sr	cI2–W	6.1.1
T_1 phases: see Si_3W_5		
T_2 phases: see B_3Cr_5		
Ta	cI2–W	6.1.1
Tc	hP2–Mg	6.2.6
TeTh	cP2–CsCl	6.1.2
TeZn	hP4–ZnO	6.3.3
α-Th	cF4–Cu	6.2.1
Th	cI2–W	6.1.1
Th_2Zn_{17}	**hR57–Th_2Zn_{17}**	6.2.8
$TiZn_3$	cP4–$AuCu_3$	3.5.5
V	cI2–W	6.1.1
W	**cI2–W**	4.1.1, 6.1.1
Wurtzite: see SZn (wurtzite)		
Xe	cF4–Cu	6.2.1
α-Y	hP2–Mg	6.2.6
Zintl phases		3.4, 6.1.4
Zn	hP2–Mg	6.2.6
β-(Cu–Zn)		4.1.1
β'-(Cu–Zn)		4.1.1
ε-Mg type		
γ-(Cu_5Zn_8)		6.1.5
μ-(Fe_7W_6)		5.3.4, Table 6
σ-phases (see (σ) Cr–Fe)	3.4	Table 6
χ-phase:see $Re_{24}Ti_5$		6.6.5
ω-phase : see ω-Cr–Ti		Table 6

References

ALBERING, J. H., Pöttgen, R., Jeitschko, W., Hoffmann, R-D., Chevalier, B., Etourneau, J., 1994, J. Alloys and Compounds, **206**, 133.

ALDINGER, F., SEIFERT, H. J., 1993, Z. Metallkd., **84**, 2.

ANDERSSON, S., HYDE, B. G., 1982, Z. Kristallogr., **158**, 119.

ANSARA, I., BERNARD, C., KAUFMAN, L., SPENCER, P., 1978, Calphad, **2**, 1.

ASM INTERNATIONAL, Monograph Series on Alloy Phase Diagrams. "Phase Diagrams of Binary Gold Alloys", 1987, H. Okamoto and T. B. Massalski (Eds.); "Phase Diagrams of Binary Berillium Alloys", 1987, H. Okamoto and L. Tanner (Eds.); "Phase Diagrams of Binary Titanium Alloys", 1987, J. L. Murray (Ed.); "Phase Diagrams of Binary Magnesium Alloys", 1988, A. A. Nayeb-Hashemi and J. B. Clark (Eds.); "Phase Diagrams of Binary Vanadium Alloys", 1989, J. F. Smith (Ed.); "Phase Diagrams of Binary Indium Alloys", 1992, C. E. T. White and H. Okamoto (Eds.).

BÄRNIGHAUSEN, H., 1980, Match (Comm. Mathematical Chemistry), **9**, 139.

BARRETT, C. S., MASSALSKI, T. B., 1966, "Structure of Metals", III Ed., (McGraw Hill Book Company, New-York).

BAUGHMAN, R. H., GALVAO, D. S., 1993, Nature, **365**, 735.

BAZELA, W, 1987, J. Less-Common Metals, **133**, 193.

BHANDARY, K. K., GIRGIS, K., 1977, Acta Crystallogr., **A33**, 903.

BILTZ, W., 1934, "Raumchemie der Festen Stoffe", (Voss-Verlag, Leipzig).

BOKII, G. B., LAPTEV, V. I., 1994, Crystallography Reports, **39**, 409; translated from Kristallografiya, 1994, **39**, 464.

BORZONE, G., CACCIAMANI, G., FERRO, R., 1990, Calphad, **14**, 139.

BORZONE, G., PARODI, N., FERRO, R., 1993, J. Phase Equilibria, **14**, 485.

BREWER, L., 1990, J. Phys. Chem., **94**, 1196.

BREWER, L., WENGERT, P. R., 1973, Metall. Trans. **4**, 83.

BROWN, I. D., SHANNON, R. D., 1973, Acta Cryst., **A29**, 266.

BRUNNER, G. O., 1977, Acta Crystallogr., **A33**, 226.

BRUNNER, G. O., SCHWARZENBACH, D., 1971, Z. Kristallogr., **133**, 127.

CAHN, R. W., 1987, "Antiphase Domains, Disordered Films and the Ductility of Ordered Alloys Based on Ni_3Al", in Stoloff, N. S., Koch, C. C., Liu, C. T. and Izumi, O. (Eds.), High-Temperature Ordered Intermetallic Alloys II, MRS, Pittsburgh, vol. 81, p. 27.

CAHN, R. W., 1990 in: "Recovery, Strain-age-hardening and Recrystallization in Deformed Intermetallics", Whang, S. H., Liu, C. T., Pope, D., and Stiegler, J. O., (Eds.), High Temperature Aluminides and Intermetallics, TSM, Warrendale, p. 245.

CARTER, F. L., 1978, Acta Cryst. **B34**, 2962.

CAVA, R. J., TAKAGI, H., BATLOGG, B., ZANDBERGEN, H. W., KRAJEWSKI, J. J., Peck, W. F. Jr., VAN DOVER, R. B., FELDER, R. J., SIEGRIST, T., MIZUHASHI, K., LEE, J. O., EISAKI, H., CARTER, S. A., UCHIDA, S., 1994a, Nature, **367**, 146.

CAVA, R. J., ZANDBERGEN, H. W., BATLOGG, B., EISAKI, H., TAKAGI, H., KRAJEWSKI, J. J., PECK, W. F. Jr., GYORGY, E. M., UCHIDA, S., 1994b, Nature, **372**, 245.

CHELIKOWSKY, R., PHILLIPS, J. C., 1977, Phys. Rev. Lett., **39**, 1687.

CHELIKOWSKY, R., PHILLIPS, J. C., 1978, Phys. Rev. B, **17**, 2453.

COLINET, C., PASTUREL, A., PERCHERON-GUEGAN, A., ACHARD, J. C., 1984a, J. Less-Common Metals, **102**, 167.

COLINET, C., PASTUREL, A., PERCHERON-GUEGAN, A., ACHARD, J. C., 1984b, J. Less-Common Metals, **102**, 239.

CORBETT, J. D., 1985, Chem. Rev., **85**, 383.

DAAMS, J. L. C., VILLARS, P., VAN VUCHT, J. H. N., 1991, "Atlas of Crystal Structure Types for Intermetallic Phases", Vol. 1–4, (Materials Park, Oh 44073: American Society for Metals).

DAAMS, J. L. C., VAN VUCHT, J. H. N., VILLARS, P., 1992, J. Alloys and Compounds, **182**, 1.

DAAMS, J. L. C., VILLARS, P., 1993, J. Alloys and Compounds, **197**, 243.

DAAMS, J. L. C., VILLARS, P., 1994, J. Alloys and Compounds, **215**, 1.

DARKEN, L. S., GURRY, R. W., 1953, "Physical Chemistry of Metals", (McGraw-Hill, New York).

DE BOER, F. R., BOOM, R., MATTENS, W. C. M., MIEDEMA, A. R., NIESSEN, A. K., 1988, "Cohesion in Metals, Transition Metal Alloys", (North Holland, Amsterdam).

DONNAY, J. D. H., HELLNER, E., NIGGLI, A., 1964, Z. Krist., **120**, 364.

DWIGHT, A. E., 1974, in: Proc. 11th Rare Earth Res. Conf., Oct. 9–10, Traverse City, Michigan, USA, p. 642.

ELLIOTT, R. P., 1965, "Constitution of Binary Alloys", First Supplement, (McGraw-Hill Book Company, New York).
ELLNER, M., PREDEL, B., 1994, in: "Intermetallic Compounds", Vol. 1, Principles, Westbrook, J. H., Fleischer, R. L., (Eds.), p. 91 (John Wiley and Sons Ltd.).
FERRO, R., DELFINO, S., BORZONE, G., SACCONE, A., CACCIAMANI, G., 1993, J. Phase Equilibria, **14,** 273.
FERRO, R., BORZONE, G., PARODI, N., CACCIAMANI, G., 1994, J. Phase Equilibria, **15,** 317.
FERRO, R., CACCIAMANI, G., SACCONE, A., 1995 to be submitted.
FERRO, R., GIRGIS, K., 1990, J. Less-Common Metals, **158,** L41.
FLIEHER, G., VÖLLENKLE, H., NOWOTNY, H., 1968a, Monatsh. Chemie, **99,** 877.
FLIEHER, G., VÖLLENKLE, H., NOWOTNY, H., 1968b, Monatsh. Chemie, **99,** 2408.
FRANK, F. C., KASPER, J. S., 1958, Acta Cryst., **11,** 184.
FRANK, F. C., KASPER, J. S., 1959, Acta Cryst., **12,** 483.
FRANZEN, H. F., 1986, "Physical Chemistry of Inorganic Crystalline Solids", (Springer-Verlag, Berlin).
FREVEL, L. K., 1985, Acta Cryst., **B41,** 304.
GIALANELLA, S., CAHN, R. W., 1993, Materials Engineering **4,** 407.
GIOVANNINI, M., SACCONE, A., FERRO, R., ROGL, P., FLANDORFER, H., EFFENBERG, G., 1994, in "Perspectives in Inorganic Chemistry", DAOLIO, S., TONDELLO, E., VIGATO, P. A., Eds. (La Photograph Publishing, Padova), p. 230.
GIOVANNINI, M., SACCONE, A., MARAZZA, R., FERRO, R., 1995a, Metall. Trans. A, **26A,** 5.
GIOVANNINI, M., SACCONE, A., FERRO, R., 1995b, J. Alloys and Compounds, **220,** 167.
GIRGIS, K., 1983, in: "Physical Metallurgy", Cahn, R. W., Haasen, P., Eds., p. 219, (North-Holland Physics Publishing, Amsterdam).
GIRGIS K., VILLARS, P., 1985, Monatsh. Chemie, **116,** 417.
GLADYSHEVSKII, R.E., CENZUAL, K., PARTHÉ, E., 1992, J. Alloys and Compounds, **189,** 221.
GRIMM, H. G., SOMMERFELD, A., 1926, Z. Physik, **36,** 36.
GRIN', Yu. N., YARMOLYUK, Ya. P., GLADYSHEVSKII, E. I., 1982, Sov. Phys. Crystallogr., **27,** 413.
GRIN', Yu. N., AKSELRUD, L. G., 1990, Acta Crystallogr., **A46** Suppl. C 338.
GRIN' Yu. N., 1992, in :"Modern Perspectives in Inorganic Crystal Chemistry", A NATO Advanced Study Institute, Director Erwin Parthe', Lecture Notes of 19th Course, Ettore Majorana Centre for Scientific Culture, Erice (Trapani), (Italy).
GSCHNEIDNER, K. A., Jr., 1969, J. Less-Common Metals, **17,** 1.
GSCHNEIDNER, K. A., Jr., 1980, in: "Theory of Alloy Phase Formation", Bennett, L. H. Ed., Proceedings 108th AIME Annual Meeting, New Orleans, USA, February 19–20, 1979, p. 1.
GSCHNEIDNER, K. A., Jr., MCMASTERS, O. D., 1971, Monatsh. Chemie, **102,** 1499.
GUILLERMET, A. F., GRIMVALL, G., 1991, J. Less-Common Metals, **169,** 257.
GUILLERMET, A. F., FRISK, K., 1992, Calphad **16,** 341.
GUINIER, A., BOKIJ, G. B., BOLL-DORNBERGER, K., COWLEY, J. M., DUROVIC, S., JAGODZINSKI, H., KRISHNA, P., DE WOLFF, P. M., ZVYAGIN, B. B., COX, D. E., GOODMAN, P., HAHN, Th., KUCHITSU, K., ABRAHAMS, S. C., 1984, Acta Cryst., **A40,** 399.
HAFNER, J., 1985, J. Phys. F., **15,** L43.
HAFNER, J., 1989, in: "The Structures of Binary Compounds. Cohesion and Structure", Vol. 2: de Boer, F. R., Pettifor, D. G. (Eds.), (North-Holland, Amsterdam), p. 147.
HÄGG, G., 1931, Z. Phys., Chem., **B12,** 33.
HAHN, T., (Ed.), 1989, "International Tables for Crystallography", (Kluwer Academic Publishers, Dordrecht).
HANSEN, M., 1936, "Der Aufbau der Zweistofflegierungen", (Springer-Verlag, Berlin).
HANSEN, M., ANDERKO, K., 1958, "Constitution of Binary Alloys", (McGraw-Hill Book Company, New York).
HAWTHORNE, F. C., 1983, Acta Cryst., **A39,** 724.
HELLNER, E. E., 1979, in: "The Frameworks (Bauverbände) of the Cubic Structure Types", Structure and Bonding, Vol. 37, (Springer-Verlag, Berlin), p. 61.
HILLERT, M., 1981, Physica B, **103,** 30.
HOCH, M., ARPSHOFEN, I., PREDEL, B., 1984, Z. Metallkd., **75,** 30.
HOFFMANN, R., 1987, Angew. Chem. Int. Ed. Engl. **26,** 846.
HOFFMANN, R., 1988, "Solids and Surfaces", (VCH Publishers, New York).

HOPPE, R., 1979, Z. Kristallogr., **150**, 23.
HOPPE, R., MEYER, G., 1980, Z. Metallkd., **71**, 347.
HYDE, B. G., ANDERSSON, S., 1989, "Inorganic Crystal Structures", (J. Wiley & Sons, New-York).
HOVESTREYDT, E., 1988, J. Less-Common Metals, **143**, 25.
HUME-ROTHERY, J., 1926, J. Inst. Metals, **35**, 295.
HUME-ROTHERY, J., MABBOT, G. W., CHANNEL EVANS, K. M., 1934, Phil. Trans. Roy. Soc., **A 233**, 1.
HUME-ROTHERY, J., 1967, in: "Phase Stability in Metals and Alloys", Rudman, P. S., Stringer, J., Jaffee, R. I. Eds., (McGraw-Hill Book Company, New-York), p. 3.
IANDELLI, A., PALENZONA, A., 1979: in "Handbook on the Physics and Chemistry of Rare Earths", Vol. 2: Gschneidner, K. A., Jr., Eyring L. (Eds.), (North-Holland, Amsterdam), p. 1.
JAGODZINSKI, H., 1954, Acta Cryst., **7**, 17.
JEITSCHKO, W., PARTHÉ, E., 1967, Acta Cryst., **22**, 417.
JENSEN, W. B., 1984, in: "Communicating Solid-State Structures to the Uninitiated", Rochester, Institute of Technology, Rochester.
JENSEN, W. B., 1989, in: "The Structures of Binary Compounds. Cohesion and Structure", Vol. 2: de Boer, F. R., Pettifor, D. G. (Eds.), (North-Holland, Amsterdam), p. 105.
KAO, C. R., PIKE, L. M., CHEN, S. -L., CHANG, Y. A., 1994, Intermetallics, **2**, 235.
KAUFMAN, L., BERNSTEIN, H., 1970, "Computer Calculation of Phase Diagrams", Vol. 4, "Refractory Materials", (Academic Press, New-York).
KAUFMAN, L., NESOR, H., 1973, Ann. Rev. Mater. Sci., R. Huggins Ed., vol. 3. p. 1.
KHACHATURYAN, A. G., 1983, "Theory of Structural Transformations in Solids", (John Wiley & Sons, New York).
KING, H. W., 1983, in: "Physical Metallurgy", Cahn, R. W., Haasen, P., Eds., (North-Holland Physics Publishing, Amsterdam), p. 37.
KISELYOVA, N. N., 1993, J. Alloys and Compounds, **197**, 159.
KLEE, H., WITTE, H., 1954, Z. Phys. Chem., **202**, p. 352.
KRIPYAKEVICH, P. I., 1963, "A Systematic Classification of Types of Intermetallic Structures", from J. Structural Chemistry, vol. 4.
KRIPYAKEVICH, P. I., 1976, Sov. Phys. Crystallogr., **21**, 273.
KRIPYAKEVICH, P. I., GLADYSHEVSKII, E. I., 1972, Acta Cryst., **A28**, Suppl.,S97.
KRIPYAKEVICH, P. I., GRIN´, Yu. N., 1979, Sov. Phys. Crystallogr., **24**, 41.
KUBASCHEWSKI, O., EVANS, E. LL., 1958, "Metallurgical Thermochemistry", (Pergamon Press, London).
KUBASCHEWSKI, O., 1967, in: "Phase Stability in Metals and Alloys", Rudman, P. S., Stringer, J., Jaffee, R. I. Eds., (McGraw-Hill Book Company, New-York), p. 63.
LAMPARTER, P., STEEB, S., 1993 in: "Structure of Amorphous and Molten Alloys", Materials Science and Technology, Cahn, R. W., Haasen, P., Kramer, E. J., (Eds.), Vol. 1, (VCH, Weinheim).
LANDOLT-BÖRNSTEIN TABLES, 1971, "Structure Data of Elements and Intermetallic Phases", Vol. 6, Hellwege, K.-H., Hellwege, A. M. (Eds.); 1991, "Phasengleichgewichte, Kristallographische und Thermodynamische Daten Binaren Legierungen", MADELUNG, O., Ed. Vol. 5a, Predel, B., (Springer-Verlag, Berlin).
LATROCHE, M., SELSANE, M., GODART, C., SCHIFFMACHER, G., THOMPSON, J. D., BEYERMANN, W. P., 1992, J. Alloys and Compounds, **178**, 223.
LAVES, F., 1930, Z. Krist., **73**, 303.
LAVES, F., 1956, in: "Theory of Alloy Phases", (Amer. Soc. Met., Cleveland (Ohio)), p. 124.
LAVES, F., 1967, in: "Phase Stability in Metals and Alloys", Rudman, P. S., Stringer, J., Jaffee, R. I. Eds., (McGraw-Hill Book Company, New-York), p. 85.
LAVES, F., WITTE, H., 1936, Metallwirtschaft, **15**, 840.
LEIGH G. J. (Ed.), 1990, "Nomenclature of Inorganic Chemistry. Recommendations 1990", Issued by the Commission on the Nomenclature of Inorganic Chemistry, (Blackwell Scientific Publications, Oxford).
LIMA-DE-FARIA, J., FIGUEIREDO, M. O., 1976, J. Solid State Chem., **16**, 7.
LIMA-DE-FARIA, J., FIGUEIREDO, M. O., 1978, Garcia de Orto, Ser. Geol. **2**, 69.
LIMA-DE-FARIA, J., HELLNER, E., LIEBAU, F., MAKOVICKY, E., PARTHÉ, E., 1990, Acta Cryst., **A46**, 1.

LIU L. -G., BASSETT, W. A., 1986, "Elements, Oxides, and Silicates - High Pressure Phases with Implications for the Earth's Interior", Oxford Monographs on Geology and Geophysics, N. 4, (Oxford University Press, New York).
LU, S. S., CHANG, T., 1957a, Sci. Rec. Peking, **1**, 41.
LU, S. S., CHANG, T., 1957b, Acta. Phys. Sinica, **13**, 150.
LUKAS, H. L., HENIG, E-Th., ZIMMERMANN, B., 1977, CALPHAD, **1**, 225.
LUKAS, H. L., WEISS, J., HENIG, E.-Th., 1982, CALPHAD, **6**, 229.
MACHATSCHKI, F., 1938, Naturwissenschaften, **26**, 67.
MACHATSCHKI, F., 1947, Monatsh. Chemie, **77**, 333.
MACHATSCHKI, F., 1953, "Spezielle Mineralogie auf Geochemischer Grundlage", (Springer, Wien), p. 1 and p. 298.
MAKINO, Y., 1994a, Intermetallics, **2**, 55.
MAKINO, Y., 1994b, Intermetallics, **2**, 67.
MALLIK, A. K., 1987, J. Alloy Phase Diagrams (Indian Institute of Metals), **3**, 12.
MANDELBROT, B., 1951, C. R. Acad. Sc., Paris, **232**, p. 1638.
MARAZZA, R., ROSSI, D., FERRO, R., 1980, J. Less-Common Metals, **75**, P25.
MARAZZA, R., ROSSI, D., FERRO, R., 1988, J. Less-Common Metals, **138**, 189.
MARTYNOV, A. I., BATSANOV, S. S., 1980, Russian J. Inorg. Chem., **25**, 1737.
MASSALSKI, T. B. (Editor in Chief), 1990, "Binary Alloy Phase Diagrams", Vol. 1–3, Second edition: Okamoto, H., Subramanian, P. R., Kacprzak, L. (Eds.), (ASM International, USA).
MASSALSKI, T. B., 1989, Metall. Trans., **20A**, 1295.
MELNIK, E. V., KRIPYAKEVICH, P. I., 1974, Kristallografiya, **19**, 645.
MERLO, F., 1988, J. Phys. F: Met. Phys., **18**, 1905.
MIEDEMA, A. R., 1973, J. Less-Common, Metals, **32**, 117.
MIEDEMA, A. R., NIESSEN, A. K., 1982, Physica **114B**, 367.
MIODOWNIK, A. P., 1993, in "Computer Aided Innovation of New Materials", M. DOYAMA *et al.* Eds., (Elsevier), p. 689.
MOFFATT, W. G., 1986, "The Handbook of Binary Phase Diagrams", Vol. 1–5, (Genium Publishing Corporation, Schenectady, New York).
MOORE, J. S., 1993, Nature, **365**, 690.
MOOSER, E., PEARSON, W. B., 1959, Acta Cryst., **12**, 1015.
MORRIS, D. G., 1992, in: "Ordered Intermetallics - Physical Metallurgy and Mechanical Behaviour", Liu, C. T., Cahn, R. W. and Sauthoff, G., (Eds.), (Kluwer Academic Publishers, Dordrecht).
NIESSEN, A. K., DE BOER, F. R., BOOM, R., DE CHATEL, P. F., MATTENS, W. C. M., MIEDEMA, A. R., 1983, CALPHAD, **7**, 51.
NIGGLI, P., 1945, Grundlagen der Stereochemie, (Birkhäuser, Basel), p. 125.
NIGGLI, P., 1948, Gesteine und Minerallagerstätten, Vol. 1, (Birkhäuser, Basel), p. 42.
OCHIAI, S., OYA, Y., SUZUKI, T., 1984, Acta Metall., **32**, 289.
OKAMOTO, H., MASSALSKI, T. B., CHAKRABARTI, D. J., LAUGHLIN, D. E., 1987 in: "Phase Diagrams of Binary Gold Alloys", Monograph Series on Alloy Phase Diagrams, Okamoto, H. and Massalski, T. B., (Eds.), (ASM International, USA), p. 76.
O'KEEFFE, M. O., 1979, Acta Cryst., **A35**, 772.
PANI, M., FORNASINI, M. L., 1990, Z. Kristallogr., **190**, 127.
PARTHÉ, E., 1961, Z. Krystallogr., **115**, 52.
PARTHÉ, E., 1963, Z. Krystallogr., **119**, 204.
PARTHÉ, E., 1964, "Crystal Chemistry of Tetrahedral Structures", (Gordon and Breach Publishers, New-York).
PARTHE, E., 1969 in: "Developments in the Structural Chemistry of Alloy Phases", Giessen, B. C. (Ed.), (Plenum Press, New York), p. 49.
PARTHÉ, E., 1980a, Acta Crystallogr., **B 36**, 1.
PARTHÉ, E., 1980b, "Valence and Tetrahedral Structure Compounds", in: Summer School on Inorganic Crystal Chemistry, Geneva, ed. E. Parthé (Parthé, Geneva).
PARTHÉ, E., 1991, J. Phase Equilibria, **12**, 404.

PARTHÉ, E., CHABOT, B., 1984 in : "Handbook on the Physics and Chemistry of Rare Earths", Vol. 6: Gschneidner, K. A., Jr., Eyring L. (Eds.), (North-Holland, Amsterdam), p. 113.
PARTHÉ, E., GELATO, L. M., 1984, Acta Cryst., **A40**, 169.
PARTHÉ, E., CENZUAL, K., GLADYSHEVSKII, R. E., 1993, J. Alloys and Compounds, **197**, 291.
PARTHÉ, E. Chabot, B. A., CENZUAL, K., 1985, Chimia, **39**, 164.
PAULING, L., 1932, J. Amer. Chem. Soc., **54**, 988.
PAULING, L., 1947, J. Amer. Chem. Soc., **69**, 542.
PEARSON, W. B., 1967, "A Handbook of Lattice Spacings and Structures of Metals and Alloys", Vol. 2, (Pergamon Press, Oxford).
PEARSON, W. B., 1972, "The Crystal Chemistry and Physics of Metals and Alloys", (Wiley-Interscience, New-York).
PEARSON, W. B., 1980, Z. Kristallogr. **151**, 301.
PEARSON, W. B., 1985a, J. Less-Common Metals, **114**, 17.
PEARSON, W. B., 1985b, J. Less-Common Metals, **109**, L3.
PEARSON, W. B., VILLARS, P., 1984, J. Less-Common Metals, **97**, 119.
PETTIFOR, D. G., 1984, Solid State Communications, **51**, 31.
PETTIFOR, D. G., 1985, J. Less-Common Metals, **114**, 7.
PETTIFOR, D. G., 1986a, J. Phys. C.: Solid State Phys., **19**, 285.
PETTIFOR, D. G., 1986b, New Scientist, May **29**, 48.
PETTIFOR, D. G., 1988a, Physica B, **149**, 3.
PETTIFOR, D. G., 1988b, Materials Science and Technology, **4**, 675.
PETZOW, G., EFFENBERG, G. (Editors), 1988 *et seq.*, "Ternary Alloys. A Comprehensive Compendium of Evaluated Constitutional Data and Phase Diagrams", (VCH, Weinheim-Germany).
PRINCE, A., 1991, "Aluminium-Copper-Nickel" in: "Ternary Alloys. A Comprehensive Compendium of Evaluated Constitutional Data and Phase Diagrams", Vol. 4, G. Petzow and G. Effenberg (Eds), (VCH, Weinheim-Germany).
RAGHAVAN, V., ANTIA, D. P., 1994, J. Phase Equilibria, **15**, 42.
RAJASEKHARAN, T., GIRGIS, K., 1983, Physical Review B, **27**, 910.
REEHUIS, M., JEITSCHKO, W., MÖLLER, M. H., BROWN, P. J., 1992, J. Phys. Chem. Solids, **53**, 687.
REIJERS, H. T. J., SABOUNGI, M. -L., PRICE, D. L., VAN DER LUGT, W., 1990, Phys. Rev., **B41**, 5661. J.
RODGERS, J. R., VILLARS, P., 1993, J. Alloys and Compounds, **197**, 167.
ROGL, P., 1984, in : "Handbook on the Physics and Chemistry of Rare Earths", Vol. 6: Gschneidner, K. A., Jr., Eyring L. (Eds.), (North-Holland, Amsterdam), p. 335.
ROGL, P., 1985, J. Less-Common Metals, **110**, 283.
ROGL, P., 1991, in: "Inorganic Reactions and Methods", A. Hagen, Ed., Vol. 13, (VCH-Publishers, New-York), p. 85.
ROSSI, D., MARAZZA, R., FERRO, R., 1979, J. Less-Common Metals, **66**, P17.
SACCONE, A., DELFINO, S., FERRO, R., 1990, CALPHAD, **14**, 151.
SACCONE, A., MACCIÓ, D., DELFINO, S., FERRO, R., 1995, J. Alloys and Compounds, **220**, 161.
SAMSON, S., 1967, Acta Cryst., **23**, 586.
SAMSON, S., 1969, in: "Development in the Structural Chemistry of Alloy Phases": Giessen, B. C. (ed.), (Plenum Press, New York), p. 65.
SAVITSKII, E. M., GRIBULYA, V. B., KISELYOVA, N. N., 1980, J. Less-Common Metals, **72**, 307.
SCHUBERT, K., 1964, "Kristallstrukturen zweikomponentiger Phasen", (Springer-Verlag, Berlin).
SCHWOMMA, O., NOWOTNY, H., WITTMANN, A., 1964a, Monatsh. Chemie, **95**, 1538.
SCHWOMMA, O., PREISINGER, A., NOWOTNY, H., WITTMANN, A., 1964b, Monatsh. Chemie, **95**, 1527.
SERENI, J. G., 1984, J. Phys. Chem. Solids, **45**, 1219.
SHOEMAKER, C. B., SHOEMAKER, D. P., 1969, in: "Development in the Structural Chemistry of Alloy Phases": Giessen, B. C. (ed.), (Plenum Press, New York), p. 107.
SHUNK, F. A., 1969, "Constitution of Binary Alloys", Second Supplement, (McGraw-Hill Book Company, New York).
SIMON, A., 1983, Angew. Chem. Int. Ed. Engl., **22**, 95.
SINGH, R. N., SOMMER, F., 1992, Z. Metallkd., **83**, 533.

SOMMER, F., 1982, Z. Metallkd., **73**, 77.
SOMMER, F., PREDEL, B., BORZONE, G., PARODI, N., FERRO, R., 1995, Intermetallics, **3**, 15.
SUNDMAN, B., JANSSON, B., ANDERSSON, J. -O., 1985, CALPHAD, **9**, 153.
SZYTULA, A., 1992, J. Alloys and Compounds, **178**, 1.
TEATUM, E. T., GSCHNEIDNER, K. A., Jr., WABER, J. T., 1968, "Compilation of Calculated Data Useful in Predicting Metallurgical Behavior of the Elements in Binary Alloy Systems", Report LA-4003, UC-25, Metals, Ceramics and Materials, TID-4500, Los Alamos Scientific Laboratory.
VAN DER LUGT, W., GEERTSMA, W., 1984, Proc. LAM V, 187.
VAN VUCHT, J. H. N., BUSCHOW, K. H. J., 1965, J. Less-Common Metals, **10**, 98.
VASSILIEV, V., GAMBINO, M., BROS, J.P., BORZONE, G., CACCIAMANI, G., FERRO, R., 1993, J. Phase Equilibria, **14**, 142.
VEGARD, L., 1921, Z. Phys., **5**, 17.
VILLARS, P., 1983, J. Less-Common Metals, **92**, 215.
VILLARS, P., 1985, J. Less-Common Metals, **109**, 93.
VILLARS, P., CALVERT, L. D., 1985, "Pearson's Handbook of Crystallographic Data for Intermetallic Phases", Vol 1–3, 1st Edition, (Materials Park, Oh 44073: American Society for Metals).
VILLARS, P., CALVERT, L. D., 1991, "Pearson's Handbook of Crystallographic Data for Intermetallic Phases", Vol. 1–4, 2nd Edition, (Materials Park, Oh 44073: American Society for Metals).
VILLARS, P., DAAMS, J. L. C., 1993, J. Alloys and Compounds, **197**, 177.
VILLARS, P., GIRGIS, K., 1982, Z. Metallkd., **73**, 455.
VILLARS, P., HULLIGER, F., 1987, J. Less-Common Metals, **132**, 289.
VILLARS, P., MATHIS, K., HULLIGER, F., 1989 in: "The Structures of Binary Compounds. Cohesion and Structure", Vol. 2: de Boer, F. R., Pettifor, D. G. (Eds.), (North-Holland, Amsterdam), p. 1.
WELLS, A. F., 1970, "Models in Structural Inorganic Chemistry", (Oxford University Press, London).
WENSKI, G., MEWIS, A., 1986, Z. Anorg. Allg. Chem., **543**, 49.
WESTBROOK, J. H., 1977, Metall. Trans., **8A**, 1327.
WESTGREN, A. F., PHRAGMEN, G., 1926, Z. Metallkd., **18**, 279.
WONDRATSCHEK, H., JEITSCHKO, W, 1976, Acta Crystallogr. **32A**, 664.
YATSENKO, S. P., SEMYANNIKOV, A. A., SEMENOV, B. G., CHUNTONOV, K. A., 1979, J. Less-Common Metals, **64**, 185.
YATSENKO, S. P., SEMYANNIKOV, A. A., SHAKAROV, H. O., FEDOROVA, E. G., 1983, J. Less-Common Metals, **90**, 95.
ZEN, E-an, 1956, Amer. Min., **41**, 523.
ZHDANOV, G. S., 1945, C. R. Acad. Sc., USSR, **48**, 39.
ZINTL, E., WOLTERSDORF, G., 1935, Z. Elektrochem., **41**, 876.
ZIPF, G. K., 1949, "Human Behavior and the Principle of Least Effort", Addison-Wesley Press.
ZUNGER, A., 1981, in: "Structure and Bonding in Crystals", Vol. I: O'Keeffe, M. and Navrotski, A. (Eds.), Academic Press, New-York), p. 73.
ZVYAGIN, B. B., 1987, Sov. Phys. Crystallogr., **32(3)**, 394.
ZVYAGIN, B. B., 1993, Sov. Phys. Crystallogr. Rep., **38**, 54.

Note: A very recent publication (Intermetallic Compounds — Principles and Practice, eds. J. H. Westbrook and R. L. Fleischer, Wiley, Chichester, 1995) includes a group of ten substantial chapters devoted to the crystal structures and crystal chemistry of intermetallic compounds and phases (Vol. 1, pages 225–491). A large collection of data has been reported in the "Handbook of Ternary Alloy Phase Diagrams", by P. Villars, A. Prince and H. Okamoto (Ten-Volume Set, ASM International, 1995): binary and ternary crystallographic data are included with ternary diagrams.

APPENDIX TO CHAPTER 4

THE STRUCTURE OF QUASICRYSTALS

WALTER STEURER

Institute of Crystallography
ETH-Zentrum, CH-8092 Zürich
Switzerland

R. W. Cahn and P. Haasen†, eds.
Physical Metallurgy; fourth, revised and enhanced edition

1. Introduction

The first years of quasicrystal structure analysis were marked by the investigation of badly characterized samples with non-crystallographic diffraction symmetry, called "quasicrystals" for short, with spectroscopic and powder diffraction techniques. It was

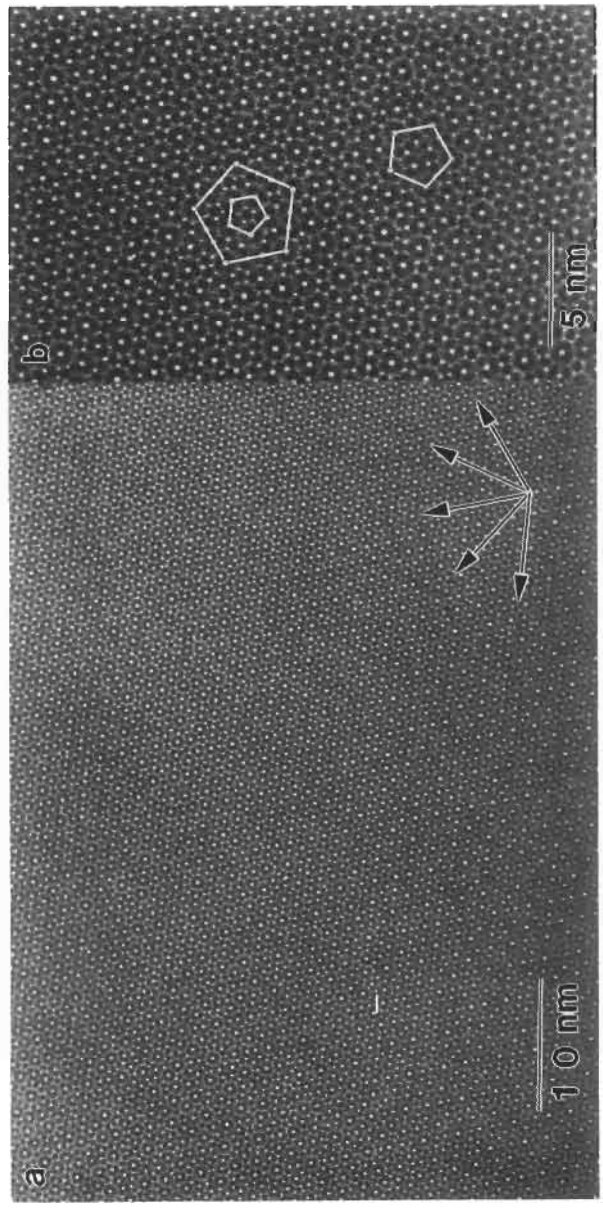

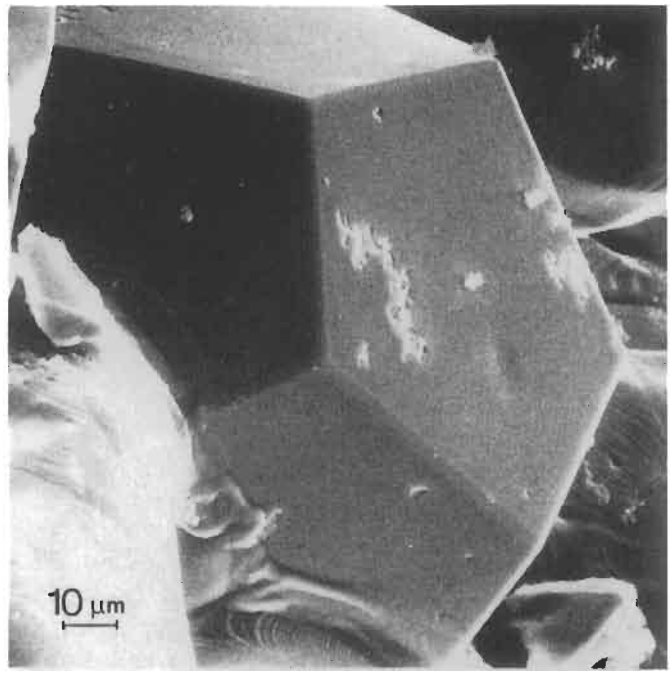

(c)

Fig. A1. (a) HRTEM image of perfectly ordered icosahedral $Al_{65}Cu_{20}Fe_{15}$ with enlarged part in (b) (from HIRAGA, ZHANG, HIRABAYASHI, INOUE and MASUMOTO [1988], and (c) REM photograph of a single crystal with pentagon-dodecahedral morphology (from TSAI, INOUE and MASUMOTO [1987].

not at all clear whether these samples were homogenous and quasiperiodically ordered (fig. A1), whether they were twinned approximants (fig. A2), i.e. closely related structures with huge unit cells, or had rather a kind of complicated crystalline nano-domain structure. The generalization of models based on single experimental results caused confusion in many cases until investigation learnt that the experimental findings were strongly dependent on chemical composition, thermal history and growth conditions of the samples. It turned out that most stable quasicrystals transform to crystalline phases at lower temperature or higher pressure running through intermediate states with sometimes complicated modulated and/or nanodomain structures. Some structural principles of quasicrystals and their relationships to approximants are now fairly well understood: both the quasiperiodic and periodic related structures are built from the same clusters. Whether the structural units order periodically or quasiperiodically can be influenced by slight changes in composition for stable samples and also by the annealing conditions for metastable ones.

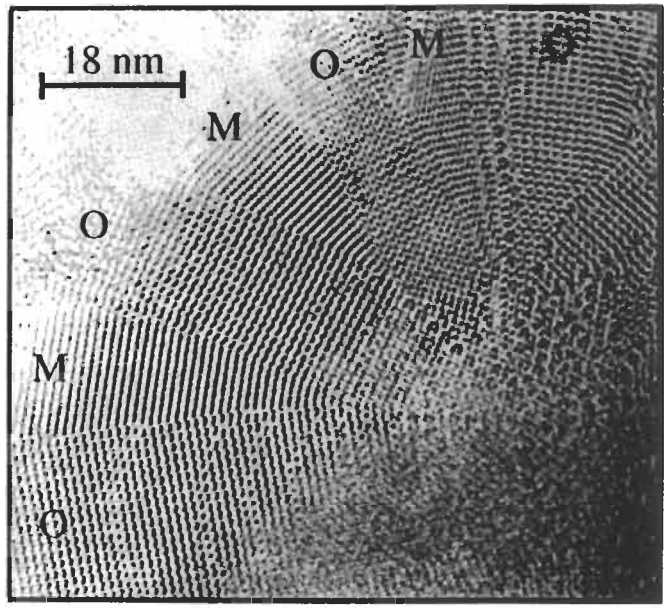

Fig. A2. Twinned $Al_{11}Mn_4$–Pd approximant with pseudo-tenfold diffraction symmetry. O and M mark the orthorhombic, and monoclinic phases, respectively (from DAULTON and KELTON [1993]).

2. *Description of quasiperiodic structures*

Regular crystal structures can be characterized by the dimensions of the unit cell, the space group, and the information what atoms occupy which Wyckoff position (cf. chapter 1 of this volume). The space group includes the information about the crystal system, the Bravais lattice type, atomic coordinates and site symmetries. A comparable description for quasiperiodic structures is possible in terms of the higher-dimensional approach (JANSSEN [1986]). Another way is the structure description by a quasilattice (quasiperiodic tiling) with two or more different unit cells, its symmetry and decoration with atomic clusters.

2.1. Decoration of quasiperiodic tilings

The classical example of a quasiperiodic tiling with five-fold orientational symmetry is the Penrose tiling (PT) (fig. A3). It can be constructed by two types of unit cells, a fat rhomb (72° and 108° angles) and a skinny rhomb (36° and 144° angles) with edge lengths all equal to a_r, and areas in the ratio τ:1, like their frequencies in the tiling. The irrational number τ, related to the golden mean, is the solution of the algebraic equation $\tau^2-\tau-1=0$, and has the value $\tau=\frac{1+\sqrt{5}}{2}=2\cos 36°=1.6180\ldots$. Since the unit tiles can also be arranged periodically or randomly, local matching rules are necessary to obtain a quasiperiodic tiling. The PT has the following characteristic properties (PAVLOVITCH and KLEMAN [1987]; LEVINE and STEINHARDT [1986]):

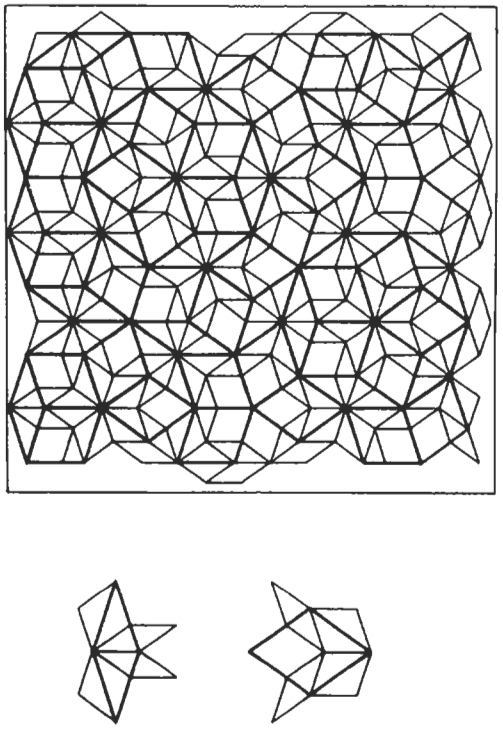

Fig. A3. Penrose tiling (bold lines) with deflated tiling drawn in (light lines). The deflation rules for the fat, and skinny rhombs are also shown in the lower part of the drawing. The edge lengths of the deflated tiles are smaller by a factor τ than the original ones (from SOCOLAR and STEINHARDT [1986]).

Quasiperiodic translational order: there is no nontrivial translation leaving the tiling invariant. The mass density function is quasiperiodic, i.e. it can be expressed as a finite sum of periodic functions with periods incommensurate to each other. For example, the function is quasiperiodic $f(x) = \cos x + \cos ax$ if a is an irrational algebraic number (i.e., an irrational solution of an equation of the type $a_n x^n + a_{n-1} x^{n-1} + ... a_o = 0$).

Orientational order: each edge of each unit tile is oriented along one of the set of orientational star axes. Except in singular cases, there is no rotational or mirror symmetry in a quasiperiodic tiling.

Indeterminacy of the construction process: the infinite pattern is not determined by a finite region. Starting from a finite region allows an uncountable infinity of ways to continue the construction. All resulting tilings belong to the same local isomorphism class and are homometric structures (i.e., have the same diffraction patterns).

Local isomorphism: any region, however large it might be, belonging to a given infinite tiling, can be found in any other different (i.e., non superposable) tiling.

References: p. 408.

Self-similarity: to any PT a different PT can be associated, whose tiles are smaller by a factor τ and which includes all the vertices of the former tiling (this operation is termed *deflation*). The local matching rules can be obtained from the deflation operation.

The Penrose tiling may serve as quasilattice for structures with two-dimensional quasiperiodicity and five-fold orientational order (decagonal phases). A three-dimensional variation of the PT, with prolate and oblate rhombohedra for unit cells (their volumes in the ratio τ:1 like their frequencies) may represent a quasilattice for the icosahedral quasicrystals (fig. A4).

In the course of a normal crystal structure analysis, the determination of the correct crystal lattice, which has to be one of the 14 Bravais lattices, never poses any problems. In the case of quasicrystal structure analysis, however, for a given diffraction symmetry an infinite number of different quasilattices are possible. Thus, the selection of the quasilattice cannot be separated from the determination of the quasicrystal structure itself. Helpful as the tiling approach may be for the understanding of the geometrical principles of a quasicrystal structure, it is not suited for performing *ab initio* structure analyses of quasicrystals. This has to be done by means of the higher-dimensional approach.

2.2. Higher-dimensional approach

Quasiperiodic structures can always be decribed as sections of higher-dimensional periodic structures (JANSSEN [1986]). Five-fold rotational symmetry, for instance, which is incompatible with three-dimensional translational order, can be a symmetry operation of a four-dimensional lattice. Thus, non-crystallographic symmetries in the three-dimensional space $\mathbb{R}^3$ can become crystallographic in $\mathbb{R}^n$ space. It is quite natural, consequently, to describe quasiperiodic structures with their non-crystallographic symmetries as periodic structures in the $\mathbb{R}^n$. For the axial quasicrystals, which are quasiperiodic in two dimensions and periodic in the third one, the five-dimensional embedding space $\mathbb{R}^5$ is necessary. The icosahedral phases can be embedded in the $\mathbb{R}^6$, and one-dimensional quasicrystals in the $\mathbb{R}^4$.

The principles of the higher-dimensional embedding method are demonstrated on the

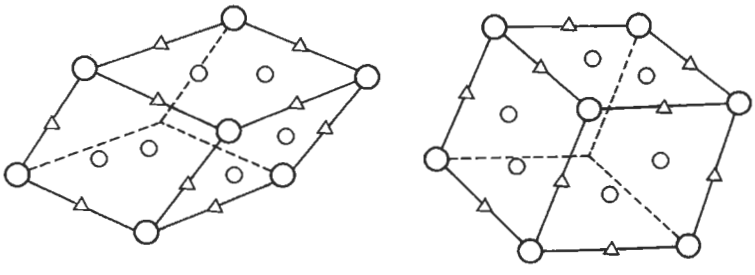

Fig. A4. Prolate (left), and oblate (right) rhombohedron, the unit tiles of the three-dimensional Penrose tiling, with special sites marked.

simple example of the one-dimensional quasiperiodic Fibonacci sequence, which can be described as a quasiperiodic section of a two-dimensional periodic lattice (fig. A5).

The Fibonacci sequence may be obtained from the substitution rule

$$\begin{pmatrix} L \\ S \end{pmatrix} \rightarrow \begin{pmatrix} 1 & 1 \\ 1 & 0 \end{pmatrix} \begin{pmatrix} L \\ S \end{pmatrix} = \begin{pmatrix} L+S \\ L \end{pmatrix},$$

where L denote 'long' and S denotes 'short'. Starting with L one obtains the sequences

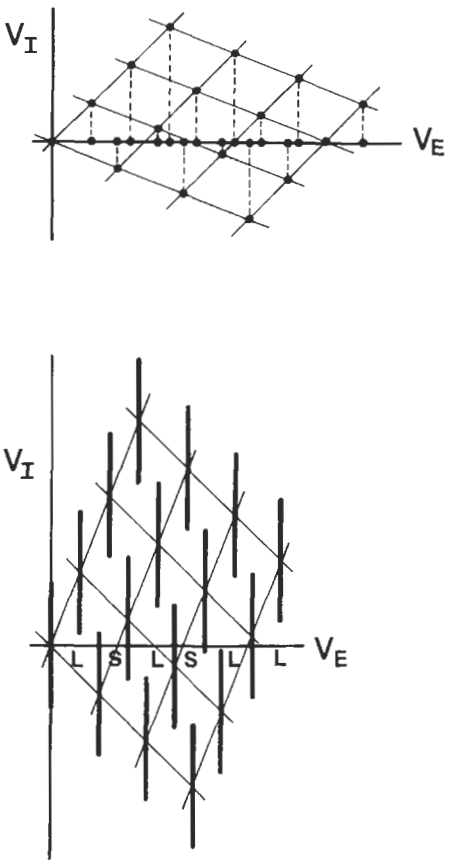

Fig. A5. Embedding of a one-dimensional quasicrystal with point atoms in the $\mathbb{R}^2$. The observed diffraction pattern of the Fibonacci sequence in the physical (external, parallel) space $\mathbf{V}_E$ corresponds to a projection of an appropriate two-dimensional reciprocal lattice down the complementary (external, perpendicular) space $\mathbf{V}_I$ (upper drawing). The quasiperiodic structure, connected via Fourier transform with reciprocal space, consequently results from a section of $\mathbf{V}_E$ with the two-dimensional hypercrystal. Since the slope of $\mathbf{V}_E$ is irrational with regard to the lattice vectors, the hyperatoms have to be extended (line-shaped) to get a non-empty intersection (lower drawing).

References: p. 408.

sequence	number of L	number of S
L	1	0
LS	1	1
LSL	2	1
LSLLS	3	2
LSLLSLSL	5	3
LSLLSLSLLSLLS	8	5
LSLLSLSLLSLLSLSLLSLSL	13	8
.	.	.
.	.	.
.	.	.
.	F_{n+1}	F_n

where $F_n = F_{n-1} + F_{n-2}$ are the Fibonacci numbers with $\lim_{n\to\infty} \frac{F_{n+1}}{F_n} = \tau$.

One finds that the substitution rule always leaves the existing sequence invariant. Thus, it corresponds to a self-similarity operation in the case of an infinite Fibonacci sequence. Replacing the letters L and S by intervals of length τ and 1 one gets, because of the relation

$$\frac{L}{S} = \frac{L+S}{L} = \tau$$

a structure invariant under scaling by a factor τ^n, n being an integer.

In fig. A6 the correlation between hyperatoms in the five-dimensional description and the actual quasiperiodic structure is illustrated on the example of decagonal $Al_{70}Co_{15}Ni_{15}$ (cf. section 3.2.2).

One big advantage of the higher-dimensional approach is that the structural information can be given in closed form. It is mainly contained in the position and shape of the hyperatoms. In terms of the tiling-decoration method, it would not be sufficient to define the type of tiling (what needs not always be possible in closed form) and the decoration of the unit tiles since, generally, the decoration can be context dependent.

2.3. Symmetry of quasicrystals

A first classification of quasicrystals, without knowing anything about their structure, can be performed by means of their diffraction symmetry. As for regular crystals, the diffraction symmetry is equivalent to the centrosymmetric point group related to the space group of the crystal structure. Experimentally observed have been phases with diffraction symmetries 8/mmm, 10/mmm, 12/mmm, and $m\bar{3}\bar{5}$ so far, called *octagonal, decagonal, dodecagonal* and *icosahedral* phases, respectively. Systematically absent reflections in the diffraction patterns (fig. A7) allow the assignment of centered lattices and symmetry elements with translation components in the higher-dimensional description.

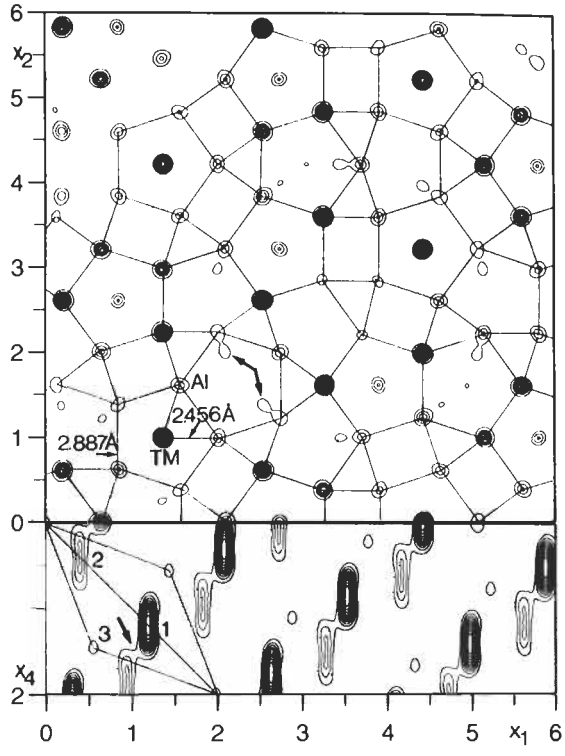

Fig. A6. Physical space electron density map (atomic structure in the (x_1, x_2)-plane) of decagonal $Al_{70}Co_{15}Ni_{15}$ with aluminum, and transition metal atoms, bond lengths, and pentagon-rectangle structure motifs marked (upper part of the drawing). In the lower part of the drawing, a section containing the perpendicular-space direction x_4 is shown to visualize the generation of real atoms from the hyperatoms marked 1, 2, and 3. The outline of one unit cell is also drawn in.

Fortunately, the number of possible superspace groups is very limited owing to the restriction that the corresponding point group has always to leave invariant the point group of the physical subspace. Thus, for the icosahedral phase, the combination of the three Bravais groups, generating the primitive (P), the body-centered (I) and the face-centered (F) hypercubic lattice, with the point groups 235 and $m\bar{3}\bar{5}$, produces only six symmorphous and five non-symmorphous superspace groups: P235, $P235_1$, I235, $I235_1$, F235, $F235_1$, $P2/m\bar{3}\bar{5}$, $P2/q\bar{3}\bar{5}$, $I2/m\bar{3}\bar{5}$, $F2/m\bar{3}\bar{5}$, $F2/q\bar{3}\bar{5}$.

3. *The structure of quasicrystals and approximants*

Depending on the preliminary character of our present knowledge of the real structure of quasicrystals, the following classification and description of quasicrystal structures may be revised in future. The fundamental relationships between quasicrystals and

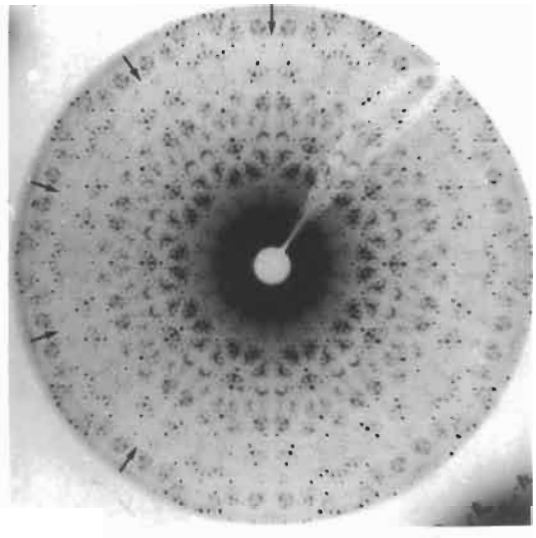

Fig. A7. First-layer X-ray precession photograph of decagonal $Al_{70.5}Mn_{16.5}Pd_{13}$ with symmetry 10/mmm. The zonal systematic extinctions (marked by arrows) obey tenfold symmetry.

*approximants** seem to be fairly reliable, however. The metastable quasicrystals mentioned in the following have all been prepared by rapid solidification methods (melt-spinning or splat-cooling); stable quasicrystals have been grown from the melt in the same way as any other metal crystals.

3.1. One-dimensional quasicrystals

There are only a few, mostly metastable phases known which are periodic in two dimensions and quasiperiodic in the third one (table A1). The structural units in these phases are ordered along one direction similarly to a Fibonacci sequence (*Fibonacci phases*). Well-studied examples are Al–Pd, Al–Cu and Al–Cu–Ni phases with basic cP2–CsCl type structure and vacancies ordered quasiperiodically along the [111] direction (CHATTOPADHYAY, LELE, THANGARAJ and RANGANATHAN [1987]). Fibonacci phases also often occur as intermediate states during the transition icosahedral ↔ crystalline or decagonal ↔ crystalline phase. Examples of the latter case were found in the systems Al–Ni–Si, Al–Co–Cu and Al–Cu–Mn (HE, LI, ZHANG and KUO [1988]; LI and KUO [1993]).

A stable one-dimensional quasicrystal as transformation product from the decagonal phase was found in a fully annealed $Al_{65}Cu_{20}Fe_{10}Mn_5$ sample. It has six-layer periodicity

* A crystalline phase with a structure closely related to that of a quasicrystal is called an *approximant*. If both structures can be transformed into each other by a rotation in superspace the crystalline phase is called a *rational approximant*.

Table A1
Systems with one-dimensional quasiperiodic (Fibonacci) phases (approximate compositions given). Stable decagonal phases are marked by a star.

GaAs–AlAs	artificial	TODD, MERLIN, CLARKE, MOHANTY and AXE [1986]
Mo–V	artificial	KARKUT, TRISCONE, ARIOSA and FISCHER [1986]
Al–Pd, Al–Cu–(Ni)		CHATTOPADHYAY, LELE, THANGARAJ and RANGANATHAN [1987]
$Al_{80}Ni_{14}Si_6$		HE, LI, ZHANG and KUO [1988]
$Al_{65}Cu_{20}Mn_{15}$		
$Al_{65}Cu_{20}Co_{15}$		
$*Al_{65}Cu_{20}Fe_{10}Mn_5$		TSAI, INOUE, MASUMOTO, SATO and YAMAMOTO [1992]
$*Al_{75}Fe_{10}Pd_{15}$		TSAI, MASUMOTO and YAMAMOTO [1992]

along the original tenfold axis and eight-layer periodicity perpendicular to it (TSAI, INOUE, MASUMOTO, SATO and YAMAMOTO [1992]). Another one was prepared from slowly cooled $Al_{75}Pd_{15}Fe_{10}$ (TSAI, MATSUMOTO and YAMAMOTO [1992]). Its structure can be derived from a decagonal quasicrystal by introducing a finite linear phason strain.*

By means of molecular beam epitaxy, Fibonacci phases were constructed from GaAs and AlAs layers (TODD, MERLIN, CLARKE, MOHANTY and AXE [1986]), as well as from Mo and V layers (KARKUT, TRISCONE, ARIOSA and FISCHER [1986]), in order to study their physical properties.

3.2. Two-dimensional quasicrystals

Two-dimensional quasicrystals consist of quasiperiodically ordered atomic layers which are stacked periodically. They combine the structural characteristics of both quasicrystals and regular crystals in one and the same sample. According to their diffraction symmetry octagonal, decagonal and dodecagonal quasicrystals are known so far.

3.2.1. Octagonal phases

The known octagonal phases (table A2) are all metastable and closely related to the cP20–βMn type, whose lattice parameter, $a = 6.315$ Å, is preserved along the translationally periodic direction of the quasiperiodic phases (fig. A8).

* A strain field introduced parallel to the perpendicular space is called a *phason-strain field.* In the case of a uniform shift of the hyperatoms along the perpendicular space coordinates one gets a *linear phason-strain field.* This is equivalent to rotating the hypercrystal relative to to the parallel space, producing a rational approximant.

Table A2
Systems with octagonal phases (approximate compositions given). In the second column the translation period along the eight-fold axis is given.

$Ni_{10}SiV_{15}$	6.3Å	WANG, CHEN and KUO [1987]
$Cr_5Ni_3Si_2$	6.3Å	
Mn_4Si	6.2Å	CAO, YE and KUO [1988]
$Al_3Mn_{82}Si_{15}$	6.2Å	WANG, FUNG and KUO [1988]
Fe–Mn–Si		WANG and KUO [1988]

3.2.2. Decagonal phases

Decagonal phases (table A3) are built in many cases from quasiperiodically packed columnar clusters with eigensymmetry $10_5/mmc$ or 10_5mc. The clusters are periodic along their tenfold axes, their translation periods can be ~4 Å, ~8 Å, ~12 Å, ~16 Å, ~24 Å and ~36 Å corresponding to stackings of 2, 4, 6, 8, 12 and 18 flat or puckered atomic layers. All decagonal phases have needle-like decaprismatic crystal morphology, indicating preferred crystal growth along the periodic direction (fig. A9).

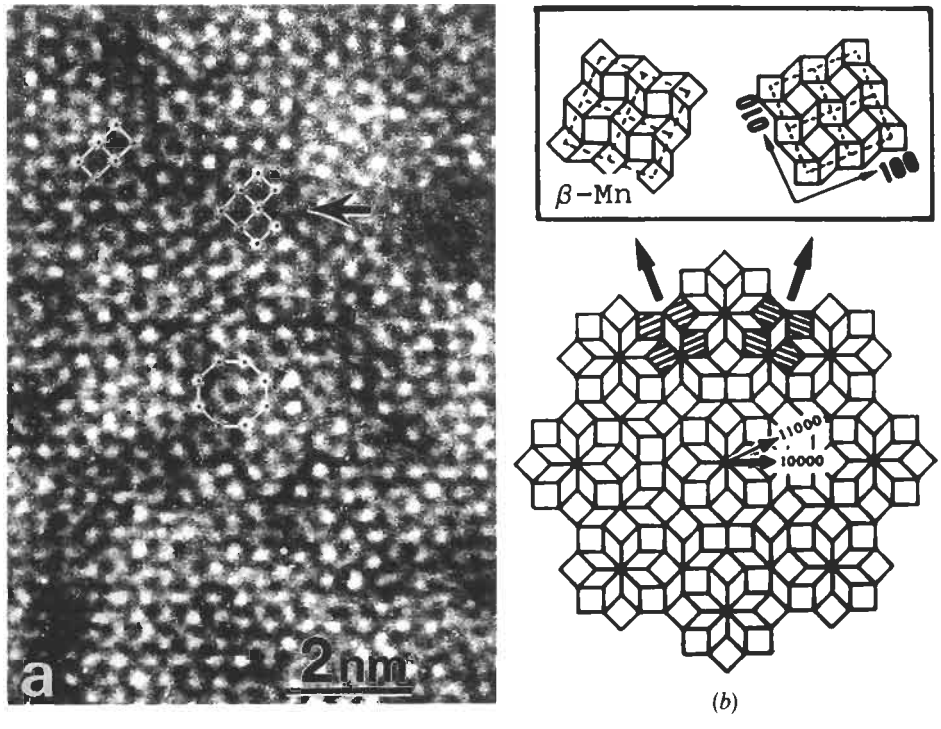

Fig. A8. (a) HRTEM image taken from octagonal Cr–Ni–Si. Nuclei of the β-Mn structure are marked by an arrow. (b) A tiling model of the octagonal phase with β-Mn structure units (hatched) indicated (from WANG and KUO [1990]).

Table A3

Systems with decagonal phases (approximate compositions given). In the second column the translation period along the tenfold axis is given. In the third column the closely related crystalline phase (approximant) is listed. Stable decagonal phases are marked by stars.

*$Al_{65}Co_{15}Cu_{20}$	4 Å	$Al_{13}Co_4$	STEURER and KUO [1990]
*$Al_{70}Co_{15}Ni_{15}$	4 Å	$Al_{13}Co_4$	STEURER, HAIBACH, ZHANG, KEK and LÜCK [1993]
*$Al_{70}Ni_{15}Rh_{15}$	4 Å	$Al_{13}Co_4$	TSAI, INOUE and MASUMTO [1989]
*$Al_{65}Cu_{15}Rh_{20}$	4 Å	$Al_{13}Co_4$	
*$Al_{71}Fe_5Ni_{24}$	4 Å	$Al_{13}Co_4$	LEMMERZ, GRUSHKO, FREIBURG and JANSEN [1994]
$Al_{75}Cu_{10}Ni_{15}$	4 Å		ZHANG and KUO [1989]
Al_4Ni	4 Å		LI and KUO [1988]
$Fe_{52}Nb_{18}$	4 Å	Zr_4Al_3	HE, YANG and YE [1990]
*$Al_{10}Co_4$	8Å	$Al_{13}Co_4$	MA and KUO [1994]
Al_4Mn	12 Å	μ-Al_4Mn	STEURER [1991]
$Al_{79}Fe_{2.6}Mn_{19.4}$	12 Å		MA and STERN [1987]
*$Al_{70.5}Mn_{16.5}Pd_{13.5}$	12 Å	μ-Al_4Mn	STEURER, HAIBACH, ZHANG, BEELI and NISSEN [1994]
Al–Cr(Si)	12 Å	$Al_{45}Cr_7$	KUO [1987]
$Al_{65}Cu_{20}Mn_{15}$	12 Å	$Al_{11}Mn_4$	HE, WU and KUO [1988]
$Al_{65}Cu_{20}Fe_{15}$	12 Å	$Al_{13}Fe_4$	
$Al_{65}Cr_7Cu_{20}Fe_8$	12 Å	$Al_{13}Fe_4$	LIU, KÖSTER, MÜLLER and ROSENBERG [1992]
Al_5Ir	16 Å	Al_3Ir	MA, WANG and KUO [1988]
Al_5Pd	16 Å	Al_3Pd	
Al_5Pt	16 Å	Al_3Pt	
Al_5Os	16 Å	$Al_{13}Os_4$	KUO [1987]
Al_5Ru	16 Å	$Al_{13}Ru_4$	BANCEL, HEINEY, STEPHENS, GOLDMAN and HORN [1985]
Al_5Rh	16 Å	Al_9Rh_2	WANG and KUO [1988]
Al_4Fe	16 Å	$Al_{13}Fe_4$	FUNG, YANG, ZHOU, ZHAO, ZHAN and SHEN [1986]
$Al_{74}Mg_5Pd_{21}$	16 Å	Al_3Pd	KOSHIKAWA, EDAGAWA, HONDA and TAKEUCHI [1993]
*$Al_{80}Fe_{10}Pd_{10}$	16 Å	$Al_{13}Fe_4$	TSAI, INOUE and MASUMOTO [1991]
*$Al_{80}Ru_{10}Pd_{10}$	16 Å	$Al_{13}Fe_4$	
*$Al_{80}Os_{10}Pd_{10}$	16 Å	$Al_{13}Fe_4$	
$Al_6Ni(Si)$	16 Å	$Al_9(Ni, Si)_2$	LI and KUO [1988, 1993]
$Al_{72}Cr_{16}Cu_{12}$	36 Å		OKABE, FURIHATA, MORISHITA and FUJIMORI [1992]

References: p. 408.

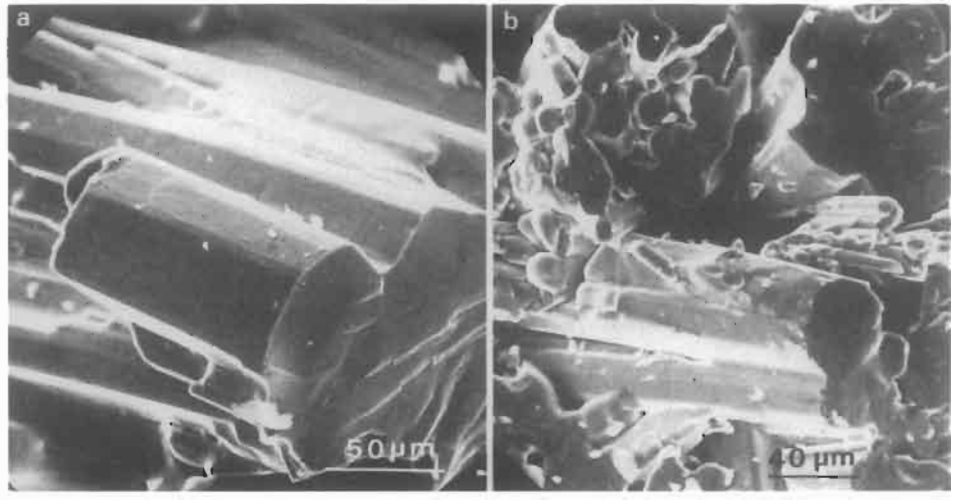

Fig. A9. Single crystals with decaprismatic growth morphology of decagonal (a) $Al_{70}Co_{15}Ni_{15}$, and (b) $Al_{65}Co_{20}Cu_{15}$ (from TSAI, INOUE and MASUMOTO [1989]).

Crystals of the decagonal phase epitaxially grown on icosahedral quasicrystals exhibit a defined orientation relationship: the tenfold axis of the decagonal phase is parallel to one of the fivefold axes of the icosahedral phase. Thus, in many cases decagonal phases can be considered as approximants of icosahedral quasicrystals. Stable decagonal phases were observed so far in the systems Al–Co–Cu (HE, ZHANG, WU and KUO [1988]), Al–Co–Ni, Al–Cu–Rh, Al–Ni–Rh (TSAI, INOUE and MASUMOTO [1989]) and Al–Me–Pd with Me=Mn, Fe, Ru, Os (BEELI, NISSEN and ROBADEY [1991]; TSAI, INOUE and MASUMOTO [1991]). The Al–Mn–Pd system is the only one for which both stable icosahedral and decagonal phases are known.

Three different basic decagonal structure types were identified hitherto: $Al_{65}Co_{15}Cu_{20}$ and $Al_{70}Co_{15}Ni_{15}$ belong to the deca-Al–Co–Cu type, $Al_{78}Mn_{22}$, $Al_{70.5}Mn_{16.5}Pd_{13}$ and $Al_{65}Cu_{20}Cr_7Fe_8$ to the deca-Al–Mn type, $Al_{80}Fe_{10}Pd_{10}$, $Al_{80}Ru_{10}Pd_{10}$, $Al_{80}Os_{10}Pd_{10}$ and $Al_{75}Mn_5Pd_{20}$ to the deca-Al–Fe–Pd type. In all cases the most probable superspace group of the average structures is $P10_5/mmc$ (table A4).

It is remarkable that all three decagonal structure types result from different stacking sequences of only three types of layers: *A*, *B* and *C*. In all cases, similar columnar clusters are formed with interplanar bonds stronger than intraplanar ones. It is also noteworthy that the electron density maps, projected along the tenfold axis, show the respective hyperatoms all centered at the same special positions on the [11110] diagonal of the five-dimensional unit cell, as is the case for a general Penrose tiling. This means that at least a substructure of any decagonal phase shows close resemblance to a decorated Penrose tiling. For the description of the full structure, however, only a context dependent decoration is adequate.

Table A4
Selected symmetry information on the five-dimensional superspace group $P10_5/mmc$. p is an integer with $0 \le p \le 4$. Reflection condition: $h_1h_2\bar{h}_2\bar{h}_1h_5=2n$.

Multiplicity	Wyckoff position	site symmetry	coordinates
4	c	5m	$\pm$(p/5 p/5 p/5 p/5 x_5) $\pm$(p/5 p/5 p/5 p/5 $\frac{1}{2}$-x_5)
2	b	$\bar{1}0$m2	$\pm$(p/5 p/5 p/5 p/5 $\frac{1}{4}$)
2	a	$\bar{5}$m2	(0 0 0 0 0), (0 0 0 0 $\frac{1}{2}$)

Deca-Al–Co–Cu type:
For Al–Co–Cu, there exist studies on phase equilibria and transformation properties (GRUSHKO [1993]; DAULTON, KELTON, SONG and RYBA [1992]; DONG, DUBOIS, DEBOISSIEU and JANOT [1991]), on structural relationships to approximants (LIAO, KUO, ZHANG and URBAN [1992]; DONG, DUBOIS, KANG and AUDIER [1992]; DAULTON and KELTON [1992]; SONG and RYBA [1992]; KUO [1993]), on twinning and microdomain structures (SONG, WANG and RYBA [1991]; LAUNOIS, AUDIER, DENOYER, DONG, DUBOIS and LAMBERT [1990]), as well as investigations using high-resolution transmission electron microscopy (HRTEM) (REYES-GASGA, LARA, RIVEROS and JOSE-YACAMAN [1992]; HIRAGA, SUN and LINCOLN [1991]), the extended X-ray absorption fine structure (EXAFS) technique (DONG, LU, YANG and SHAN [1991]), scanning tunneling microscopy (KORTAN, BECKER, THIEL and CHEN [1990]), or fast-ion channeling (PLACHKE, KUPKE, CARSTANJEN and EMRICK [1993]). For Al–Co–Ni the stability range between 500° C and the melting point was investigated (KEK [1991]), and a wealth of HRTEM and electron diffraction studies of the decagonal phase in comparison with its approximant phases was performed (e.g., HIRAGA, LINCOLN and SUN [1991]; EDAGAWA, ICHIHARA, SUZUKI and TAKEUCHI [1992]). Also a large number of theoretical studies have been published dealing with structure modelling or tiling decoration to understand the rules governing the formation of quasiperiodic phases (HENLEY [1993]; ROMEU [1993]; WIDOM and PHILLIPS [1993]; KANG and DUBOIS [1992]; BURKOV [1991]; BURKOV [1992]).

From the results of the five-dimensional single crystal X-ray structure analyses of decagonal $Al_{65}Co_{15}Cu_{20}$ (STEURER and KUO [1990]) and $Al_{70}Co_{15}Ni_{15}$ (STEURER, HAIBACH, ZHANG, KEK and LÜCK [1993]), the following characteristics of the deca-Al-Co–Cu structure type can be derived:

(1) Two-layer structure with approximate translation period 4 Å. There are two planar layers stacked with sequence *Aa* (*a* means *A* rotated around 36° under the action of the 10_5–screw axis). At lower temperature a disordered superstructure doubling the translation period is observed.
(2) There are two hyperatoms per asymmetric unit on the special Wyckoff position (b): one with p = 2 consisting mainly of transition metal (marked 1), and one with p = 4 (marked 2) consisting of Al atoms (fig. A10).

References: p. 408.

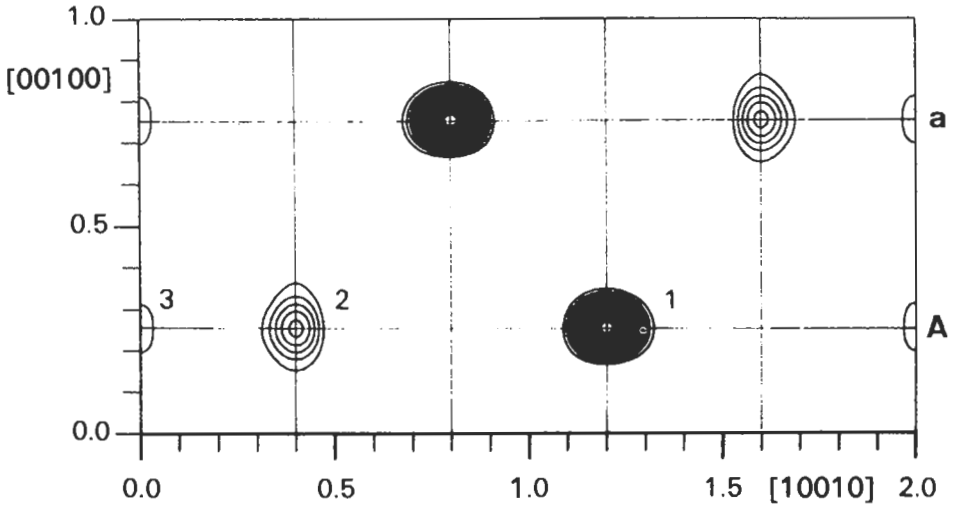

Fig. A10. Characteristic (10110) section of the five-dimensional electron density of decagonal $Al_{70}Co_{15}Ni_{15}$. The hyperatoms 1, and 2 generate an atomic layer A separated by ≈2 Å from the symmetrically equivalent layer a generated by the 10_5–screw axis which is parallel to [00100].

(3) Shape and chemical composition of the hyperatoms are roughly compatible with tiling models like the binary tiling model (BURKOV [1991]), for instance.

(4) Columnar clusters (Ø ≈ 20 Å) with eigensymmetry 10_5/mmc can be identified as basic structural units (fig. A11). Their cross sections can be described as parts of a Penrose tiling with edge lengths $a_r \approx 2.5$ Å. The unit rhombs are decorated by atoms on the vertices and in some cases on the diagonals.

(5) The global structure can be described as a rhombic tiling with unit tiles of edge length $a_r \approx 20$ Å (equivalent to the distance between two ≈ 20 Å columnar clusters), decorated by the columnar clusters at the vertices and at one position on the long diagonal of the fat rhomb (fig. A12).

(6) The formation of a network of icosagonal rings of pentagonal and rectangular structure motifs may act as weak matching rule stabilizing quasiperiodic tilings (fig. A13).

(7) A closely related approximant structure is that of monoclinic $Al_{13}Co_4$ (HUDD and TAYLOR [1962]; BARBIER, TAMURA and VERGER-GAUGRY [1993]). It contains locally similar structure motifs (pentagon-rectangle strips) which are arranged in a different way (wavy bands instead of icosagons), however (fig. A14).

Deca-Al–Mn type:

Decagonal $Al_{78}Mn_{22}$, $Al_{70.5}Mn_{16.5}Pd_{13}$ and $Al_{65}Cu_{20}Cr_7Fe_8$ are representatives of the deca-Al–Mn type with ~ 12 Å translational period. Stable decagonal $Al_{70.5}Mn_{16.5}Pd_{13}$, may be considered as Pd-stabilized $Al_{78}Mn_{22}$. There exist several HRTEM (BEELI, NISSEN and ROBADEY [1991]; HIRAGA, SUN, LINCOLN, KANEKO and MATSUO [1991]; HIRAGA and

SUN [1993]; BEELI and NISSEN [1993]) and X-ray diffraction investigations (FREY and STEURER [1993]; STEURER, HAIBACH, ZHANG, BEELI and NISSEN [1994]) and also structure determinations of the approximants Al_3Mn (HIRAGA, KANEKO, MATSUO and HASHIMOTO [1993]) and μ-$Al_{4.12}Mn$ (SHOEMAKER [1993]). Stable decagonal $Al_{65}Cu_{20}Cr_7Fe_8$, i.e., Fe-stabilized metastable (?) $Al_{65}Cu_{20}Cr_{15}$, and its approximants were studied by (LIU, KÖSTER,

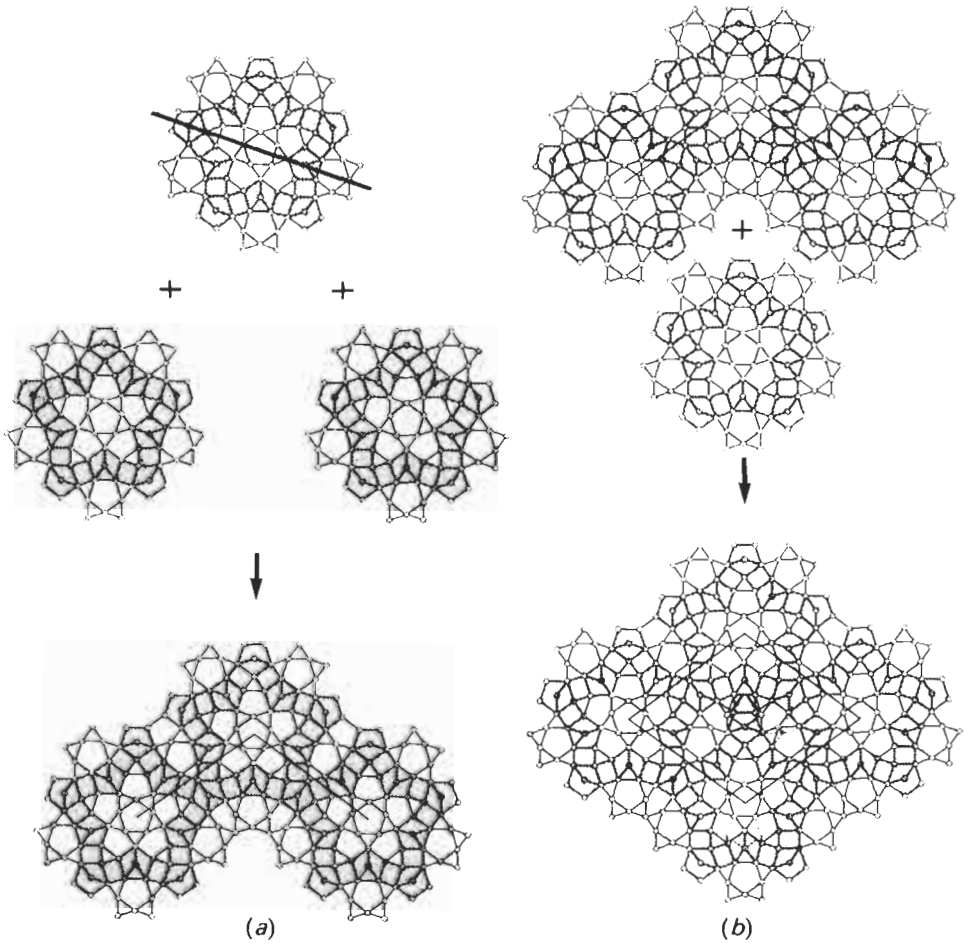

(*a*) (*b*)

References: p. 408.

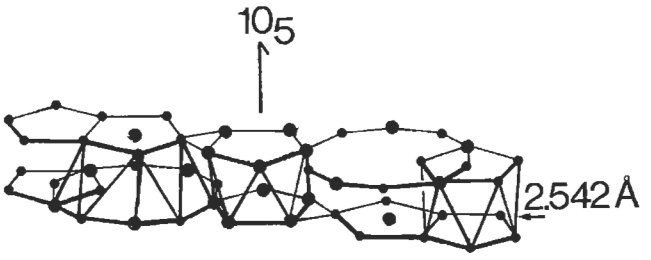

Fig. A11. (a), and (b): Schematic drawings illustrating how the ≈ 20 Å columnar clusters (shown in sections) agglomerate to a fat decorated Penrose unit rhomb. (c) Stacking principle of the layers *A* and *a* along the line drawn in the uppermost section of (a).

MÜLLER and ROSENBERG [1992]; KANG, DUBOIS, MALAMAN and VENTURINI [1992]).

The X-ray single-crystal structure analyses of $Al_{78}Mn_{22}$ (STEURER [1991]) and $Al_{70.5}Mn_{16.5}Pd_{13}$ (STEURER, HAIBACH, ZHANG, BEELI and NISSEN [1994]) allow the characterization of the deca-Al–Mn type in the following way:

(1) Six-layer structure with approximate translation period 12 Å. One puckered (±0.3 Å) layer *A* (related to the layer *a* of the deca-Al–Co–Cu type) and one planar layer *B* are stacked with sequence *ABAaba*.

(2) Four hyperatoms per asymmetric unit: two on the Wyckoff position (c); one with $p=1$, $x_5=0.063$ (marked 1), consisting in its core region of transition metal (TM) and in its remaining part of Al, and one with $p=3$, $x_5=0.113$ (marked 2), consisting of Al. Two further hyperatoms are located on Wyckoff position (b), one with $p=0$ (marked 4), consisting mainly of Al, and one with $p=3$ (marked 5), of similar chemical composition as hyperatom 1 (fig. A15).

(3) Shape and chemical composition of the hyperatoms are roughly compatible with tiling models such as the triangular tiling model (BURKOV [1992]; WELBERRY [1989]), for instance.

(4) Columnar clusters (diameter ≈ 20 Å) with point symmetry 10_5/mmc can be identified as basic structural units. Their cross sections can be described as sections of a Penrose tiling with edge lengths $a_r \approx 2.5$ Å of the unit rhombs (fig. A16).

(5) The global structure can be described as a random Robinson-triangle tiling with unit tiles of edge lengths $S \approx 20$ Å, and $L = \tau S$, decorated by the columnar clusters on the vertices (fig. A17).

(6) The decagonal phase shows close resemblance to the respective icosahedral phase, orthorhombic Al_3Mn (HIRAGA, KANEKO, MATSUO and HASHIMOTO [1993]), and hexagonal μ-$Al_{4.12}Mn$ (SHOEMAKER [1993]), which has nearly all Mn atoms icosahedrally coordinated.

(7) Contrary to the phases with deca-Al–Co–Cu type, those with deca-Al–Mn type show icosahedral pseudosymmetry and can be considered as rational approximants of icosahedral quasicrystals. There is also a larger amount of Mackay icosahedra (MI) or fragments of MI present in this structure type than in the other decagonal ones.

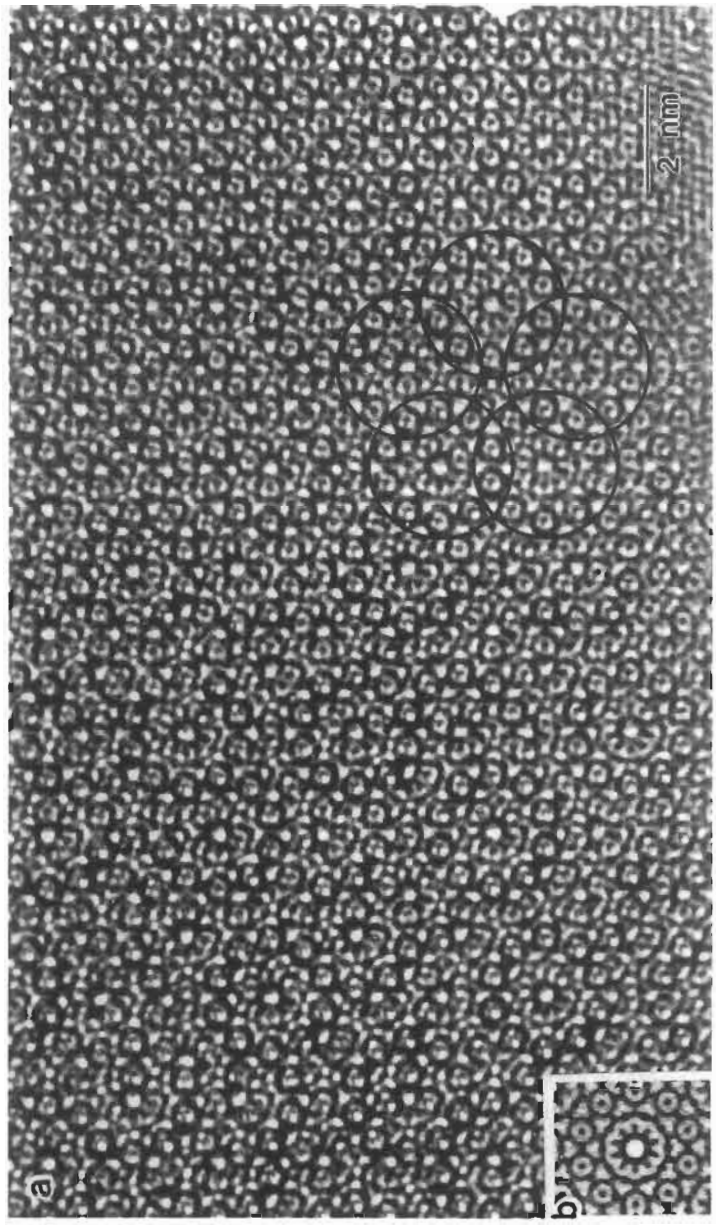

Fig. A12. (a) HRTEM image of decagonal $Al_{70}Co_{15}Ni_{15}$ (b) simulation image calculated from the 20 Å columnar cluster (from HIRAGA [1992]).

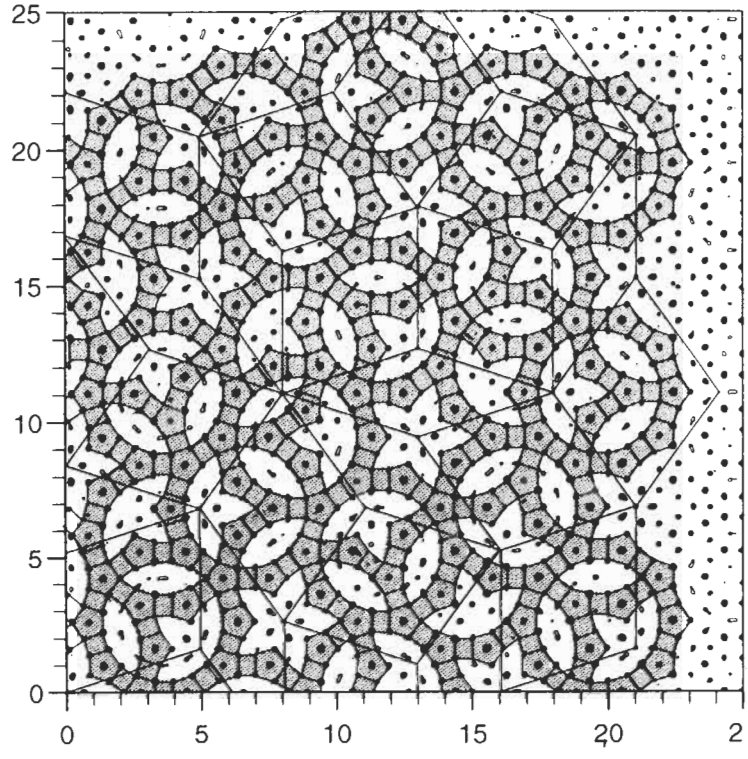

Fig. A13. Parallel space section with Penrose tiling from the type of $a_r \approx 20$ Å rhombs shown in fig. A11 indicated. The pentagonal and rectangular structure motifs form a network of interconnected icosagons.

Deca-Al–Fe–Pd type:

The stable decagonal phases $Al_{80}Fe_{10}Pd_{10}$, $Al_{80}Ru_{10}Pd_{10}$, $Al_{80}Os_{10}Pd_{10}$ (TSAI, INOUE and MASUMOTO [1991]) and $Al_{75}Mn_5Pd_{20}$ (TSAI, YOKOYAMA, INOUE and MASUMOTO [1991]) belong to the deca-Al–Fe–Pd type with 16 Å translational periodicity. $Al_{80}Fe_{10}Pd_{10}$ is the only one of this group studied so far by X-ray single-crystal diffraction (HAIBACH, ZHANG and STEURER [1994]), electron diffraction and HRTEM (TSAI, INOUE and MASUMOTO [1993]), and also by Mössbauer spectroscopy (LAWTHER and DUNLAP [1993]). A stable one-dimensional quasiperiodic phase, a rational approximant of the decagonal phase, was also identified in the system Al–Fe–Pd (TSAI, MASUMOTO and YAMAMOTO [1992]). On the basis of early results, the deca-Al–Fe–Pd type may be characterized in the following way:

(1) Eight-layer structure with approximate translation period 16 Å. Two puckered (± 0.3 Å) layers *A* and *C*, and one planar layer *B* are stacked with sequence *CABACaba*, with *C* identical to *c*.

(2) Four hyperatoms per asymmetric unit: one on the Wyckoff position (a), one on the Wyckoff position (c) with $p = 1$, $x_5 = 0.125$, and two with $p = 0$ and 2 on (b).

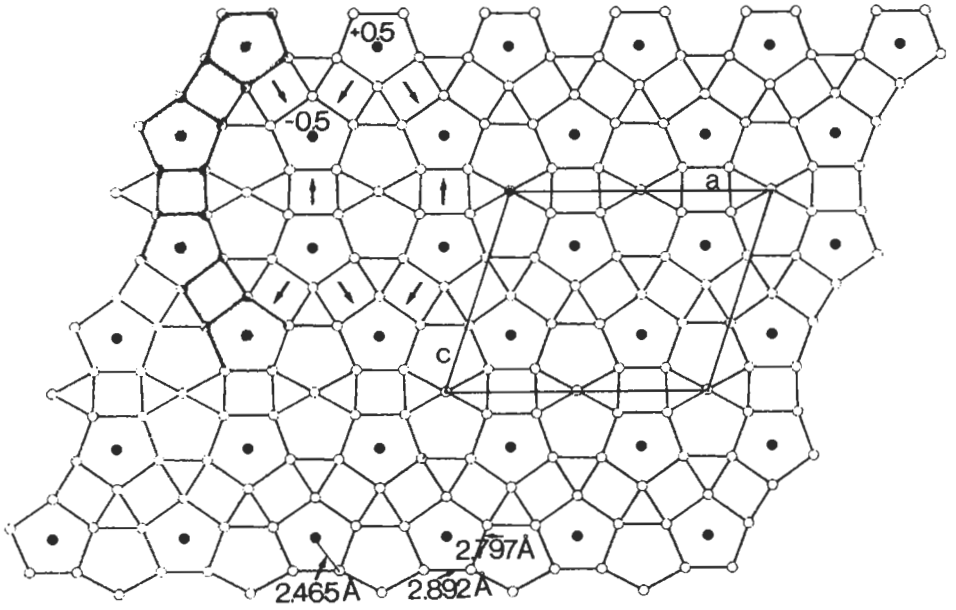

Fig. A14. Schematic drawing of the puckered atomic layer of the monoclinic approximant $Al_{13}Co_4$ with the same pentagon-rectangle strips as found in the decagonal phase. One unit cell is also drawn in.

(3) Shape and chemical composition of the hyperatoms are roughly compatible with tiling models like the binary tiling model (BURKOV [1991]), for instance.
(4) Columnar clusters ($Ø \approx 20$ Å) with point symmetry 10_5/mmc can be identified as basic structural units. Their cross sections can be described as section of a Penrose tiling with edge lengths $a_r \approx 2.5$ Å of the unit rhombs.
(4) The global structure can be described as a rhombic tiling with unit tiles of edge lengths $a_r \approx 20$ Å decorated by the columnar clusters at the vertices and at one site on the long diagonal of the fat rhombs.

3.2.3. Dodecagonal phases

Beside one, probably stable, dodecagonal Ta_xTe phase (KRUMEICH, CONRAD and HARBRECHT [1994]), only metastable dodecagonal phases are known so far (table A5). These phases are closely related to the tP30–σCrFe type phases, which are built up from hexagon-triangle and triangle-square layers (fig. A18). The c lattice parameter of the σ-phase corresponds with 4.544 Å to the translation period of the dodecagonal phases.

3.3. Icosahedral phases

The icosahedral phases discovered so far (table 6) can be grouped into two main classes (HENLEY and ELSER [1986]): the ico-Al–Mn structure type (A) with quasilattice constant $a_r \sim 4.6$ Å and free electron per atom ratio of ~ 1.75, and the ico-Al–Mg–Zn

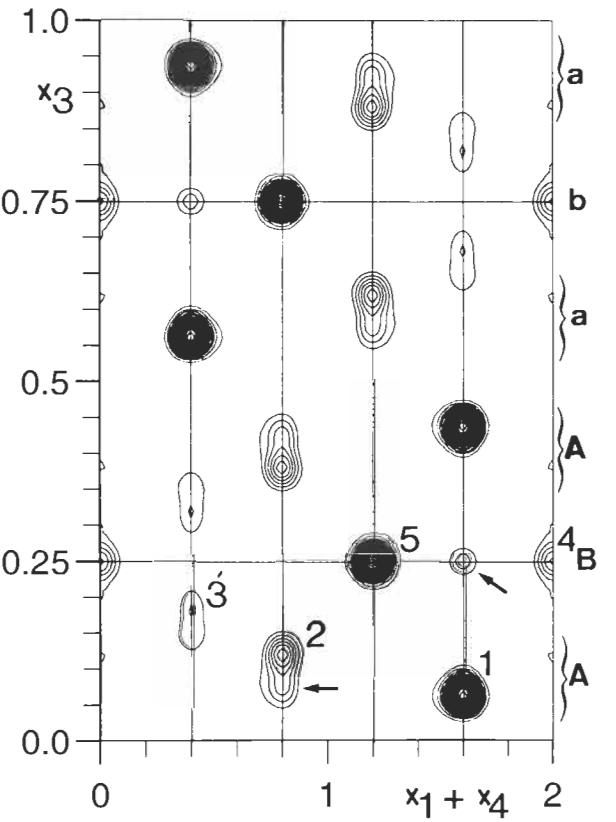

Fig. A15. Characteristic (10110) section of the five-dimensional electron density of decagonal $Al_{70.5}Mn_{16.5}Pd_{13}$. The hyperatoms create a six-layer structure *ABAaba*.

structure type (B) with $a_r \sim 5.2$ Å and free electron per atom ratio of ~ 2.1. The A type phases contain 54–atom Mackay icosahedra as structural building elements which also occur in the approximant α-Al–Mn–Si, while the B type consists of 137–atom Bergmann rhombic triacontahedra which are also typical for Frank–Kasper phases like

Table A5
Systems with dodecagonal phases (approximate compositions given). In the second column the translation period along the twelve-fold axis is given. Stable dodecagonal phases are marked by a star.

$Cr_{70.6}Ni_{29.4}$		Ishimasa, Nissen and Fukano [1985]
Ni_2V_3	4.5 Å	Chen, Li and Kuo [1988]
$Ni_{10}SiV_{15}$	4.5 Å	
*Ta_xTe	20.7 Å	Krumeich, Conrad and Harbrecht [1994]

$Mg_{32}(Al,Zn)_{42}$, for instance. The A-type icosahedral phases are mostly aluminum-transition metal compunds contrary to the B-type phases which rarely contain transition metals.

The first quasicrystal structure ever studied was that of metastable ico-Al–Mn and

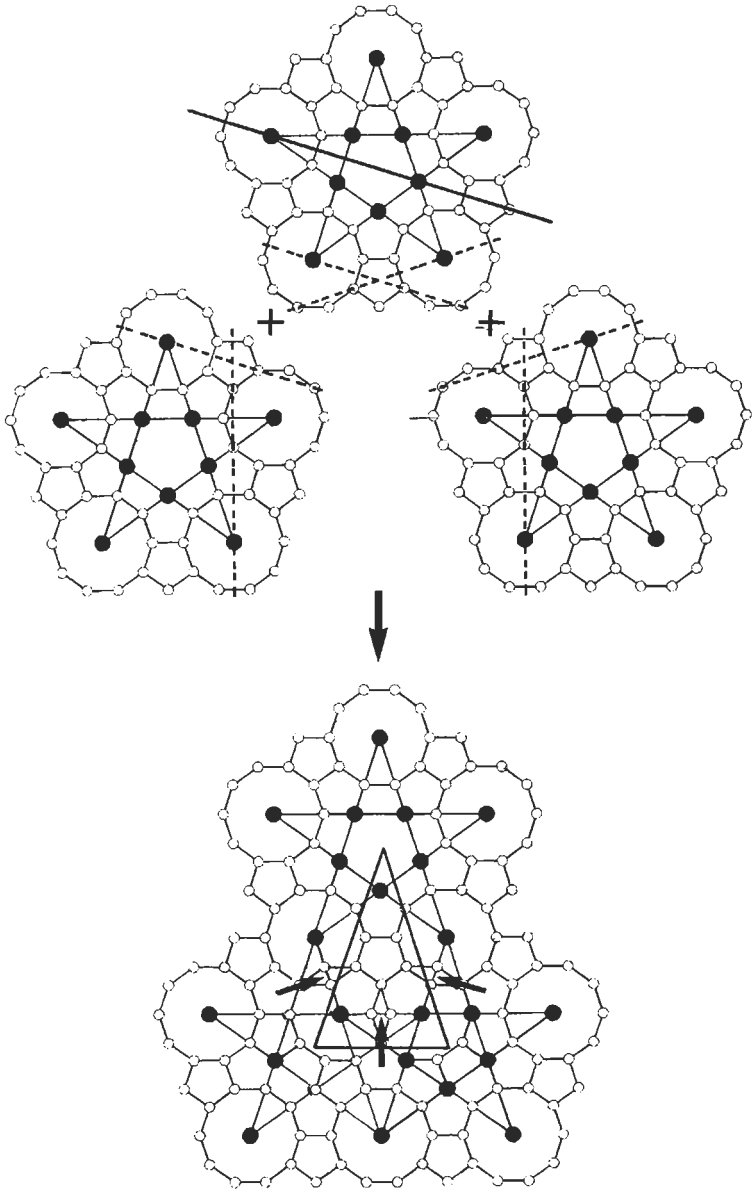

(a)

Figure continued on p. 394

isotypic, higher-quality ico-Al–Mn–Si, respectively (CAHN, GRATIAS and MOZER [1988]). Single-crystal X-ray and neutron diffraction methods became possible with the discovery of stable ico-Al–Cu–Li (DE BOISSIEU, JANOT, DUBOIS, AUDIER and DUBOST [1991]; VAN SMAALEN, DE BOER and SHEN [1991]; YAMAMOTO [1992]; QIU and JARIC [1993]) also allowing for a further developement of six-dimensional structure analytical techniques. The existence of closely related cubic α-$Al_{73}Mn_{16}Si_{11}$ (COOPER and ROBINSON [1966]) and R-Al_5CuLi_3 (AUDIER, PANNETIER, LEBLANC, JANOT, LANG and DUBOST [1988]), both rational (1,1)-approximants of the respective icosahedral phases, was very helpful for their structure analyses.

Ico-Al–Cu–Li and shortly later found stable ico-Ga–Mg–Zn (OHASHI and SPAEPEN [1987]) could both be prepared only with poor quality setting a limit for the achievable

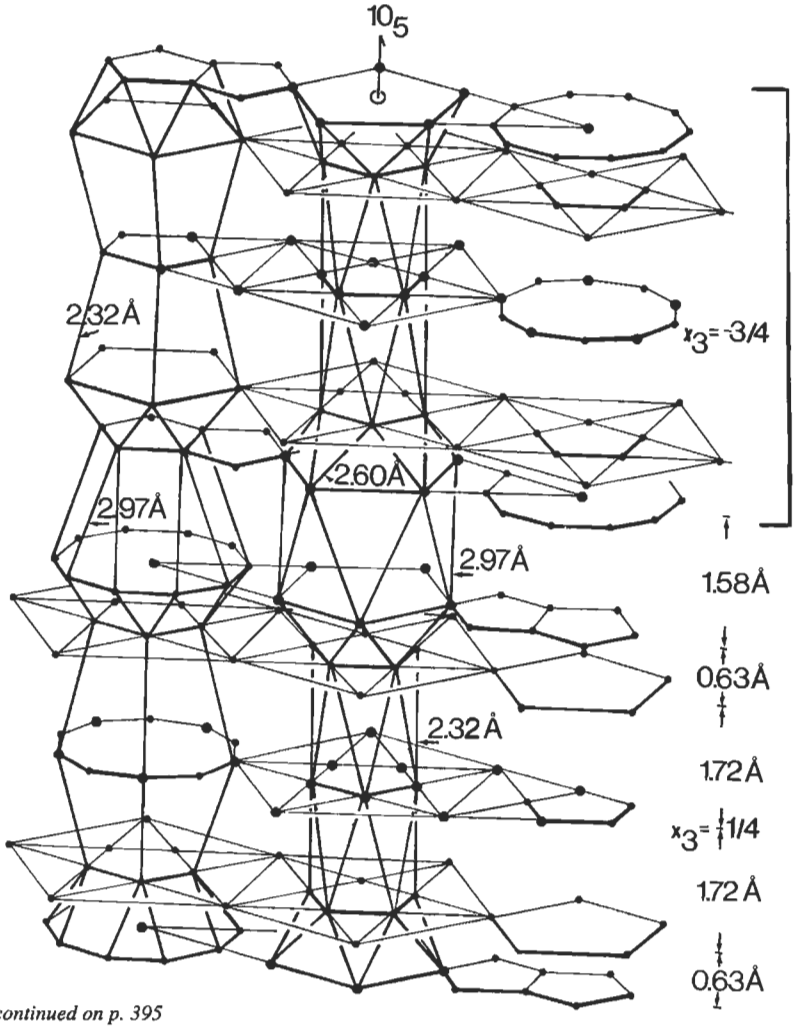

(b)

Figure continued on p. 395

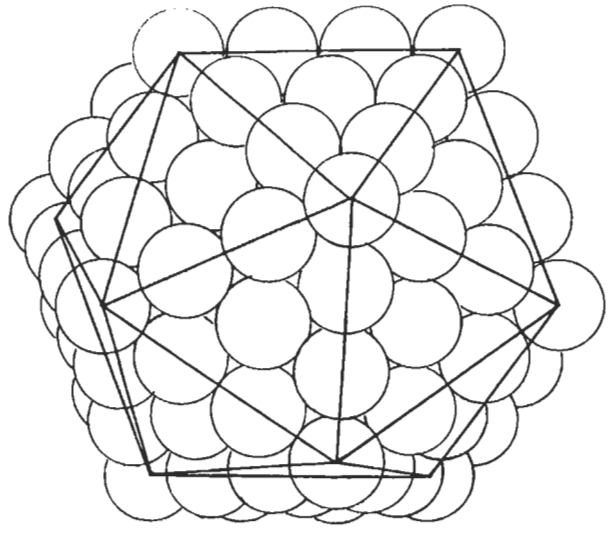

(c)

Fig. A16. (a) Schematical drawings illustrating how the ≈20 Å columnar clusters (shown in sections) agglomerate to a Robinson triangle (coincidence lines are dotted). (b) Stacking principle along the full line drawn in the uppermost section of (a). The pentagons and decagons in the right upper part marked by a bracket form one half of a 54-atom Mackay icosahedron illustrated in (c).

structural resolution. The discovery of very well ordered icosahedral quasicrystals in the systems Al–Cu–Me, with Me = Fe, Ru, Os (TSAI, INOUE and MASUMOTO [1987]; TSAI, INOUE and MASUMOTO [1988]b) and Al–Me–Pd, with Me = Mg, Mn, Re (TSAI, INOUE, YOKOYAMA and MASUMOTO [1990]; KOSHIKAWA, SAKAMOTO, EDAGAWA and TAKEUCHI [1992]) brought the turning point. During the last years, structure analyses focused on ico-Al–Cu–Fe (CORNIER-QUIQUANDON, QUIVY, LEFEBVRE, ELKAIM, HEGER, KATZ and GRATIAS [1991]; CORNIER-QUIQUANDON, BELLISENT, CALVAYRAC, CAHN, GRATIAS and MOZER [1993]) and ico-Al–Mn–Pd (BOUDARD, DEBOISSIEU, AUDIER, JANOT, HEGER, BEELI, NISSEN, VINCENT, IBBERSON and DUBOIS [1992]). In both cases, the ternary phase diagrams have been intensively investigated and the phase transitions studied (AUDIER, DURAND-CHARRE and DE BOISSIEU [1993]).

3.3.1. Primitive hypercubic icosahedral phases

Representatives of stable quasicrystals with superspace group $Pm\bar{3}\bar{5}$ are ico-$Al_{73}Mn_{21}Si_6$ (JANOT, DEBOISSIEU, DUBOIS, and PANNETIER [1989]), ico-Al_6CuLi_3 (DEBOISSIEU, JANOT, DUBOIS, AUDIER and DUBOST [1991]; YAMAMOTO [1992]), ico-$Ga_{20.4}Mg_{36.7}Zn_{42.9}$ (OHASHI and SPAEPEN [1987]) and ico-$Al_{38}Mg_{47}Pd_{15}$ (KOSHIKAWA, SAKAMOTO, EDAGAWA and TAKEUCHI [1992]). The structures of ico-$Al_{73}Mn_{21}Si_6$ and ico-Al_6CuLi_3 (fig. A19) were analysed using X-ray powder diffraction and neutron scattering techniques. Of the large number of papers dealing with other structure sensitive methods, only two HRTEM studies will be quoted (HIRAGA [1991]; NISSEN and BEELI [1993]). The results are shortly summarized as follows:

References: p. 408.

Table A6

Systems with icosahedral phases (approximate compositions given). The quasilattice constant $a_r = 1/a^*_{100000}$ is listed in the second column. The structures with face-centered hypercubic unit cells are marked by F, the ico-Al–Mn–Si structure type is labeled by A, and that of ico-(Al, Zn)–Mg by B. Stable quasicrystals are marked by asterisks.

$Al_{85}Cr_{15}$	4.65 Å		A	Zhang, Wang and Kuo [1988]
$Al_{86}Fe_{14}$			A	Bancel, Heiney, Stephens, Goldman and Horn [1985]
$Al_{86}Mn_{14}$	4.60 Å		A	Shechtman, Blech, Gratias and Cahn [1984]
Al–Mo			A	Chen, Phillips, Villars, Kortan and Inoue [1987]
$Al_{78}Re_{22}$			A	Bancel and Heiney [1986]
Al_4Ru			A	Anlage, Fultz and Krishnan [1988]
Al_4V	4.75 Å		A	Chen, Phillips, Villars, Kortan and Inoue [1987]
Al–W			A	
$Al(Cr_{1-x}Fex)$			A	Schurer, Koopmans and van der Woude [1988]
$Al(Mn_{1-x}Fe_x)$			A	
$Al_{62}Cr_{19}Si_{19}$	4.60 Å		A	Inoue, Kimura, Masumoto, Tsai and Bizen [1987]
$Al_{65}Cr_{20-x}Fe_xGe_{15}$			A	Srinivas, Dunlap, Bahadur and Dunlap [1990]
Al–Cr–Ru			A	Bancel and Heiney [1986]
$*Al_{65}Cu_{20}Cr_{15}$			A	Tsai, Inoue and Masumoto [1988a]
$*Al_{65}Cu_{20}Fe_{15}$	4.45 Å	F	A	Ebalard and Spaepen [1989]; Tsai, Inoue and Masumoto [1988d]
$Al_{65}Cu_{20}Mn_{15}$		F	A	He, Wu and Kuo [1988]
$*Al_{65}Cu_{20}Os_{15}$	4.51 Å	F	A	Tsai, Inoue and Masumoto [1988b]
$*Al_{65}Cu_{20}Ru_{15}$	4.53 Å	F	A	
$Al_{65}Cu_{20}V_{15}$	4.59 Å		A	Tsai, Inoue and Masumoto [1988a]
$Al_{70}Fe_{20}Ta_{10}$	4.55 Å		A	Tsai, Inoue and Masumoto [1988c]
$Al_{73}Mn_{21}Si_6$	4.60 Å		A	Gratias, Cahn and Mozer [1988]
$Al_{60}Mn_{20}Ge_{20}$			A	Tsai, Inoue and Masumoto [1988d]
$Al_{75.5}Mn_{17.5}Ru_4Si_3$			A	Heiney, Bancel, Goldman and Stephens [1986]
$Al_{74}Mn_{17.6}Fe_{2.4}Si_6$	4.59 Å		A	Ma and Stern [1988]
$Al_{75}Mn_{15}Cr_5Si_5$			A	Nanao, Dmowski, Egami, Richardson and Jorgensen [1987]
$*Al_{70.5}Mn_{8.5}Pd_{21}$	4.56 Å	F	A	Tsai, Inoue, Yokoyama and Masumoto [1990]
$*Al_{70.5}Pd_{20.5}Re_9$	4.60 Å	F	A	
*Al–Mn–Pd–B	4.55 Å	F	A	Yokoyama, Inoue and Masumoto [1992]
*Al–Cu–Mn–B	4.51 Å	F	A	

Table A6–*Continued*

$Al_{72}Pd_{25}V_3$		F	A	Tsai, Yokoyama, Inoue and Masumoto [1990]
$Al_{70}Fe_{13}Pd_{17}$		F	A	
$Al_{72}Cr_8Pd_{20}$		F	A	
$Al_{75}Co_{10}Pd_{15}$		F	A	
*Al–Pd–Cr–Fe		F	A	Yokoyama, Tsai, Inoue, Masumoto and Chen [1991]
*Al–Pd–Co–V		F	A	
*Al–Pd–Mo–Ru		F	A	
*Al–Pd–W–Os		F	A	
$Al_{52}Mg_{17}Pd_{31}$	4.63 Å	F	A	Koshikawa, Edagawa, Honda and Takeuchi [1993]
$Al_{70}Mg_8Rh_{22}$		F	A	
Ti_2Fe	4.72 Å	F	A	Kelton, Gibbons and Sabes [1988]
Ti_2Mn	4.79 Å	F	A	
Ti_2Co	4.82 Å	F	A	
$Ti_2(Ni,V)$		F	A	Zhang, Ye and Kuo [1985]
$Ti_{56}Ni_{28}Si_{16}$		F	A	Chatterjee and O'Handley [1989]
$V_{41}Ni_{36}Si_{23}$			A	Kuo, Zhou and Li [1987]
$Pd_{58.8}U_{20.6}Si_{20.6}$	5.14 Å		A	Poon, Drehmann and Lawless [1985]
*$Al_{43}Mg_{44}Pd_{13}$	5.13 Å		B	Koshikawa, Sakamoto, Edagawa and Takeuchi [1992]
*Al_6CuLi_3	5.04 Å		B	Saintfort and Dubost [1986]
Al_6CuMg_4	5.21 Å		B	Sastry, Rao, Ramachandrarao and Anantharaman [1986]
$Al_{51}Cu_{12.5}$–$(Li_xMg_{36.5-x})$	5.05 Å		B	Shen, Shiflet and Poon [1988]
$Al_{50}Li_{25}Mg_{25}$	5.17 Å	F	B	Niikura, Tsai, Inoue, Masumoto and Yamamoto [1993]
Al_6AuLi_3	5.11 Å		B	Chen, Phillips, Villars, Kortan and Inoue [1987]
$Al_{51}Zn_{17}Li_{32}$	5.11 Å		B	
$Al_{50}Mg_{35}Ag_{15}$	5.23 Å		B	Mukhopadhyay, Chattopadhyay, and Raganathan [1988]
Al–Ni–Nb			B	
$(Al,Zn)_{49}Mg_{32}$	5.15 Å		B	Henley and Elser [1986]
$(Al,Zn,Cu)_{49}Mg_{32}$	5.15 Å		B	Mukhopadhyay, Thangaraj, Chattopadhyay and Ranganathan [1987]
*$Ga_{16}Mg_{32}Zn_{52}$	5.09 Å		B	Ohashi and Spaepen [1987]
*Mg–Y–Zn			B	Luo, Zhang, Tang and Zhao [1993]
*Mg–Y–Zn–Zr			B	Tang, Zhao, Luo, Sheng and Zhang [1993]
Nb–Fe			B	Kuo [1987]

References: p. 408.

Table A7
Selected symmetry information on the six-dimensional superspace group $Pm\bar{3}\bar{5}$.

Multiplicity	Wyckoff position	site symmetry	coordinates
6	c	$m\bar{5}$	$\frac{1}{2}$(1 0 0 0 0 0)
1	b	$m\bar{3}\bar{5}$	$\frac{1}{2}$(1 1 1 1 1 1)
1	a	$m\bar{3}\bar{5}$	(0 0 0 0 0 0)

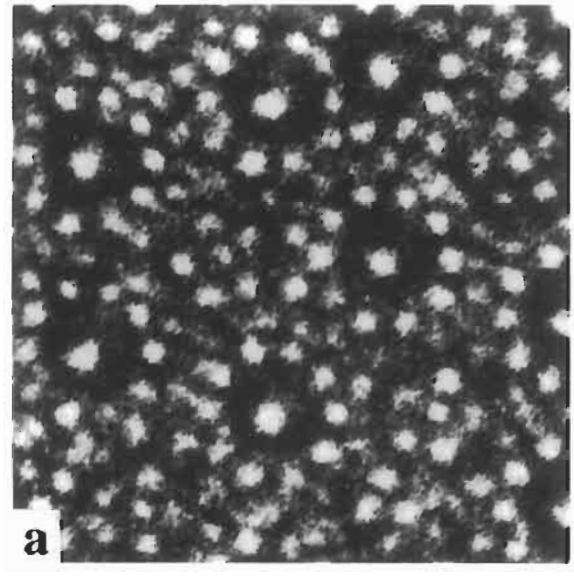

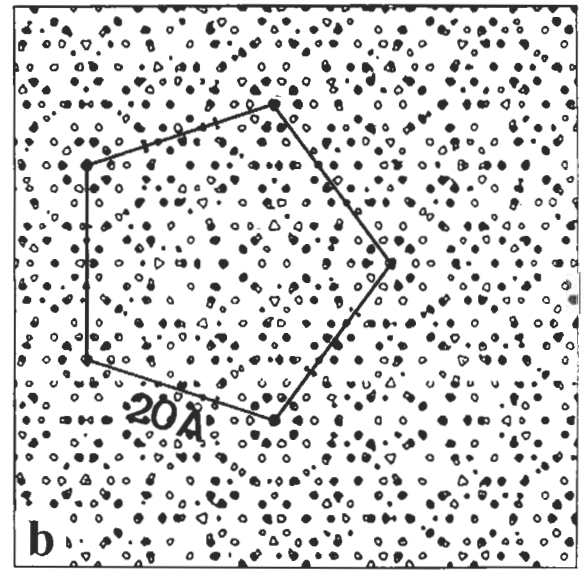

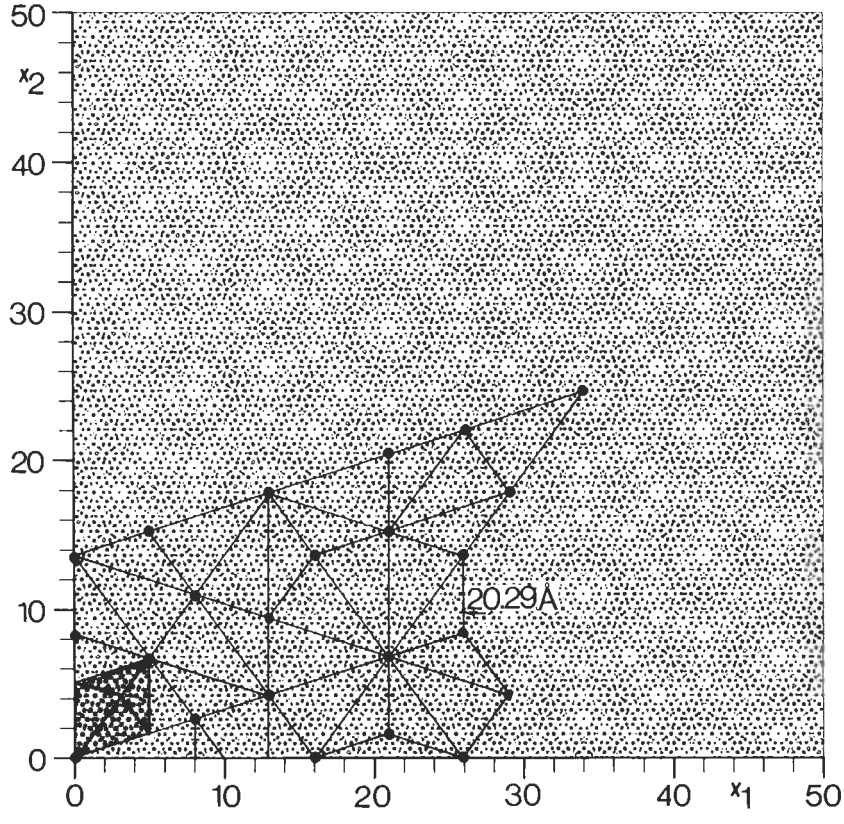

Fig. A17. (a) HRTEM image of decagonal $Al_{70.5}Mn_{16.5}Pd_{13}$ with a point to point resolution of 2 Å, and (b) comparison with the projected decagonal Al–Mn structure (from BEELI and NISSEN [1993]). (c) Physical space projection of the electron density of decagonal $Al_{70.5}Mn_{16.5}Pd_{13}$ with large, and small ROBINSON triangles drawn in.

(1) The hyperatoms occupy the Wyckoff positions (a), (b) and (c) (table A7), i.e., the vertices, the body center and the mid-edge positions of the six-dimensional hypercubic unit cell. In the case of ico-$Al_{73}Mn_{21}Si_6$, one hyperatom is centered at (a), its core consisting of Mn and the surrounding part of Al/Si. The second hyperatom is located at the body center (b), (c) remains unoccupied. Ico-Al_6CuLi_3 has Al/Cu-hyperatoms at (a) and (c), and one Li-hyperatom at (b) (figs. A20 and A21).

(2) The structures of ico-$Al_{73}Mn_{21}Si_6$, ico-Al_6CuLi_3 and their related crystalline phases show close resemblance in the six-dimensional description. This confirms the assumption that cubic α-$Al_{73}Mn_{16}Si_{11}$ and R–Al_5CuLi_3 are (1,1)-approximants related to the icosahedral phases merely by a hyperspace rotation.

(3) There exist orientation relationships for epitaxially grown α-$Al_{73}Mn_{16}Si_{11}$ on icosahedral $Al_{73}Mn_{21}Si_6$: [100] of the cubic phase is parallel to a twofold direction of the icosahedral phase, and [111] is parallel to a threefold one.

References: p. 408.

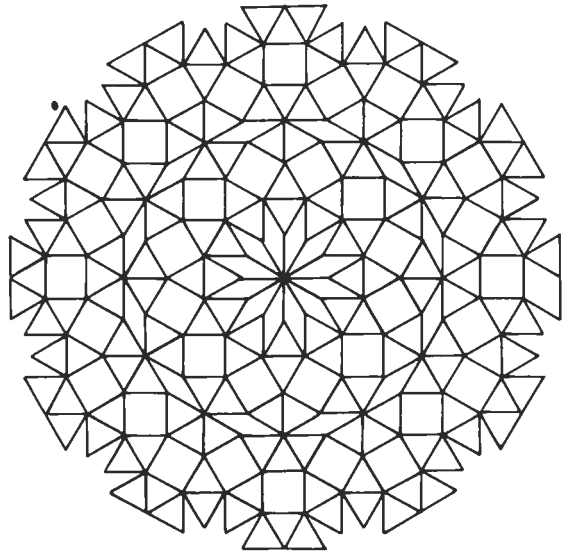

Fig. A18. Dodecagonal tiling as example for a quasilattice with twelve-fold symmetry.

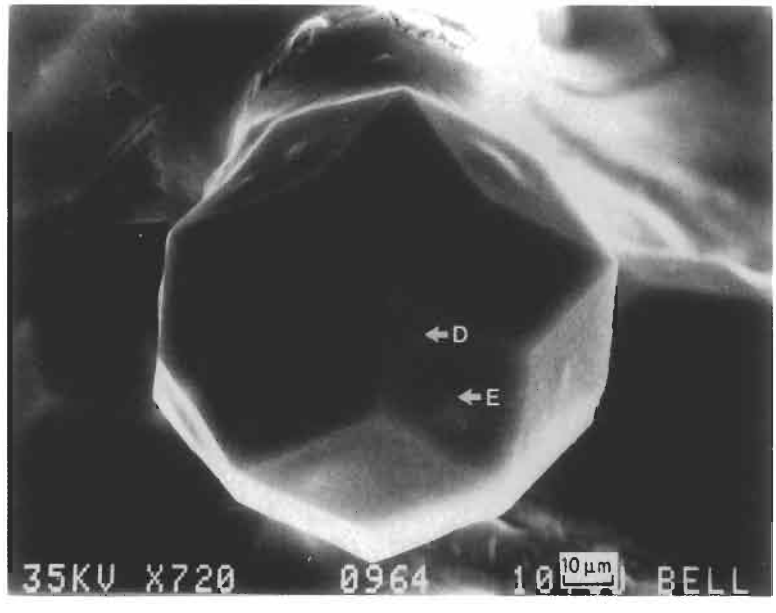

Fig. A19. Single crystal of ico-$Al_{5.1}CuLi_3$ with triacontahedral shape (from KORTAN, CHEN, PARSEY and KIMERLING [1989]).

(4) α-$Al_{73}Mn_{16}Si_{11}$ contains a high percentage of atoms forming slightly distorted Mackay icosahedra (78.3%), and its structure can be described by a near-bcc packing of these 54–atom polyhedra. Ico-$Al_{73}Mn_{21}Si_6$, on the other hand, contains 66.6% of atoms in regular but often fragmented Mackay icosahedra.

(5) R–Al_5CuLi_3 can be described as bcc packing of distorted Pauling triacontahedra or 104–atoms Samson complexes (fig. A22). These structure motifs are also locally present in ico-Al_6CuLi_3. In the Penrose tiling description, there are icosahedral clusters placed on the twelvefold vertices.

3.3.2. Face-centered hypercubic icosahedral phases

The face-centering of the six-dimensional hypercubic unit cell results from chemical

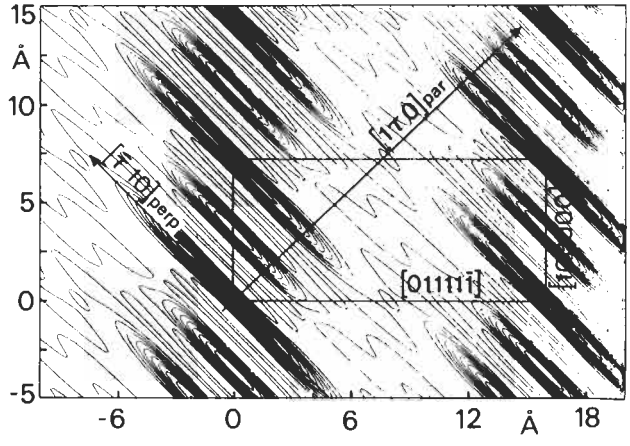

(a)

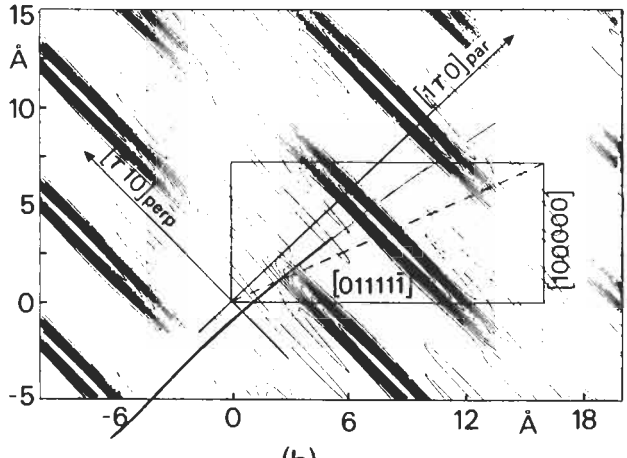

(b)

References: p. 408.

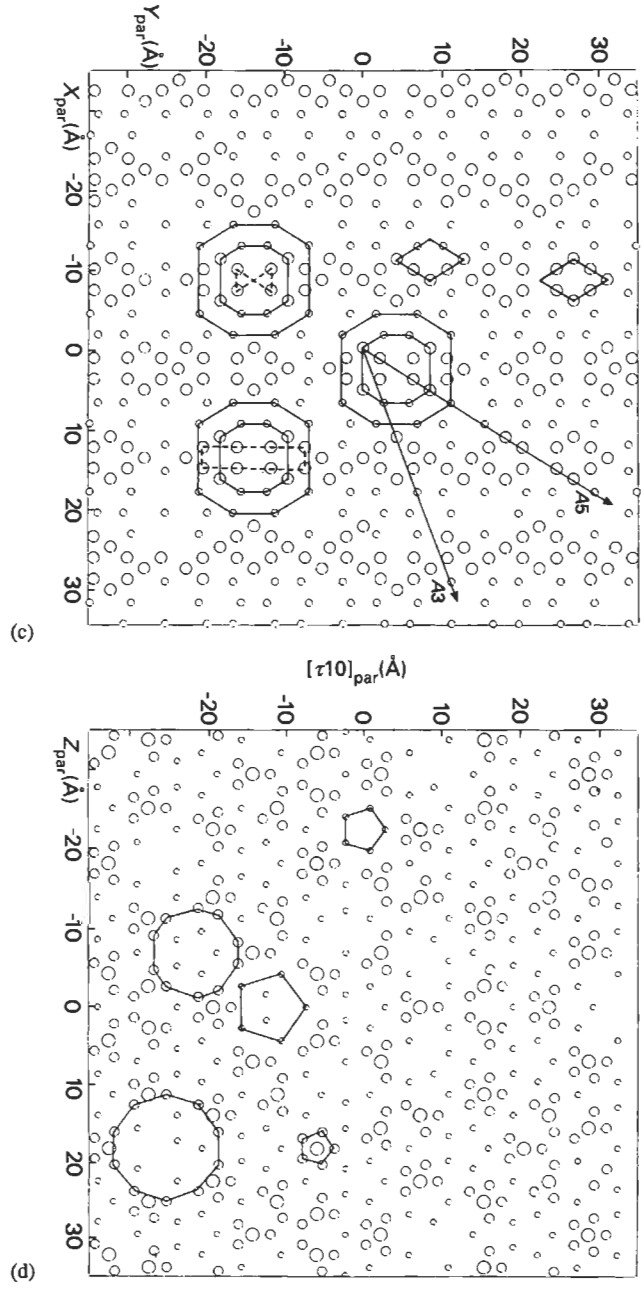

Fig. A20. Cuts of six-dimensional partial hyperatomic density of ico-Al_6CuLi_3. (a) Al/Cu hyperatoms at the vertices, and mid-edge positions, (b) Li at the body center. Parallel-space atomic planes as obtained by a cut of the six-dimensional model; layer with twofold symmetry in (c), with fivefold symmetry in (d) (from JANOT [1992]).

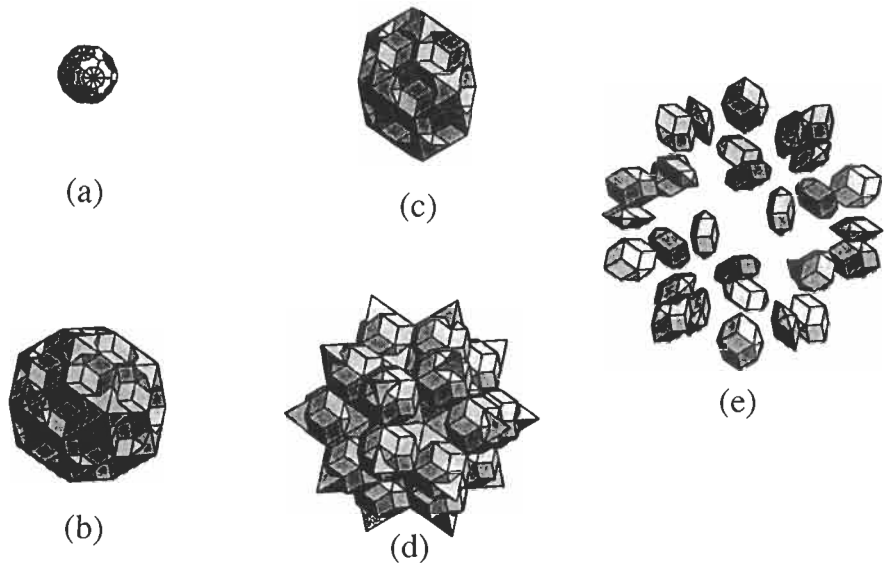

Fig. A21. Hyperatoms of the ideal ico-Al_6CuLi_3 structure derived from the R-Al_5CuLi_3 structure: (a) vacant twelve-fold, (b) vertex Al/Cu, (c) mid-edge Al/Cu, (d) body-center Li surrounded by (e) Al/Cu hyperatoms. The domain (a) has to be subtracted from (b) to remove unoccupied twelve-fold vertices (from YAMAMOTO [1992]).

ordering of the atoms. Therefore, the resulting structure may also be described as a superstructure, with twice the lattice parameters of the primitive hypercubic unit cell used in the preceding paragraph: the Wyckoff positions occupied are often named $n_1 = (0\ 0\ 0\ 0\ 0\ 0)$, $n_2 = \frac{1}{2}(1\ 0\ 0\ 0\ 0\ 0)$, $bc_1 = \frac{1}{4}(1\ 1\ 1\ 1\ 1\ 1)$ and $bc_2 = \frac{1}{4}(1\ 1\ 1\ 1\ 1\ \bar{1})$.

Representatives of stable quasicrystals with superspace group $Fm\bar{3}\bar{5}$ are ico-Al–Cu–Me, with Me=Fe, Ru, Os (TSAI, INOUE and MASUMOTO, 1989; TSAI, INOUE and MASUMOTO [1988b]) and ico-Al–Me–Pd, with Me=Mn, Re (TSAI, INOUE, YOKOYAMA and MASUMOTO [1990]). Ico-$Al_{63}Cu_{25}Fe_{12}$ (CORNIER-QUIQUANDON, QUIVY, LEFEBVRE, ELKAIM, HEGER, KATZ and GRATIAS [1991]; CORNIER-QUIQUANDON, BELLISENT, CALVAYRAC, CAHN, GRATIAS and MOZER [1993]) and ico-$Al_{70.5}Mn_{8.5}Pd_{21}$ (BOUDARD, DEBOISSIEU, AUDIER, JANOT, HEGER, BEELI, NISSEN, VINCENT, IBBERSON and DUBOIS [1992]) were analysed using X-ray diffraction and neutron scattering techniques on single- and polycrystalline samples, and by HRTEM (BEELI, NISSEN and ROBADEY [1991]; HIRAGA [1991]; KRAKOW, DI VINCENZO, BANCEL, COCKAYNE and ELSER [1993]). Ico-$Al_{65}Cu_{20}Ru_{15}$ was investigated by anomalous X-ray diffraction on polycristalline samples (HU, EGAMI, TSAI, INOUE and MASUMOTO [1992]). The results of the structure analyses can be summarized briefly:

(1) The hyperatoms occupy the positions n_1, n_2, bc_1 and bc_2, i.e. the vertices, mid-edge positions, and body centers of the subhypercubes of the six-dimensional face-centered hypercubic unit cell. In the case of ico-$Al_{63}Cu_{25}Fe_{12}$, Fe is concentrated at

References: p. 408.

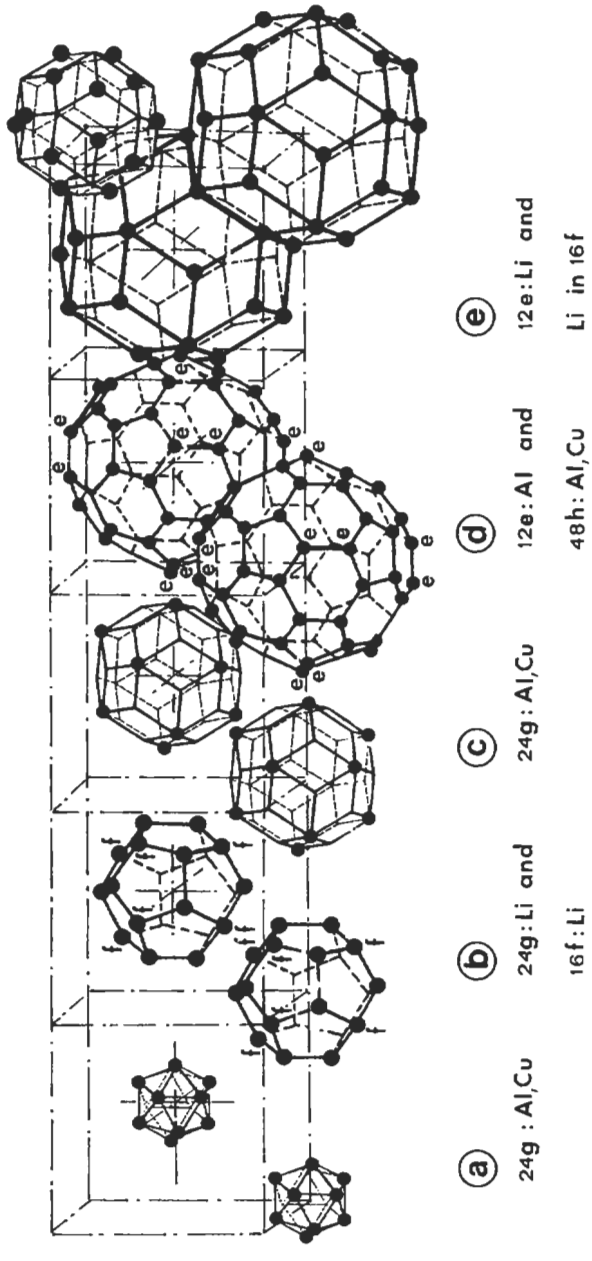

Fig. A22. Schematical illustration of the structure, and bcc packing of Pauling triacontahedra in R-Al_5CuLi_3 (from AUDIER, PANNETIER, LEBLANC, JANOT, LANG and DUBOST [1988]).

the core of hyperatoms centered on n_1 and n_2 and surrounded by successive shells of Cu and Al. Cu also occupies the body center bc_1, while bc_2 remains unoccupied. For ico-$Al_{70.5}Mn_{8.5}Pd_{21}$ (fig. A23) was found that Mn occupies the core of the

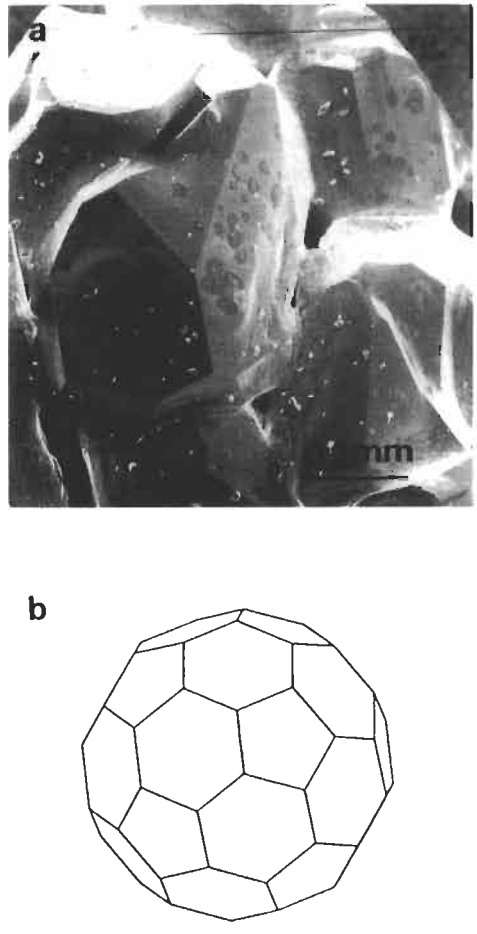

Fig. A23. (a) Single crystal of ico-$Al_{70}Mn_{20}Pd_{10}$ with shape like an (b) icosidodecahedron (from TSAI, INOUE, YOKOYAMA and MASUMOTO [1990]).

hyperatom on n_1 surrounded by an intermediate Pd and one outer Al shell, the hyperatom at n_2 consists of Mn surrounded by Al; at bc_2 a small Pd and at bc_1 possibly a small Al hyperatom may be located (fig. A24).

(2) The shapes of the hyperatoms for $Al_{63}Cu_{25}Fe_{12}$ were assumed as a large triacontahedron at n_1, a truncated triacontahedron of the same size at n_2 and a small polyhedron bounded by twofold planes at bc_1 (fig. A25). For $Al_{70.5}Mn_{8.5}Pd_{21}$ only spherical hyperatomic shapes were used in the refinements.

(3) Since the hyperatoms at the lattice nodes have a subset in common with the triacontahedra generating a canonical Penrose rhombohedra tiling, also a subset of the atoms in the three-dimensional quasicrystal structure is located on the vertices

of a Penrose tiling. The location of the other atoms, however cannot be described by a simple decoration of the unit tiles, a context dependent decoration would be necessary.

(4) In the three-dimensional structure of ico-$Al_{70.5}Mn_{8.5}Pd_{21}$ two types of pseudo-Mackay cluster are present: type 1 refers to a large icosahedron of Mn/Al and a icosidodecahedron of Pd/Al, type 2 to a large icosahedron of Mn/Pd and a icosidodecahedron of Al. The small icosahedron core of MI is absent.

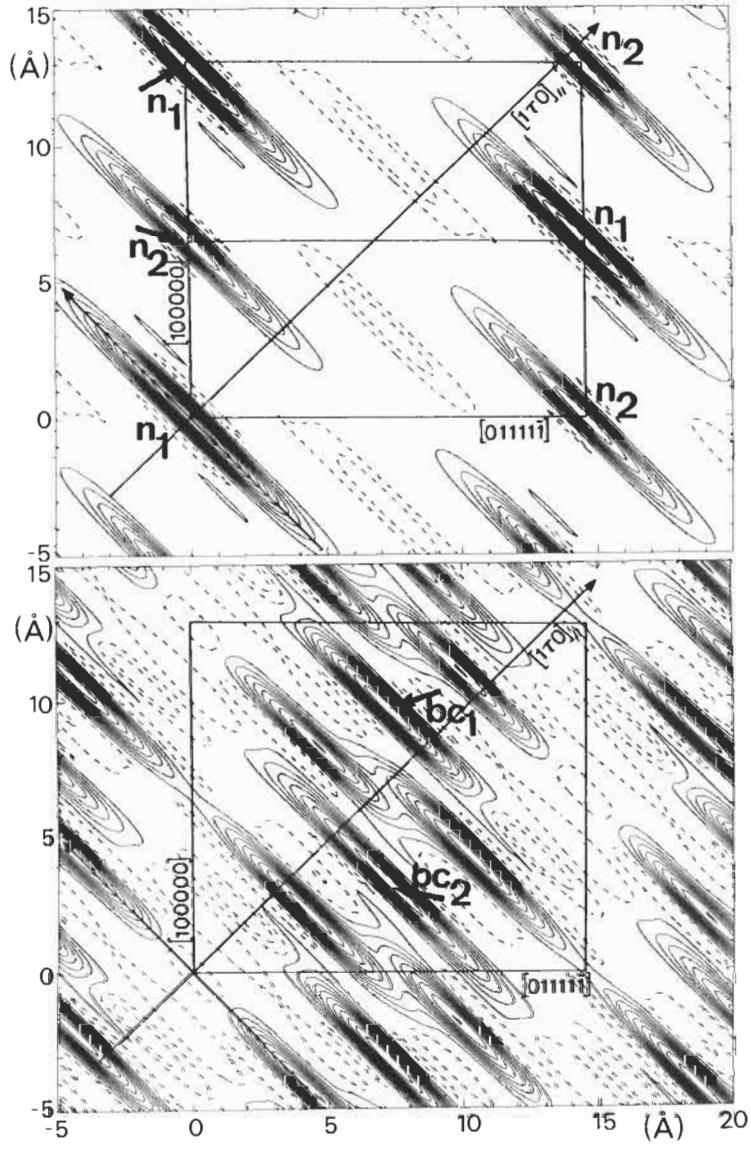

(a)

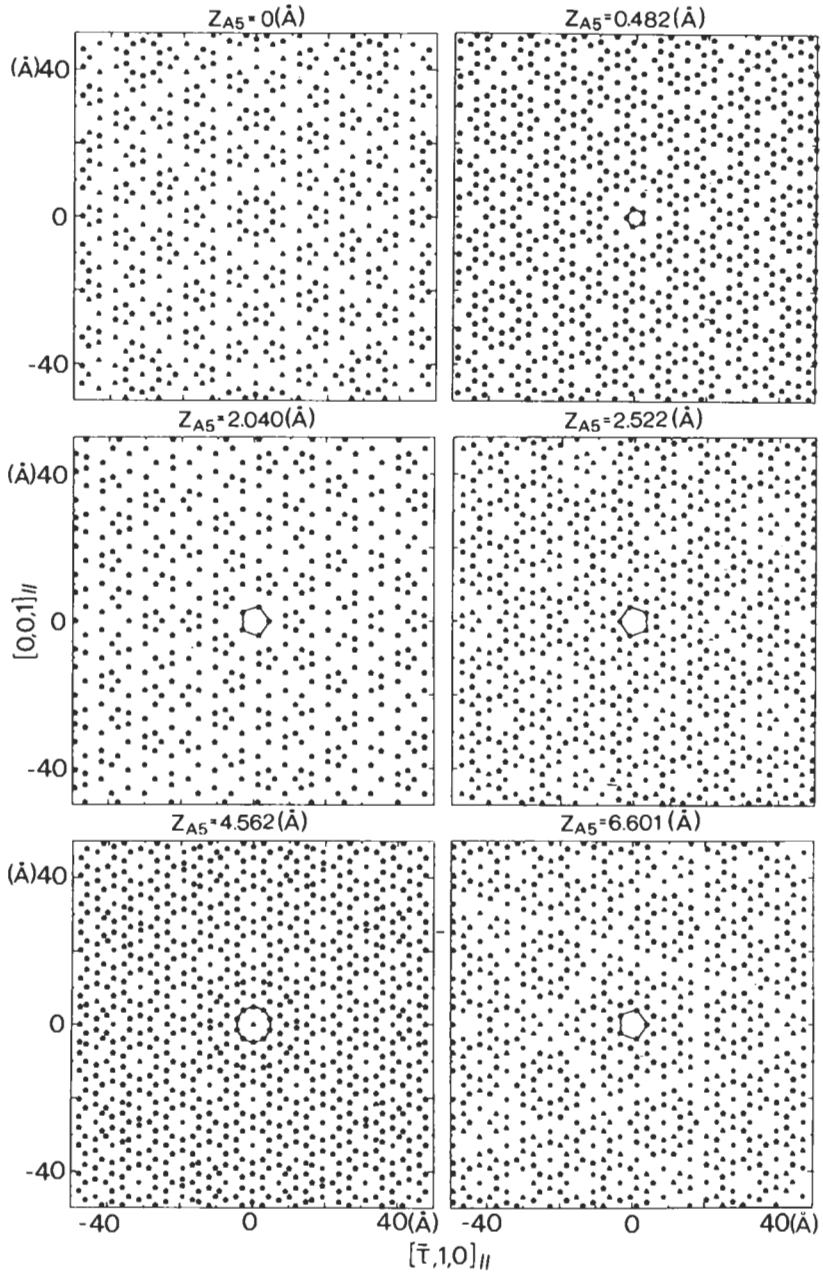

(b)

Fig. A24. (a) Cuts of six-dimensional partial hyperatomic density of ico-$Al_{70.5}Mn_{8.5}Pd_{21}$ for lattice nodes n_1, and mid-edge positions n_2 (upper drawing), and the body centers bc_1 of the subhypercubes of the F-hypercell (lower drawing). (b) Parallel-space atomic planes as obtained by cuts of the six-dimensional model (from BOUDARD, DEBOISSIEU, JANOT, DUBOIS and DONG [1991]).

References: p. 408.

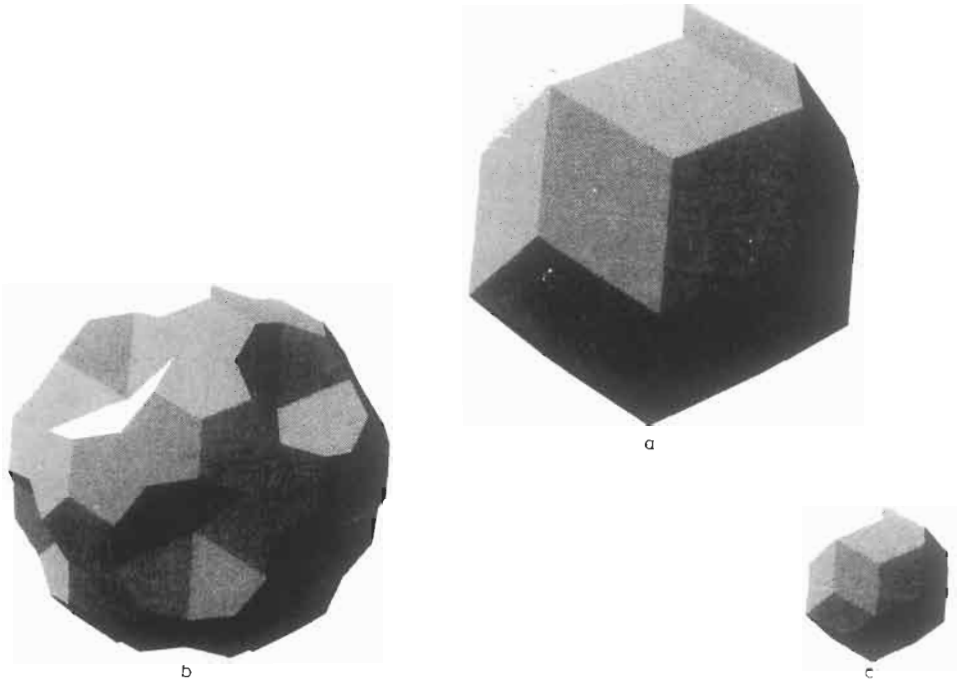

Fig. A25. The shapes of the hyperatoms in ico-$Al_{63}Cu_{25}Fe_{12}$. (a) Fe/Cu/Al triacontahedral hyperatom in the origin n_1, (b) mid-edge (n_2) Fe/Cu/Al hyperatom, and (c) Cu/Al hyperatom at bc_1 (from CORNIER–QUIQUANDON, QUIVY, LEFEBVRE, ELKAIM, HEGER, KATZ and GRATIAS [1991]).

References

ANLAGE, S.M., B. FULTZ and K.M. KRISHNAN, 1988, J. Mater. Res. **3,** 421–5.
AUDIER, M., M. DURAND-CHARRE and M. DEBOISSIEU, 1993, Phil. Mag. **B68**, 607–18.
AUDIER, M., J. PANNETIER, M. LEBLANC, C. JANOT, J.M. LANG and B. DUBOST, 1988 Physica **B153**, 136–42.
BANCEL, P.A., and P.A. HEINEY, 1986, Phys. Rev. **B33**, 7917–22.
BANCEL, P.A., P.A. HEINEY, P.W. STEPHENS, A.I. GOLDMAN and P.M. HORN, 1985, Phys. Rev. Lett. **54**, 2422–5.
BARBIER, J.-N., N. TAMURA and J.-L. VERGER-GAUGRY, 1993, J. Non-Crystall. Solids **153, 154**, 126–31.
BEELI, C., and H.-U. NISSEN, 1993, J. Non-Crystall. Solids **153, 154**, 463–7.
BEELI, C., H.-U. NISSEN and J. ROBADEY, 1991, Phil. Mag. Lett. **63**, 87–95.
BOUDARD, M., M. DEBOISSIEU, C. JANOT, J.M. DUBOIS and C. DONG, 1991, Phil. Mag. Lett. **64**, 197–206.
BOUDARD, M., M. DEBOISSIEU, M. AUDIER, C. JANOT, G. HEGER, C. BEELI, H.-U. NISSEN, H. VINCENT, R. IBBERSON and J.M. DUBOIS, 1992, J. Phys.: Condens. Matt. **4**, 10149– 68.
BURKOV, S.E., 1991, Phys. Rev. Lett. **67**, 614–7.
BURKOV, S.E., 1992, Phys. Rev. **B47**, 12325–8.
CAHN, J.W., D. GRATIAS and B. MOZER, 1988, J. Phys. France **49,** 1225–33.
CAO, W., H.Q. YE and K.H. KUO, 1988, Phys. Status Solidi (a) **107**, 511–9.

CHATTERJEE, R., and R.C. O'HANDLEY, 1989, Phys. Rev. **B39**, 8128–31.
CHATTOPADHYAY, K., S. LELE, N. THANGARAJ and S. RANGANATHAN, 1987, Acta Metall. **35**, 727–33.
CHEN, H., D.X. LI and K.H. KUO, 1988, Phys. Rev. Lett. **60**, 1645–8.
CHEN, H.S., J.C. PHILLIPS, P. VILLARS, A.R. KORTAN and A. INOUE, 1987, Phys. Rev. **B35**, 9326–9.
COOPER, M., and K. ROBINSON, 1966, Acta Crystallogr. **20**, 614–17.
CORNIER-QUIQUANDON, M., R. BELLISENT, Y. CALVAYRAC, J.W. CAHN, D. GRATIAS and B. MOZER, 1993, J. Non-Crystall. Solids **153, 154**, 10–4.
CORNIER-QUIQUANDON, M., A. QUIVY, S. LEFEBVRE, E. ELKAIM, G. HEGER, A. KATZ and D. GRATIAS, 1991, Phys. Rev. **B44**, 2071–84.
DAULTON, T.L., and K.F. KELTON, 1992, Phil. Mag. **B66**, 37–61.
DAULTON, T.L., and K.F. KELTON, 1993, Phil. Mag. **B68**, 697–711. .
DAULTON, T.L., K.F. KELTON, S. SONG and E.R. RYBA, 1992, Phil. Mag. Lett. **65**, 55–65.
DEBOISSIEU, M., C. JANOT, J.M. DUBOIS, M. AUDIER and B. DUBOST, 1991,
J. Phys.: Condens. Matt. **3**, 1–25.
DONG, C., J.M. DUBOIS, M. DEBOISSIEU and C. JANOT, 1991, J. Phys.: Cond. Matt. **3**, 1665–73.
DONG, C., J.M. DUBOIS, S.S. KANG and M. AUDIER, 1992, Phil. Mag. **B65**, 107–26.
DONG, J., K. LU, H. YANG and Q. SHAN, 1991, Phil. Mag. **B64**, 599–609.
EBALARD, S., F. SPAEPEN, 1989, J. Mater. Res. **4**, 39–43.
EDAGAWA, K., M. ICHIHARA, K. SUZUKI and S. TAKEUCHI, 1992, Phil. Mag. Lett. **66**, 19–25.
FREY, F., and W. STEURER, 1993, J. Non-Crystall. Solids **153, 154**, 600–5.
FUNG, K.K., C.Y. YANG, Y.Q. ZHOU, J.G. ZHAO, W.S. ZHAN and B.G. SHEN, 1986, Phys. Rev. Lett. **56**, 2060–3.
GRATIAS, D., J.W. CAHN, B. MOZER, 1988, Phys. Rev. **B38**, 1643–6.
GRUSHKO, B., 1993, Mater. Trans. JIM **34**, 116–21.
HAIBACH, T., B. ZHANG and W. STEURER, 1994, in preparation.
HE, L.X., X.Z. LI, Z. ZHANG and K.H. KUO, 1988, Phys. Rev. Lett. **61**, 1116–8.
HE, L.X., Y.K. WU, K.H. KUO, 1988, J. Mater. Sci. **7**, 1284–6.
HE, A.Q., Q.B. YANG and H.Q. YE, 1990, **61**, 69–75.
HE, L. X, Z. ZHANG, Y.K. WU and K.H. KUO, 1988, Inst. Phys. Conf. Ser. No. 93, **2**, 501–2.
HEINEY, P.A., P.A. BANCEL, A.I. GOLDMAN and P.W. STEPHENS, 1986, Phys. Rev. **B34**, 6746–51.
HENLEY, C.L., 1993, J. Non-Crystall. Solids **153, 154**, 172–6.
HENLEY, C.L., and V. ELSER, 1986, Phil. Mag. **B53**, L59–66.
HIRAGA, K., 1991, J. Electron Microsc. **40**, 81–91.
HIRAGA, K., 1992, Electron Microscopy **2**, EUREM 92, Granada, Spain.
HIRAGA, K., M. KANEKO, Y. MATSUO and S. HASHIMOTO, 1993, Phil. Mag. **B67**, 193–205.
HIRAGA, K., F.J. LINCOLN and W. SUN, 1991, Mater. Trans. **32**, 308–14.
HIRAGA, K., and W. SUN, 1993, Phil. Mag. Lett. **67**, 117–23.
HIRAGA, K., W. SUN and F.J. LINCOLN, 1991, Jap. J. Appl. Phys. **30**, L302–5.
HIRAGA, K., W. SUN, F.J. LINCOLN, M. KANEKO and Y. MATSUO, 1991, Jap. J. Appl. Phys. **30**, 2028–34.
HIRAGA, K., B.P. ZHANG, M. HIRABAYASHI, A. INOUE and T. MASUMOTO, 1988, Jpn. J. Appl. Phys. **27**, L951–3.
HU, R., T. EGAMI, A.P. TSAI, A. INOUE and T. MASUMOTO, 1992, Phys. Rev. **B46**, 6105–14.
HUDD, R.C., and W.H. TAYLOR, 1962, Acta Crystallogr. **15**, 441–2.
INOUE, A., H.M. KIMURA, T. MASUMOTO, A.P. TSAI and Y. BIZEN, 1987, J. Mater. Sci. Lett. **67**, 771–4.
ISHIMASA, T., H.-U. NISSEN and Y. FUKANO, 1985, Phys. Rev. Lett. **85**, 511–3.
JANOT, C., 1992, Quasicrystals. A Primer (Clarendon Press, Oxford).
JANOT, C., M. DEBOISSIEU, J.M. DUBOIS and J. PANNETIER, 1989, J. Phys.: Condens. Matt. **1**, 1029–48.
JANSSEN, T., 1986, Acta Crystallogr. **A42**, 261–71.
KANG, S., and J.M. DUBOIS, 1992, J. Phys.: Condens. Matt. **4**, 10169–98.
KANG, S.S., J.M. DUBOIS, B. MALAMAN and G. VENTURINI, 1992, Acta Crystallogr. **B48**, 770–6.
KARKUT, M.G., J.M. TRISCONE, D. ARIOSA and Ø. FISCHER, 1986, Phys. Rev. **B34**, 4390–3.
KEK, S., 1991, Thesis, Univ. Stuttgart, FRG.
KELTON, K.F., P.C. GIBBONS and P.N. SABES, 1988, Phys. Rev. **B38**, 7810–3.

KORTAN, A.R., R.S. BECKER, F.A. THIEL and H.S. CHEN, 1990, Phys. Rev. Lett. **64**, 200–3.
KORTAN, A.R., H.S. CHEN, J.M. PARSEY and L.C. KIMERLING, 1989, J. Mater. Sci. **24**, 1999–2005.
KOSHIKAWA, N., K. EDAGAWA, Y. HONDA and S. TAKEUCHI, 1993, Phil. Mag. Lett. **68**, 123–9.
KOSHIKAWA, N., S. SAKAMOTO, K. EDAGAWA and S. TAKEUCHI, 1992, Jpn. J. Appl. Phys. **31**, 966–9.
KRAKOW, W., D.P. DIVINCENZO, P.A. BANCEL, E. COCKAYNE and V. ELSER, 1993, J. Mater. Res. **8**, 24–7.
KRUMEICH, F., M. CONRAD and B. HARBRECHT, 1994, 13th International Congress on Electron Microscopy, ICEM, Paris.
KUO, K.H., 1987, Mater. Sci. Forum **22–24**, 131–40.
KUO, K.H., 1993, J. Non-Crystall. Solids **153, 154**, 40–4.
KUO, K.H., D.S. ZHOU and D.X. LI, 1987, Phil. Mag. Lett. **B55**, 33–7.
LAUNOIS, P., M. AUDIER, F. DENOYER, C. DONG, J.M. DUBOIS and M. LAMBERT, Europhys. Lett. **13**, 629–34.
LAWTHER, D.W., and R.A. DUNLAP, 1993, J. Non-Crystall. Solids **153, 154**, 611–4.
LEMMERZ, U., B. GRUSHKO, C. FREIBURG and M. JANSEN, 1994, Phil. Mag. Lett. **69**, 141–6.
LEVINE, D., and P.J. STEINHARDT, 1986, Phys. Rev. **B34**, 596–616.
LI, X.Z., and K.H. KUO, 1988, Phil. Mag. Lett. **58**, 167–71.
LI, X.Z., and K.H. KUO, 1993, J. Mater. Res. **8**, 2499–503.
LIAO, X.Z., K.H. KUO, H. ZHANG and K. URBAN, 1992, Phil. Mag. **B66**, 549–58.
LIU, W., U. KÖSTER, F. MÜLLER and M. ROSENBERG, 1992, Phys. Stat. Sol. (a) **132**, 17–34.
LUO, Z., S. ZHANG, Y. TANG and D. ZHAO, 1993, Scr. Metall. and Mater. **28**, 1513–8.
MA, X.L., and K.H. KUO, 1994, Met. and Mater. Trans. **25A**, 47–56.
MA, Y., and E.A. STERN, 1987, Phys. Rev. **B35**, 2678–81.
MA, Y., and E.A. . STERN, 1988, Phys. Rev. **B38**, 3754–65.
MA, L., R. WANG and K.H. KUO, 1988, Scr. Metall. **22**, 1791–6.
MUKHOPADHYAY, N.K., K. CHATTOPADHYAY and S. RANGANATHAN, 1988, Met. Trans. **A20**, 805–12.
MUKHOPADHYAY, N.K., N. THANGARAJ, K. CHATTOPADHYAY and S. RANGANATHAN, 1987, J. Mater. Res. **2**, 299–304.
NANAO, S., W. DMOWSKI, T. EGAMI, J.W. RICHARDSON and J.D. JORGENSEN, 1987, Phys. Rev. **B35**, 435–40.
NIIKURA, A., A.P. TSAI, A. INOUE, T. MASUMOTO and A. YAMAMOTO, 1993, Jpn. J. Appl. Phys. **32**, L1160–3.
NISSEN, H.-U., and C. BEELI, 1993, J. Non-Crystall. Solids **153, 154**, 68–71.
OHASHI, W., and F. SPAEPEN, 1987, Nature **330**, 555–6.
OKABE, T., J.I. FURIHATA, K. MORISHITA and H. FUJIMORI, 1992, Phil. Mag. Lett. **66**, 259–64.
PAVLOVITCH, A., and M KLEMAN, 1987, J. Phys. A: Math. Gen. **20**, 687–702.
PLACHKE, D., T. KUPKE, H.D. CARSTANJEN and R.M. EMRICK, 1993, J. Non-Crystall. Solids **153, 154**, 72–6.
POON, S.J., A.J. DREHMANN and K.R. LAWLESS, 1985, Phys. Rev. Lett. **55**, 2324–7.
QIU, S.-Y., and M.V. JARIC, 1993, J. Non-Crystall. Solids **153, 154**, 221–6.
REYES-GASGA, J., A. LARA, H. RIVEROS and M. JOSE-YACAMAN, 1992, Mater. Sci. Eng. **A150**, 87–99.
ROMEU, D., 1993, Phil. Mag. **B67**, 77–96.
SAINTFORT, P., and B. DUBOST, 1986, J. Phys. France **47**, C3-321–30.
SASTRY, G.V.S., V.V. RAO, P. RAMACHANDRARAO and T.R. ANANTHARAMAN, 1986, Scr. metall. **20**, 191–3.
SCHURER, P.J., B. KOOPMANS, F. VAN DER WOUDE, 1988, Phys. Rev. **B37**, 507–10.
SHECHTMAN, D., I. BLECH, D. GRATIAS and J.W. CAHN, 1984, Phys. Rev. Lett. **53**, 1951–3.
SHEN, Y., G.J. SHIFLET and S.J. POON, 1988, Phys. Rev. **B38**, 5332–7.
SHOEMAKER, C.B., 1993, Phil. Mag. **B67**, 869–81.
VAN SMAALEN, S., J.L. DE BOER and Y. SHEN, 1991, Phys. Rev. **B43**, 929–37.
SOCOLAR, J.E.S., and P.J. STEINHARDT, 1986, Phys. Rev. **B34**, 617–47.
SONG, S., and E.R. RYBA, 1992, Phil. Mag. Lett. **65**, 85–93.
SONG, S., L. WANG and E.R. RYBA, 1991, Phil. Mag. Lett. **63**, 335–44.
SRINIVAS, V., R.A. DUNLAP, D. BAHADUR and E. DUNLAP, 1990, Phil. Mag. **B61**, 177–88.
STEURER, W., 1991, J. Phys.: Condens. Matter **3**, 3397–410.
STEURER, W., T. HAIBACH, B. ZHANG, C. BEELI and H.-U. NISSEN, 1994, J. Phys.: Condens. Matter **6**, 613–32.
STEURER, W., T. HAIBACH, B. ZHANG, S. KEK and R. LÜCK, 1993, Acta Crystallogr. **B49**, 661–75.
STEURER, W., and K.H. KUO, 1990, Acta Crystallogr. **B46**, 703–12.

TANG, Y., D. ZHAO, Z. LUO, N. SHENG and S. ZHANG, 1993, Mater. Lett. **18**, 148–50.
TODD, J., R. MERLIN, R. CLARKE, K.M. MOHANTY and J.D. AXE, 1986, Phys. Rev. Lett. **57**, 1157–60.
TSAI, A.P., A. INOUE and T. MASUMOTO, 1987, Jpn. J. Appl. Phys. **26**, L1505–7.
TSAI, A.P., A. INOUE and T. MASUMOTO, 1988a, Trans. JIM **29**, 521–4.
TSAI, A.P., A. INOUE and T. MASUMOTO, 1988b, J.J. Appl. Phys. **27**, L1587–90
TSAI, A.P., A. INOUE and T. MASUMOTO, 1988c, J.J. Appl. Phys. **27**, L5–8.
TSAI, A.P., A. INOUE and T. MASUMOTO, 1988d, J. Mater. Sci. Lett. **7**, 322–6.
TSAI, A.P., A. INOUE and T. MASUMOTO, 1989, Mater. Trans. JIM **30**, 463–73.
TSAI, A.P., A. INOUE and T. MASUMOTO, 1991, Phil. Mag. Lett. **64**, 163–7.
TSAI, A.P., A. INOUE and T. MASUMOTO, 1993, Mater. Trans. JIM **34**, 155–61.
TSAI, A.P., A. INOUE, T. MASUMOTO, A. SATO and A. YAMAMOTO, 1992, Jpn. J. Appl. Phys. **31**, 970–3.
TSAI, A.P., A. INOUE, Y. YOKOYAMA and T. MASUMOTO, 1990, Mater. Trans. JIM **31**, 98–103.
TSAI, A.P., T. MASUMOTO and A. YAMAMOTO, 1992, Phil. Mag. Lett. **66**, 203–8.
TSAI, A.-P., Y. YOKOYAMA, A. INOUE and T. MASUMOTO, 1990, Jpn. J. Appl. Phys. **29**, L1161–4.
TSAI, A.-P., Y. YOKOYAMA, A. INOUE and T. MASUMOTO, 1991, J. Mater. Res. **6**, 2646–52.
WANG, N., H. CHEN and K.H. KUO, 1987, Phys. Rev. Lett. **59**, 1010–13.
WANG, N., K.K. FUNG and K.H. KUO, 1988, Appl. Phys. Lett. **52**, 2120–22.
WANG, N., and K.H. KUO, 1988, Acta Crystallogr. **A44**, 857–63.
WANG, N., and K.H. KUO, 1990, Phil. Mag. Lett. **61**, 63–8.
WELBERRY, T.R., 1989, J. Appl. Cryst. **22**, 308–14.
WIDOM, M., and R. PHILLIPS, 1993, J. Non-Crystall. Solids **153, 154**, 282–7.
YAMAMOTO, A., 1992, Phys. Rev. **B45**, 5217–27.
YOKOYAMA, Y., A. INOUE and T. MASUMOTO, 1992, Mater. Trans. JIM **33**, 1012–9.
YOKOYAMA, Y., A.P. TSAI, A. INOUE, T. MASUMOTO and H.S. CHEN, 1991, Mater. Trans. JIM **32**, 421–8.
ZHANG, H., and K.H. KUO, 1989, Scr. Metall. **23**, 355–8.
ZHANG, H., D.H. WANG and K.H. KUO, 1988, Phys. Rev. **B37**, 6220–5.
ZHANG, Z., H.Q. YE and K.H. KUO, 1985, Phil. Mag. **A52**, L49–52.

Further reading

FUJIWARA, T., and T. OGAWA, (eds.) 1990, Quasicrystals, Springer Series in Solid State Science **93**.
GOLDMAN, A.I., and K.F. KELTON, 1993, Rev. Mod. Phys. **65**, 213–30.
KELTON, K.F., 1995, in: Intermetallic Compounds — Principles and Practice, eds. J.H. Westbrook and R.L. Fleischer (Wiley, Chichester), Vol. 1, pp. 453–491.
JANOT, C., 1992, Quasicrystals. A Primer (Clarendon Press, Oxford).
JANSSEN, T., 1988, Phys. Rep. **168**, 55–113.
STEURER, W., 1990, Z. Kristallogr. **190**, 179–234.

CHAPTER 5

METALLURGICAL THERMODYNAMICS

D.R. GASKELL

School of Materials Engineering
Purdue University
West Lafayette, IN 47907, USA

R. W. Cahn and P. Haasen†, eds.
Physical Metallurgy; fourth, revised and enhanced edition

1. Introduction

Metallurgical thermodynamics is concerned with the equilibrium states of existence available to systems, and with the effects of external influences on the equilibrium state. The thermodynamic state of a system is defined in terms of state variables (or *state functions*) and the state variables occur in two categories; *intensive* variables such as pressure, P, and temperature, T, the values of which are independent of the size of the system, and *extensive* variables such as internal energy, U, and volume, V, the values of which are dependent on the size of the system. The simplest equation of state is the ideal gas law,

$$PV = nRT \tag{1}$$

where n is the number of moles of the gas and R is the universal gas constant. In considering a fixed quantity of ideal gas, only two of the state functions in eq. (1) are independent and the other is dependent. Thus, in a three-dimensional diagram employing P, V and T as ordinates, the equilibrium states of existence of the fixed quantity of gas lie on a definite surface. In any *reversible* change of state of the gas the path of the process lies on this equilibrium surface, such that, in moving from the initial to the final state, the gas passes through a continuum of equilibrium states. Under such conditions the *work*, w, done on or by the gas during the process is given by:

$$w = \int_{V_{initial}}^{V_{final}} P dV, \tag{2}$$

and thus the magnitude of w is dependent on the actual process path taken over the equilibrium surface between the final and initial states. In an *irreversible* process the state of the gas momentarily leaves the equilibrium surface while moving between the initial and final states.

1.1. The First and Second Laws of Thermodynamics

When a system undergoes a process in which it moves from one state to another, the change in the internal energy of the system, ΔU, is given by:

$$\Delta U = U_2 - U_1 = q - w, \tag{3}$$

where q is the heat entering or leaving the system and w is the work done on or by the system during the change of state. For an increment of the process the change is:

$$dU = dq - dw. \tag{4}$$

Equations (3) and (4) are statements of the *First Law of Thermodynamics*. By convention, heat entering the system and work done *by* the system are positive quantities. Equation (3) is remarkable in that, although the individual values of q and w are dependent on the path taken by the system between the initial and final states, their algebraic sum (which is the difference between U_2 and U_1) is independent of the process path. Thus integration of eq. (4) to obtain eq. (3) requires that the process path be known and that the process

be conducted reversibly.

The *Second Law of Thermodynamics* states that, for a reversible change of state, the integral of dq/T is independent of the process path. As one of the properties of a state function is that the difference between the values of the function in any two thermodynamic states is independent of the process path taken by the system in moving between the two states, the term dq/T is the differential of a state function. The state function *entropy*, S, is thus defined as:

$$dS = dq_{rev} / T. \tag{5}$$

If change in volume against an external pressure is the only form of work performed during a reversible change of state of a closed system, the work performed is given by eq. (2), and substitution of eqs. (2) and (5) into eq. (4) gives:

$$dU = TdS - PdV. \tag{6}$$

Equation (6), which is a combination of the First and Second Laws of Thermodynamics, gives the variation of U (as the dependent variable) with S and V (as the independent variables).

From consideration of the difference between reversible and irreversible processes and the Second Law, eq. (6) gives the following criteria for thermodynamic equilibrium in a closed system of fixed composition:

(i) S is a maximum at constant U and V;

(ii) U is a minimum at constant S and V.

Equation (6) involves the extensive thermodynamic properties S and U as independent variables. Although it is possible to measure and, with sufficient ingenuity on the part of the experimenter, to control the volume of a system, experimental control of the entropy of a system is virtually impossible, and consequently the criteria for equilibrium obtained from eq. (6) are not of practical use. From the practical point of view it would be desirable to have an equation as simple in form as eq. (6) but in which the independent variables are the intensive properties P and T, both of which are amenable to experimental measurement and control. Such an equation would also provide a criterion for equilibrium in a constant pressure–constant temperature system.

1.2. Auxiliary thermodynamic functions

The required auxiliary state functions are generated by Legendre transformations of U. For example, in eq. (6), written as

$$U = U(S, V),$$

a Legendre transform, H, of U is obtained using:

$$-P = \left(\frac{\partial U}{\partial V}\right)_S = \frac{U - H}{V - 0}. \tag{7}$$

At constant S, the tangent to the variation of U with V passes through the points $U = U$, $V = V$ and $U = H$, $V = 0$. Rearrangement of eq. (7) gives:

$$H = U + PV,$$

which, on differentiation, gives:

$$dH = dU + PdV + VdP. \tag{8}$$

Substitution of eq. (6) into eq. (8) gives:

$$dH = TdS + VdP, \tag{9}$$

in which the extensive variable V has been replaced by the intensive variable P. The transform H is called the *enthalpy*.

Writing eq. (9) as

$$H = H(S, P),$$

a Legendre transform, G, of H is obtained as:

$$T = \left(\frac{\partial H}{\partial S}\right)_P = \frac{H - G}{S - 0} \tag{10}$$

or: $G = H - TS,$

which, on differentiation, gives:

$$dG = dH - TdS - SdT = -SdT + VdP, \tag{11}$$

in which the extensive variable S has been replaced by the intensive variable T. This transform, G, is called the *Gibbs free energy*. Being dependent on the independent variables T and P, the Gibbs free energy is the most useful of thermodynamic functions and provides the practical criterion that, at constant T and P, thermodynamic equilibrium is established when the Gibbs free energy is minimized.

A third Legendre transform yields the *Helmholtz free energy*, or work function A, defined as

$$A = U - TS.$$

In a multicomponent system containing n_1 moles of component 1, n_2 moles of component 2, n_i moles of component i, etc.:

$$G = G(T, P, n_1, n_2, ..., n_i)$$

and thus,

$$dG = \left(\frac{\partial G}{\partial T}\right)dT + \left(\frac{\partial G}{\partial P}\right)dP + \left(\frac{\partial G}{\partial n_1}\right)dn_1 + \ldots \left(\frac{\partial G}{\partial n_i}\right)dn_i \tag{12}$$

The derivative

$$\left(\frac{\partial G}{\partial n_i}\right)_{T, P, n_j}$$

is of particular significance and is called the *chemical potential*, μ_i, or the partial molar free energy, $\overline{G_i}$, of the component i. Thus, in view of eq. (11), eq. (12) can be written as

$$dG = -SdT + VdP + \sum \overline{G}_i dn_i, \tag{13}$$

and the equilibrium state of any system undergoing any type of reaction at constant temperature and pressure can be determined by application of this equation.

2. *Metallurgical thermochemistry*

2.1. The measurement of changes in enthalpy

In order to distinguish between the value of an extensive property of a system containing n moles and the molar value of the property, the former will be identified by the use of a prime ($'$), e.g., with respect to enthalpy, $H' = nH$.

From eqs. (5) and (9), for a process occurring reversibly at constant pressure P:

$$dH' = dq_P,$$

which, on integration, gives:

$$\Delta H' = q_P.$$

Thus, in a system undergoing a process in which the only work performed is the work of expansion or contraction against the constant pressure P, the change in enthalpy, $\Delta H'$, can be measured as the heat q_P entering or leaving the system during the constant pressure process. In the case of heat entering the system the process involves an increase in the temperature of the system and the *constant pressure molar heat capacity*, c_P, is defined as:

$$c_p = \frac{dq_p}{dT} = \left(\frac{\partial H}{\partial T}\right)_p. \tag{14}$$

The constant pressure molar heat capacity of a system can be measured by the methods of calorimetry. In metallurgical applications the measured values are fitted to an equation of the form

$$c_p = a + bT + cT^{-2}.$$

For example, the constant pressure molar heat capacity of solid silver varies with temperature in the range 298–1234 K as:

$$c_{p,Ag(s)} = 21.3 + 8.54 \times 10^{-3} T + 1.51 \times 10^{5} T^{-2} \text{ J/K mole}$$

and hence, from eq. (14), the difference between the molar enthalpy of solid Ag at a temperature T and the molar enthalpy at 298 K is

$$\Delta H = \int_{298}^{T} c_{P,Ag} \mathrm{d}T$$
$$= 21.3(T - 298) + 4.27 \times 10^{-3}\left(T^2 - 298^2\right)$$
$$- 1.51 \times 10^{5}\left(\frac{1}{T} - \frac{1}{298}\right) \mathrm{J/mole},$$

which is thus the quantity of heat required to raise the temperature of one mole of solid Ag from 298 K to T.

Transformation of a low-temperature phase to a high-temperature phase involves the absorption of the latent heat of the phase change, e.g., the transformation of one mole of silver from the solid to the liquid state at the normal melting temperature of 1234 K requires a heat input of 11.09 kJ. Thus at 1234 K the molar enthalpy of melting of Ag, ΔH_m, is

$$\Delta H_{m,Ag.1234\mathrm{K}} = H_{Ag(l),1234\mathrm{K}} - H_{Ag(s),1234\mathrm{K}} = 11.09\mathrm{kJ}.$$

The molar heat capacity of liquid Ag is independent of temperature, $c_{P,\mathrm{Ag(l)}} = 30.5$ J/K mole, and the difference between the molar enthalpy of liquid Ag at a temperature T and the molar enthalpy of solid Ag at 298 K is

$$H_{Ag(l),T} - H_{Ag(s),298\mathrm{K}} = \int_{298}^{1234} c_{p,Ag(s)} \mathrm{d}T + \Delta H_{m,Ag.1234\mathrm{K}} + \int_{1234}^{T} c_{p,Ag(l)} \mathrm{d}T.$$

As chemical reactions involve the absorption or evolution of heat, they also necessarily involve changes in enthalpy. For example, when conducted at *298* K, the oxidation reaction

$$2\mathrm{Ag}_{(s)} + \tfrac{1}{2}\mathrm{O}_{2(g)} = \mathrm{Ag_2O}_{(s)}$$

is accompanied by the evolution of 30.5 kJ of heat per mole of Ag_2O produced. Thus,

$$q = \Delta H = -30.5k\mathrm{J},$$

or the system existing as one mole of Ag_2O has an enthalpy of 30.5 kJ less than the system existing as two moles of Ag and half a mole of oxygen gas at 298 K.

As the enthalpies of substances are not measurable quantities, i.e., only changes in enthalpy can be measured (as the evolution or absorption of heat), it is conventional to designate a reference state in which the relative enthalpy is zero. This reference state is the elemental substance existing in its stable form at 298 K and $P = 1$ atm. In practice the designation of $P = 1$ atm is relatively unimportant as the enthalpies of condensed phases are not significantly dependent on pressure and the enthalpy of an ideal gas is independent of pressure. Thus, in the above example:

$$\Delta H_{298} = H_{\mathrm{Ag_2O(s)},298} - 2H_{\mathrm{Ag(s)},298} - \tfrac{1}{2} H_{\mathrm{O_2(g)},298}.$$

As $H_{Ag(s),298}$ and $H_{O_2(g),298}$ are arbitrarily assigned values of zero, the relative molar enthalpy of Ag_2O at 298 K is simply equal to the experimentally-measured molar heat of formation of Ag_2O at 298 K. At any other temperature T:

$$\begin{aligned}\Delta H_T &= H_{Ag_2O,T} - 2H_{Ag,T} - \tfrac{1}{2} H_{O_2,T} \\ &= H_{Ag_2O,298} + \int_{298}^{T} c_{p,Ag_2O} dT - 2H_{Ag,298} - 2\int_{298}^{T} c_{p,Ag} dT \\ &\quad - \tfrac{1}{2} H_{O_2,298} - \tfrac{1}{2}\int_{298}^{T} c_{p,Ag} dT \\ &= \Delta H_{298} + \int_{298}^{T} \Delta c_p dT,\end{aligned}$$

where

$$\Delta c_p = c_{p,Ag_2O} - 2c_{p,Ag} - \tfrac{1}{2} c_{p,O_2}.$$

The enthalpy–temperature diagram for the oxidation of silver is shown in fig. 1.

2.2. The measurement of entropy

From eqs. (5) and (14), we find:

$$dS = \frac{dq_p}{T} = \frac{c_p dT}{T}.$$

Thus, the variation of entropy with temperature at constant pressure is obtained from measured heat capacities as

$$S_T = S_0 + \int_0^T \frac{c_p}{T} dT.$$

Nernst's heat theorem, which is also known as the *Third Law of Thermodynamics*, states that all substances at complete internal equilibrium have zero entropy at 0 K, i.e., $S_0 = 0$. Thus, in contrast to enthalpies, the entropies of substances have absolute values.

According to Gibbs, entropy is a measure of the degree of disorder in a system. Thus the entropy of the gaseous state is greater than that of the liquid state, which, in turn, is greater than that of the solid state. The transformation of a solid to a liquid at the normal melting temperature, T_m, involves the absorption of ΔH_m per mole. Thus, at T_m, the molar entropy of the liquid exceeds that of the solid by the molar entropy of fusion, ΔS_m, given by eq. (5) as:

$$\Delta S_m = \Delta H_m / T_m.$$

This corresponds with the fact that the liquid state is more disordered than the solid state, and ΔS_m is a measure of the difference in degree of order. For simple metals, with similar crystal structures and similar liquid structures, ΔS_m lies in the range 8–16 J/K. This correlation is known as *Richard's rule*. Similarly, at the normal boiling temperature, T_b, the molar entropy of boiling, ΔS_b, is obtained from the molar heat of boiling as:

References: p. 469.

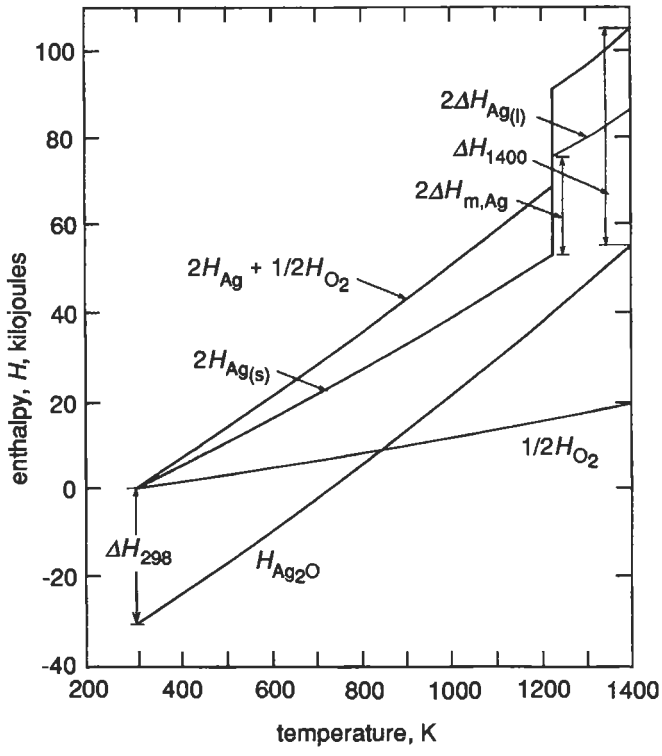

Fig. 1. The enthalpy–temperature diagram for the reaction $2Ag + \frac{1}{2}O_2 = Ag_2O$.

$$\Delta S_b = \Delta H_b / T_b.$$

For simple metals $\Delta S_b \approx 88$ J/K, which indicates that the difference in disorder between the gaseous state at 1 atm pressure and the liquid state significantly exceeds the corresponding difference between the liquid and solid states. The correlation $\Delta H_b = 88 T_b$ is known as *Trouton's rule*.

Although the degrees of disorder, and hence the entropies of condensed states, are not noticeably dependent on pressure, the entropy of a gas is a significant function of pressure. As the internal energy, U', of an ideal gas is dependent only on T, an isothermal compression of an ideal gas from P_1 to P_2 does not involve a change in U'. Thus, from eq. (3), the work of compression, w, equals the heat transferred from the gas to the isothermal surroundings at the temperature T. This transfer of heat from the gas decreases its entropy by the amount

$$\Delta S' = \frac{q}{T} = \frac{w}{T} = \int_1^2 \frac{P \mathrm{d}V'}{T},$$

which, from eq. (1), gives:

$$\Delta S' = \int_1^2 \frac{nR\,dV}{V} = -\int_1^2 nR\,d\ln P.$$

Thus

$$S_2' - S_1' = nR\ln(P_1/P_2),$$

which corresponds with the fact that a gas at high pressure is a less disordered state than a gas at low pressure.

As changes in entropy are caused by the transfer of heat, chemical reactions involving heat changes necessarily involve changes in entropy. At 298 K and 1 atm pressure, the molar entropies of $Ag_{(s)}$, $O_{2(g)}$ and $Ag_2O_{(s)}$ are 42.7, 205 and 122 J/K, respectively. Thus the entropy change for the oxidation

$$2Ag_{(s)} + \tfrac{1}{2}O_{2(g)} = Ag_2O_{(s)}$$

at 298 is:

$$\Delta S = 122 - (2 \times 42.7) - (0.5 \times 205) = -65.9\ \text{J/K mole}.$$

This can be viewed in two ways: (i) the entropy decrease is due to the loss of the heat of oxidation from the reacting system, or (ii) the degree of disorder in the system existing as one mole of Ag_2O is less than that when the system exists as two moles of Ag and half a mole of oxygen gas at 1 atm pressure.

The variation, with temperature, of the entropy change for the reaction is determined by the heat capacities of the reactants and products as:

$$\Delta S_T = \Delta S_{298} + \int_{298}^{T} (\Delta c_p/T)dT$$

The entropy–temperature diagram corresponding to fig. 1 is shown in fig. 2.

From the definition of Gibbs free energy, eq. (10), the change in Gibbs free energy due to a chemical reaction occurring at a temperature T, ΔG_T, is

$$\begin{aligned}\Delta G_T &= \Delta H_T - T\Delta S_T \\ &= \Delta H_{298} + \int_{298}^{T} \Delta c_p dT - T\Delta S_{298} - T\int_{298}^{T} (\Delta c_p/T)dT.\end{aligned} \tag{15}$$

Thus, the variation of the change in Gibbs free energy with temperature can be determined from measurement of the variation, with temperature, of the constant pressure molar heat capacities of the reactants and products and measurement of the enthalpy change of the reaction at one temperature. For the oxidation of solid silver, such data give

$$\begin{aligned}\Delta G_T = &-34200 + 87.9T - 1.76T\ln T - 10.8 \times 10^{-3}T^2 \\ &+ 3.2 \times 10^5 T^{-1}\ \text{J/mole}\ Ag_2O.\end{aligned} \tag{16}$$

References: p. 469.

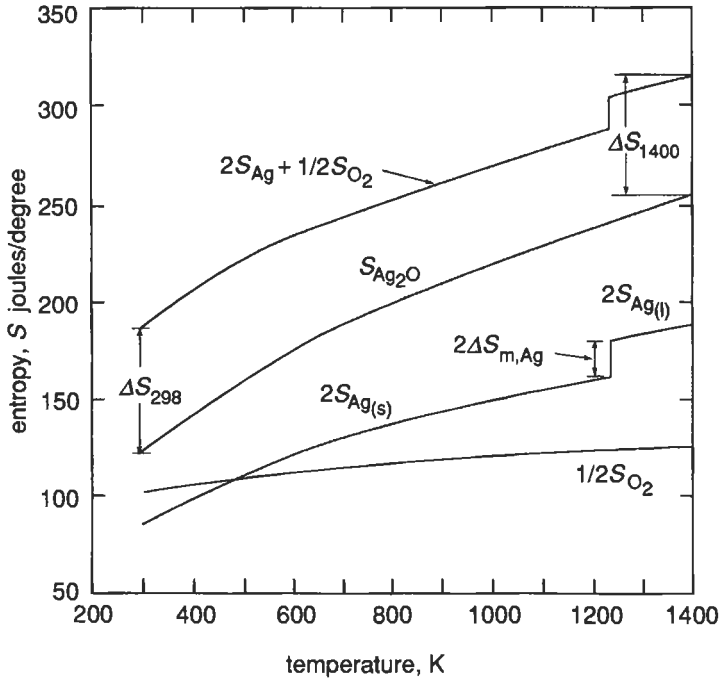

Fig. 2. The entropy–temperature diagram for the reaction $2Ag + \frac{1}{2}O_2 = Ag_2O$.

3. *Phase equilibrium in a one-component system*

At constant T and P the equilibrium state is that in which the Gibbs free energy has its minimum possible value. In a one-component system the states of existence available are the gaseous and liquid states and the various allotropic or polymorphic forms of the solid state. At any T and P the state with the lowest Gibbs free energy is the stable state. For the transformation

solid $\rightarrow$ liquid:

$$\Delta G_m(P,T) = G_{(l)}(P,T) - G_{(s)}(P,T) = \Delta H_m(P,T) - T\Delta S_m(P,T). \tag{17}$$

If ΔG_m is negative, the transformation decreases the Gibbs free energy of the system and hence the liquid is stable relative to the solid. Conversely, if ΔG_m is positive the solid is stable relative to the liquid. As absolute values of enthalpy cannot be measured it follows that absolute values of Gibbs free energy cannot be measured. Thus only changes in G can be measured.

The solid and liquid phases coexist in equilibrium with one another in that state at which $\Delta G_m = 0$, i.e., where $G_{(l)} = G_{(s)}$. From eq. (15), at any pressure P this equilibrium occurs at the temperature T_m given by

$$T_m = \Delta H_m / \Delta S_m,$$

and hence T_m is the equilibrium melting temperature of the solid at the pressure P. From eq. (10), G is decreased by decreasing H and increasing S and hence nature prefers states of low enthalpy and high entropy. As $H_{(l)} > H_{(s)}$ and $S_{(l)} > S_{(s)}$ the enthalpy contribution to G favors the solid as the stable state and the entropy contribution favors the liquid as the stable state. In eq. (17) the entropy contribution to ΔG is temperature–dependent and the enthalpy contribution is not. Thus, at high temperatures the former contribution dominates, at low temperatures the latter contribution dominates, and at a unique temperature T_m the two contributions cancel to make $\Delta G = 0$.

For the two-phase equilibrium to exist,

$$G_{(l)} = G_{(s)},$$

and maintenance of the two-phase equilibrium with variation in T and P requires that T and P be varied in such a manner that

$$dG_{(l)} = dG_{(s)}$$

or, from eq. (11), such that

$$-S_{(l)}dT + V_{(l)}dP = -S_{(s)}dT + V_{(s)}dP,$$

i.e.,

$$(dP / dT)_{eq} = \left(S_{(l)} - S_{(s)}\right) / \left(V_{(l)} - V_{(s)}\right) = \Delta S_m / \Delta V_m$$

As equilibrium between the two phases is maintained, $\Delta H_m = T\Delta S_m$:

$$\left(dP/dT\right)_{eq} = \Delta H_m / T\Delta V_m. \tag{18}$$

Equation (18) is the *Clapeyron equation*, which, on integration, gives the variation of T and P required for maintenance of the two-phase equilibrium. Strictly, integration requires knowledge of the pressure and temperature dependences of ΔH_m and ΔV_m. However, for relatively small departures from the state $P = 1$ atm, T_m, ΔH_m and ΔV_m can be taken as constants, in which case:

$$P_2 - P_1 = \frac{\Delta H_m}{\Delta V_m} \ln\left(\frac{T_2}{T_1}\right).$$

Equation (18) can be applied to condensed phase–vapor phase equilibria by making the approximation $\Delta V = V_{(v)} - V_{(\text{condensed phase})} \approx V_{(v)}$ and assuming ideal behavior of the vapor phase, i.e., $V_{(v)} = RT/P$, i.e.,

$$\left(dP/dT\right)_{eq} = \frac{P\Delta H_b}{RT^2}. \tag{19}$$

Equation (19) is the *Clausius–Clapeyron equation.*

References: p. 469.

If ΔH_b (the molar enthalpy of boiling) is not a function of temperature (which requires $c_{p(v)} = c_{p(l)}$), integration of eq. (19) gives

$$\ln P = -\frac{\Delta H_b}{RT} + \text{const.},$$

and if ΔH_b is a linear function of T (which requires that Δc_p be independent of temperature) given by $\Delta H_{b,T} = \Delta H_0 + \Delta c_p T$, integration gives

$$\ln P = -\frac{\Delta H_0}{RT} + \frac{\Delta c_p}{R} \ln T + \text{const.}$$

as either (i) the variation of the saturated vapor pressure with temperature or (ii) the variation of the equilibrium boiling temperature with pressure. Experimentally measured vapor pressures are normally fitted by an equation of the type

$$\ln P = -A/T + B \ln T + C.$$

The solid, liquid and vapor states exist on surfaces in G–T–P space. The solid- and liquid-surfaces intersect at a line (along which $G_{(l)} = G_{(s)}$) and projection of this line onto the basal P–T plane of the G–T–P diagram gives the pressure dependence of T_m. Similarly the vapor- and liquid-surfaces intersect at a line, projection of which onto the basal P–T plane gives the variation, with temperature, of the saturated vapor pressure of the liquid. Similar projection of the line of intersection of the surfaces for the solid and vapor states gives the variation, with temperature, of the saturated vapor pressure of the solid. The three lines of two-phase equilibrium in G–T–P space intersect at a point, called the *triple point*, at which all three phases are in equilibrium with one another. Consideration of the geometry of the intersections of the surfaces in G–T–P space shows that, in a one-component system, a maximum of three phases can exist in equilibrium. Alternatively, as the three phases co-exist in equilibrium at fixed values of T and P the equilibrium is invariant, i.e., has no degrees of freedom. The phase diagram for H_2O is shown in fig. 3 and a schematic representation of the section of G–T–P space at 1 atm pressure is shown in fig. 4. In fig. 4, the slope of any line at any point is $-S$ for that state and hence the "steepness" of the lines increases in the order solid, liquid, vapor. Also the curvatures of the lines are $(\partial^2 G/\partial T^2)_p = -(\partial S/\partial T)_p = -c_p/T$.

4. *Chemical reaction equilibrium*

From eq. (13), at constant T and P, the Gibbs free energy varies with composition in a chemically reacting system as

$$dG' = \sum \overline{G}_i \, dn_i.$$

The reaction proceeds spontaneously in that direction which involves a decrease in Gibbs free energy, and reaction equilibrium is attained when, thereby, the Gibbs free energy is minimized, i.e., when $dG' = 0$.

Consider the water–gas reaction

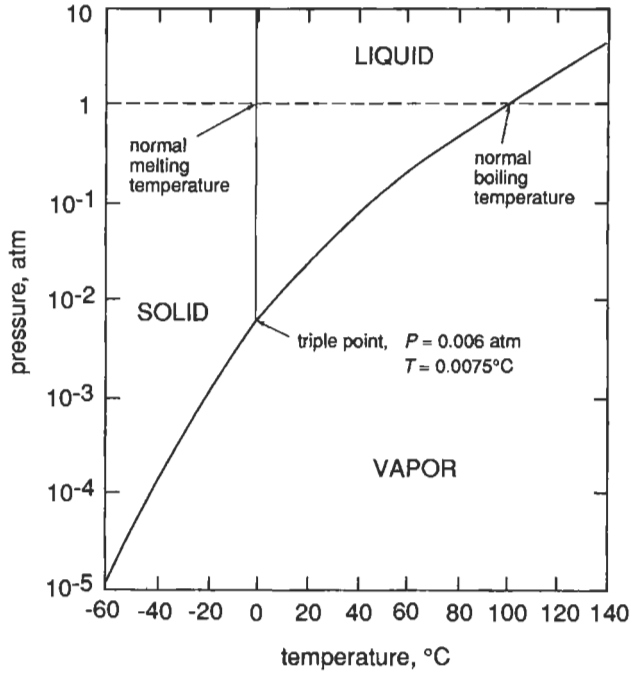

Fig. 3. The phase diagram for H_2O.

$$H_2O_{(g)} + CO_{(g)} = H_{2(g)} + CO_2.$$

At equilibrium:

$$dG = \overline{G}_{H_2} dn_{H_2} + \overline{G}_{CO_2} dn_{CO_2} - \overline{G}_{H_2O} dn_{H_2O} - \overline{G}_{CO} dn_{CO} = 0$$

or, in view of the stoichiometry requirement

$$-dn_{H_2O} = -dn_{CO} = dn_{H_2} = dn_{CO_2}:$$

$$dG = \left(\overline{G}_{H_2} + \overline{G}_{CO_2} - \overline{G}_{H_2O} - \overline{G}_{CO}\right) dn_{H_2} = 0$$

Thus, at equilibrium:

$$\left(\overline{G}_{H_2} + \overline{G}_{CO_2}\right) = \left(\overline{G}_{H_2O} + \overline{G}_{CO}\right). \tag{20}$$

The isothermal transfer of a mole of ideal gas i from the pure state at the pressure P_i and temperature T to an ideal gas mixture at the *partial pressure* p_i involves a change in Gibbs free energy:

$$\Delta G = \overline{G}_i - G_i = RT \ln\left(p_i / P_i\right). \tag{21}$$

References: p. 469.

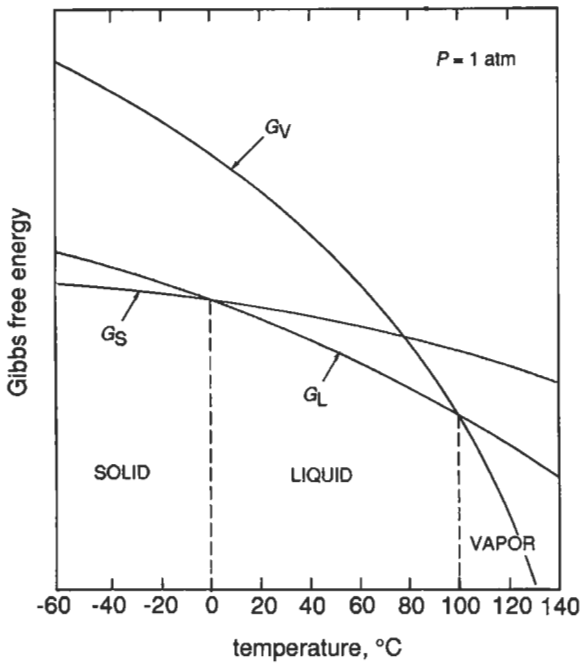

Fig. 4. Schematic representation of the variations of $G_{(s)}$, $G_{(l)}$ and $G_{(v)}$ with temperature at $P = 1$ atm for H_2O.

Again, as only changes in Gibbs free energy can be measured, it is convenient to select a standard state for the gas and consider the Gibbs free energy of the gas in any other state in terms of the difference between the free energy of the gas in this state and the free energy of the gas in the standard state. The standard state for an ideal gas at the temperature T is the pure gas at 1 atm pressure and in this state the Gibbs free energy is the standard free energy, designated G^0. Thus eq. (21) can be written as:

$$\overline{G}_i = G_i^0 + RT \ln p_i. \tag{22}$$

Substitution of eq. (22) into eq. (20) and rearrangement gives:

$$\left(G^0_{H_2} + G^0_{CO_2} - G^0_{H_2O} - G^0_{CO}\right) = -RT \ln \frac{p_{H_2} p_{CO_2}}{p_{H_2O} p_{CO}}. \tag{23}$$

Being the difference between the standard free energies of the products and the standard free energies of the reactants, the left-hand side of eq. (23) is termed the *standard free energy* for the reaction at the temperature T, ΔG_T^0, and, being dependent only on T, it has a definite fixed value at any T. Consequently the quotient of the partial pressures of the reactants and products occurring in the logarithm term on the right-hand side of eq. (23) has a fixed value at any T. This term is called the *equilibrium constant*, K_p, and hence the equilibrium state in any reacting system is such that

$$\Delta G_T^0 = -RT \ln K_p. \tag{24}$$

For the general reaction

$$aA + bB = cC + dD: \quad K_p = \frac{p_C^c p_D^d}{p_A^a p_B^b}.$$

Dalton's law of partial pressures in an ideal gas mixture gives

$$p_i = X_i P,$$

where X_i, being the ratio of the number of moles of i in the gas to the total number of moles of all species, is the *mole fraction* of i in the gas and P is the total pressure of the gas. Thus

$$K_p = \frac{X_C^c X_D^d}{X_A^a X_B^b} P^{c+d-a-b} = K_X P^{c+d-a-b}, \tag{25}$$

where K_X is the equilibrium constant expressed in terms of the mole fractions of the reactants and products occurring at reaction equilibrium. From the definition of ΔG_T^0, K_p is independent of pressure and hence, from eq. (25), K_X is only independent of pressure if $c+d-a-b=0$.

From eqs. (24) and (15):

$$\Delta G_T^0 = -RT \ln K_p = \Delta H_T^0 - T\Delta S_T^0.$$

Thus

$$\ln K_p = -\frac{\Delta H_T^0}{RT} + \frac{\Delta S_T^0}{R},$$

$$\text{or} \quad \frac{\partial \ln K_p}{\partial T} = \frac{\Delta H_T^0}{RT^2}.$$

For the water–gas reaction:

$$CO + H_2O = CO_2 + H_2;$$

$$\Delta G_T^0 = -36400 + 32.0T \text{ J/mole};$$

thus

$$K_p = \exp\left(\frac{36400}{8.3144T}\right)\exp\left(\frac{-32.0}{8.3144}\right).$$

The reaction of a moles of CO with b moles of H_2O produces x moles of each CO_2 and H_2 and leaves $(a - x)$ moles of CO and $(b - x)$ moles of H_2. Thus at any point along the reaction coordinate in a reacting mixture at the constant pressure P:

References: p. 469.

$$p_{CO} = \frac{a-x}{a+b}P, \qquad p_{H_2O} = \frac{b-x}{a+b}P, \qquad \text{and} \qquad p_{CO_2} = p_{H_2} = \frac{x}{a+b}P,$$

and at reaction equilibrium:

$$\frac{p_{CO_2}p_{H_2}}{p_{CO}p_{H_2O}} = \frac{x^2}{(a-x)(b-x)} = K_p = \exp\left(\frac{36400}{8.3144T}\right)\exp\left(\frac{-32.0}{8.3144}\right)$$

If one or more of the reactants and/or products occurs in a condensed state the attainment of equilibrium involves both phase and reaction equilibrium. For example, at a temperature T the equilibrium

$$2Ag_{(s)} + \tfrac{1}{2}O_{2(g)} = Ag_2O_{(s)} \tag{26}$$

requires the establishment of the phase equilibria

$$Ag_{(s)} = Ag_{(v)} \quad \text{and} \quad Ag_2O_{(s)} = Ag_2O_{(v)},$$

and, in the vapor or gas phase, requires establishment of the reaction equilibrium

$$2Ag_{(v)} + \tfrac{1}{2}O_{2(g)} = Ag_2O_{(v)}. \tag{27}$$

Conditions for the phase equilibria are $p_{Ag} = p^0_{Ag}$ (the saturated vapor pressure of solid silver at temperature T) and $p_{Ag_2O} = p^0_{Ag_2O}$ (the saturated vapor pressure of solid Ag_2O at temperature T), and thus, as the equilibrium constant K for the vapor phase reaction, given by eq. (27), has a fixed value at temperature T, the equilibrium oxygen pressure, p_{O_2}, is uniquely fixed by:

$$K = \frac{p^0_{Ag_2O}}{\left(p^0_{Ag}\right)^2 p^{1/2}_{O_2}}.$$

Alternatively, reaction equilibrium in the vapor phase requires that:

$$2\overline{G}_{Ag(v)} + \tfrac{1}{2}\overline{G}_{O_{2(g)}} = \overline{G}_{Ag_2O(v)}, \tag{28}$$

and the two-phase equilibria require that:

$$\overline{G}_{Ag(v)} = \overline{G}_{Ag(s)} \tag{29}$$

and

$$\overline{G}_{Ag_2O(v)} = \overline{G}_{Ag_2O(s)}. \tag{30}$$

From eq. (11), at constant T, $dG = VdP$, and hence eq. (29) can be written as:

$$G^0_{Ag(v)} + RT\ln p^0_{Ag} = G^0_{Ag(s)} + \int_1^{p^0_{Ag}} V_{Ag(s)}dP, \tag{31}$$

where $G^0_{Ag(s)}$ is the standard molar free energy of solid Ag at temperature T. The integral

on the right-hand side of eq. (31) is negligibly small and hence eq. (31) can be written as:

$$G^0_{Ag(v)} + RT \ln p^0_{Ag} = G^0_{Ag(s)}. \tag{32}$$

Similarly, eq. (30) can be written as:

$$G^0_{Ag_2O(v)} + RT \ln p^0_{Ag_2O} = G^0_{Ag_2O(s)}. \tag{33}$$

Substitution of eqs. (32) and (33) into eq. (28) gives:

$$2G^0_{Ag(s)} + \tfrac{1}{2} G^0_{O_2(g)} + RT \ln p^{1/2}_{O_2} = G^0_{Ag_2O(s)}.$$

or
$$\Delta G^0_T = -RT \ln \frac{1}{p^{1/2}_{O_2(eq.T)}}, \tag{34}$$

where ΔG^0_T is the standard free energy change for the reaction given by eq. (26) and $p_{O_2(eq,T)}$ is the value of p_{O_2} required for equilibrium between $Ag_{(s)}$, $Ag_2O_{(s)}$ and oxygen gas at temperature T. The variations of ΔH^0_T, $-T\Delta S^0_T$ and ΔG^0_T [given by eq. (16)] are shown in fig. 5. Thus, from eq. (34), $p_{O_2(eq.\,485\,K)} = 1$ atm, at which temperature $\Delta G^0 = 0$. At $T < 485$ K, ΔG^0_T is a negative quantity and hence $p_{O_2(eq,T)} < 1$ atm. At $T > 485$ K, ΔG^0_T is a positive quantity and hence $p_{O_2(eq.T)} > 1$ atm.

5. *Ellingham diagrams*

In 1944 ELLINGHAM published diagrams showing the variation, with temperature, of the standard free energies of formation of a number of oxides and sulfides, and pointed out that these diagrams "would show at a glance the relative stabilities of the various substances within a given class at any temperature, and would thus indicate, in a direct fashion, the range of conditions required for their reduction to the corresponding elements. It would provide, in fact, what might be described as a ground plan of metallurgical possibilities with respect to the reduction of compounds of the specified class". Such diagrams, which are now available for a wide range of classes of compounds, are known as *Ellingham diagrams*, and the Ellingham diagram for oxides is shown in fig. 6. (See also ch. 14, § 2.1).

In order to facilitate comparison of the stabilities of the various oxides, the standard free energies are for the reaction

$$(2x/y)M + O_2 = (2/y)M_xO_y,$$

i.e., for reactions involving the consumption of one mole of O_2. By choosing this basis:

$$\Delta G^0_T = RT \ln p_{O_2(eq.T)},$$

and hence, in addition to being a plot of ΔG^0_T versus temperature, the Ellingham diagram is a plot of the variation, with temperature, of the oxygen pressure, $p_{O_2(eq,T)}$, required for equilibrium between the metal and its oxide. The free energy change for the change of state $O_2(T, P = 1$ atm$) \rightarrow O_2(T, P = p_{O_2})$ is:

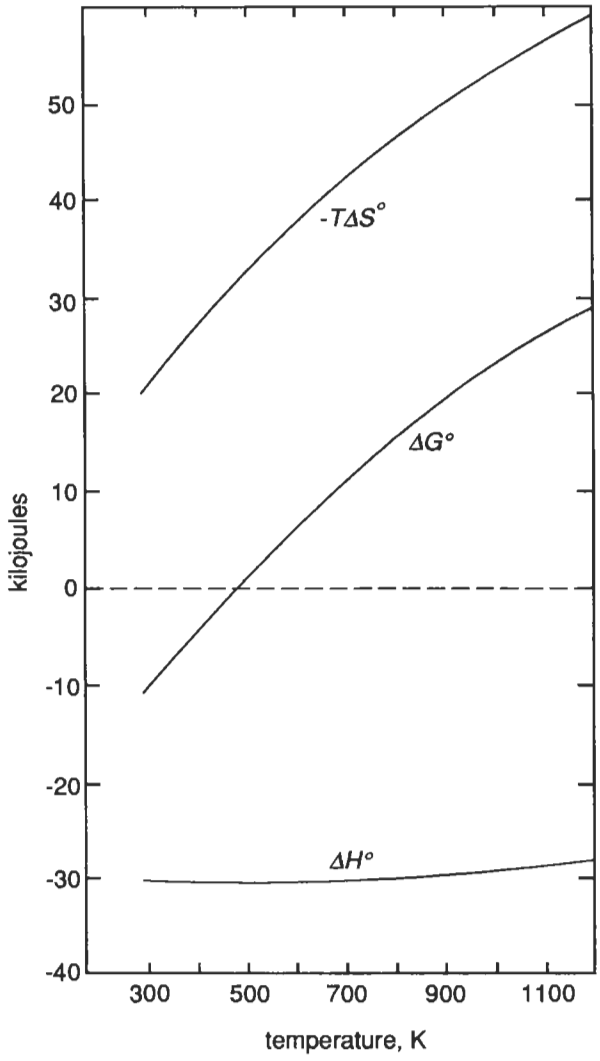

Fig. 5. The variations of ΔH_T^0, $-T\Delta S_T^0$ and ΔG_T^0 with temperature for the reaction $2Ag + \frac{1}{2}O_2 = Ag_2O$.

$$\Delta G_T = RT \ln p_{O_2},$$

and thus, in the Ellingham diagram, lines of constant p_{O_2} radiate from the origin, $\Delta G^0 = 0$, $T = 0$ K, with slopes of $R \ln p_{O_2}$. Consequently, a nomographic scale of p_{O_2} can be placed on the edges of the diagram and $p_{O_2(eq)}$ at any point on an Ellingham line is obtained as the reading on the nomographic scale which is collinear with the given point and the origin of the diagram. The Ellingham diagram is thus a stability diagram, in that any point in the diagram lying **above** the Ellingham line for a given oxide is a state in which $p_{O_2(T)} > p_{O_2(eq.\ T)}$

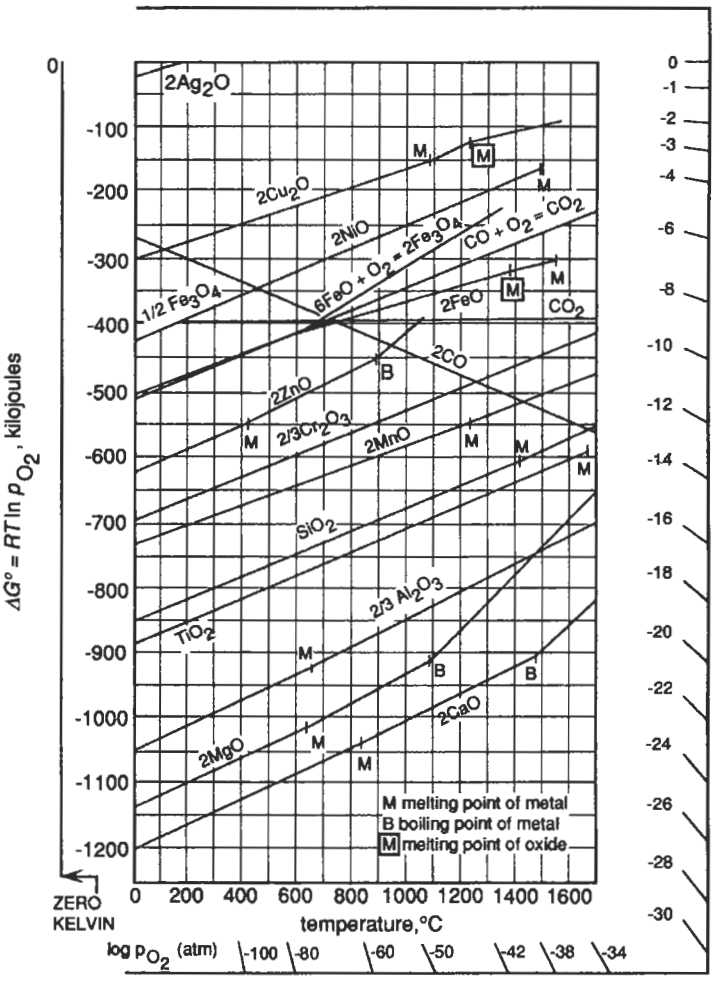

Fig. 6. The Ellingham diagram for several oxides.

and hence, in all states above the line the oxide is stable relative to the metal. Conversely, any point lying **below** the Ellingham line for the given oxide is a state in which $p_{O_2(T)} < p_{O_2(eq.\ T)}$ and hence, below the line, the metal is stable relative to the oxide. The Ellingham line thus divides the diagram into stability fields and, if it is required that a given oxide be reduced, the thermodynamic state must be moved from a point above the Ellingham line for the oxide to a point below the line, i.e., must be moved from a position within the oxide stability field to a position within the metal stability field.

The magnitude of ΔG_T^0 is a measure of the relative stability of the oxide and hence, with increasing stability, the Ellingham lines occur progressively lower in the diagram. Consequently, in principle, the element A can reduce the oxide B_xO_y, if, in the diagram,

References: p. 469.

the Ellingham line for A_xO_y, lies below that for B_xO_y.

Over the ranges of temperature in which no phase transitions occur the Ellingham lines are virtually linear, being given by

$$\Delta G_T^0 = A + BT.$$

In this expression A, the intercept of the line with the $T=0$ K axis, is identified with ΔH^0, the standard enthalpy change for the oxidation, and B, the slope of the line, is identified with $-\Delta S^0$, the standard entropy change for the reaction. The Ellingham lines for the oxidation of solid and liquid metals are more or less parallel with one another, with slopes corresponding to the disappearance of one mole of oxygen gas in the standard oxidation equation. Consequently, the stabilities of these oxides are determined primarily by the magnitudes of their enthalpies of formation.

At the temperature of a phase change the slope of the Ellingham line changes by an amount equal to the entropy change for the phase transition. The slope increases at the transition temperatures of the metal and decreases at the transition temperatures of the oxide. These changes in slope are most noticeable at normal boiling temperatures, e.g., at 1090°C the slope of the Ellingham line for MgO increases by 190.3 J/K, which is the entropy of boiling of 2Mg, and at 1484°C the slope of the Ellingham line for CaO increases by 174.2 J/K, the entropy of boiling of 2Ca.

Carbon is unique in that it forms two gaseous oxides, CO and CO_2, and the positions of the Ellingham lines for these oxides are of particular significance in extraction metallurgy. The Ellingham line for CO has a negative slope due to the fact that the oxidation

$$2C + O_2 = 2CO$$

involves the net production of one mole of gas, and, because the oxidation

$$C + O_2 = CO_2$$

does not involve a change in the number of moles of gas, the Ellingham line for CO_2 is virtually horizontal. The enthalpy change for the oxidation of C to form CO as $C + \frac{1}{2}O_2 = CO$ is −111 700 J and the enthalpy change for the oxidation of CO to CO_2 as $CO + \frac{1}{2}O_2 = CO_2$ is −282 400 J. Thus the standard enthalpy change for the Ellingham line for CO is $2 \times (-111700) = -223400$ J and the standard enthalpy change for the Ellingham line for CO_2 is $(-111700) + (-282400) = -394100$ J. Thus, on the basis that the stability of an oxide is determined primarily by the magnitude of ΔH^0, it would appear that CO_2 should be more stable than CO. However, as the Ellingham line for CO has a negative slope, which means that the stability of CO increases with increasing temperature, the Ellingham lines for the two oxides intersect. Consequently, although CO_2 is more stable than CO at lower temperature, the reverse is the case at higher temperatures. The gaseous phase in equilibrium with solid carbon is a CO–CO_2 mixture in which the ratio p_{CO}/p_{CO_2} increases with increasing temperature. For a total pressure of 1 atm, the equilibrium gas contains less than 1% CO at temperatures less than 400°C, contains less than 1% CO_2 at temperatures greater than 980°C, and is an equimolar mixture at 674°C. The "carbon

line" in the diagram, which is the continuum of states in which carbon is in equilibrium with a CO–CO_2 mixture at 1 atm pressure, follows the CO_2 Ellingham line up to about 400°C and then curves down gently to tangentially meet and join the Ellingham line for CO at about 1000°C. Along the carbon line the ratio p_{CO}/p_{CO_2} is fixed by the equilibrium

$$C + CO_2 = 2CO,$$

and, by virtue of the equilibrium

$$CO + \tfrac{1}{2}O_2 = CO_2$$

the oxygen pressure is also fixed. Thus the carbon line divides the other oxides into two classes, those with Ellingham lines which lie above the carbon line, and those with Ellingham lines which lie below the carbon line. With respect to the former class, the carbon line lies in the stability field of the metal and hence carbon is a potential reducing agent for these oxides, whereas, with respect to the latter class, the carbon line lies in the oxide stability field and hence carbon cannot reduce the oxide. Furthermore, if the Ellingham line for a metal oxide intersects the carbon line, the temperature of intersection is the minimum temperature at which the oxide may be reduced by carbon. Thus, for example, FeO cannot be reduced by carbon at temperatures less than 675°C.

Whether or not carbon can be used as a reducing agent is determined by the stability of any carbide phase which may form, i.e., by the sign of the standard free energy for formation of the carbide from metal and carbon. For example, in the Ellingham diagram the carbon line intersects with the Ellingham line for SiO_2 at 1676°C, and hence above this temperature liquid Si is stable relative to SiO_2 in the presence of C and its equilibrium CO–CO_2 gas mixture at 1 atm pressure. However, for the reaction

$$Si_{(l)} + C = SiC,$$

the standard free energy change is $\Delta G_T^0 = -122600 + 37.0T$ J and hence SiC is stable relative to liquid Si in the presence of carbon at 1676°C and $P = 1$ atm.

The stability fields in the system Si–O–C at 1676°C are shown in fig. 7 as functions of log p_{CO} and log p_{CO_2}. Line A is the variation of p_{CO} and p_{CO_2} required for the equilibrium

$$Si_{(l)} + 2CO_2 = SiO_2 + 2CO.$$

Line B is the corresponding variation required for the equilibrium

$$Si_{(l)} + 2CO = SiC + CO_2,$$

and line C is the variation for the equilibrium

$$SiC + 3CO_2 = SiO_2 + 4CO.$$

These lines divide the diagram into stability fields for Si, SiC and SiO_2 and meet at the values of p_{CO} and p_{CO_2} required for the four-phase equilibrium involving the three condensed phases Si, SiC and SiO_2 and the CO–CO_2 gas phase. Line D is the variation of p_{CO} and p_{CO_2} required for the equilibrium between carbon and the gas phase at 1676°C

References: p. 469.

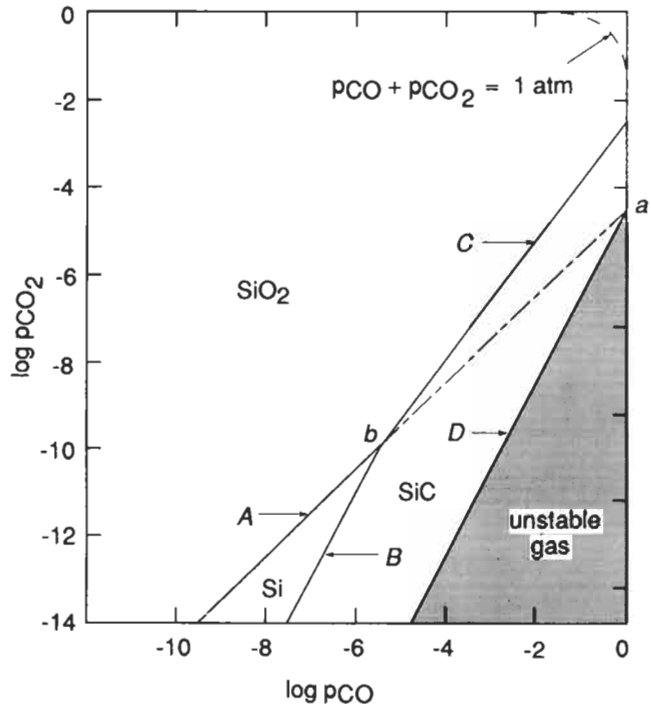

Fig. 7. The stability diagram for the system Si–O–C at 1949 K.

and, as such, represents the compositions of CO–CO_2 gas mixtures which are saturated with carbon. The field below line D is designated "unstable" gas, as any gas mixture in this field is supersaturated with carbon and hence will spontaneously undergo the carbon deposition reaction

$$2CO \rightarrow C_{(graphite)} + CO_2,$$

until, thereby, the composition of the gas lies on line D. The dashed line is the $(p_{CO} + p_{CO_2}) = 1$ atm isobar. Consequently, the system containing solid carbon and a gas phase at 1 atm pressure exists at the state **a**, and as this state is in the field of stability of SiC, SiO_2 is not reduced to Si by carbon at 1676°C. However, if the standard free energy for formation of SiC had been positive, lines B and C would have occurred below line D in the diagram and, as shown by the dashed–dotted extension of line A, the equilibrium Si–SiO_2–C would occur at the state **a**, which is the state of intersection of the carbon line with the Ellingham line for SiO_2 in the Ellingham diagram.

6. *The thermodynamic properties of solutions*

6.1. Mixing processes

The relationship between entropy and the "degree of mixed-up-ness" is quantified by Boltzmann's expression as:

$$S' = k \ln W,$$

where S' is the entropy of the system and W is the number of microstates available to the system*. In the simplest of mixing processes, W is the number of distinguishable arrangements of the constituent atoms on the sites available to them. Consider the mixing of N_A atoms of solid A and N_B atoms of solid B as the process:

$$\text{state 1} \rightarrow \text{state 2},$$

i.e., unmixed A and B $\rightarrow$ mixed A and B.

In state 1, interchange of the positions of A atoms in the crystal of pure A and/or interchange of the positions of B atoms in the crystal of pure B does not produce a distinguishably different arrangement and hence W sub1 = 1. However, the N_A atoms of A and N_B atoms of B can be placed on the $N_A + N_B$ lattice sites of the mixed crystal (state 2) in $(N_A + N_B)!$ ways, of which $(N_A + N_B)!/N_A!N_B!$ are distinguishable. Thus

$$W_2 = \frac{(N_A + N_B)!}{N_A!\,N_B!}.$$

Thus, for the process:

$$\Delta S' = S'_2 - S'_1 = k \ln W_2 - k \ln W_1 = k \ln \frac{(N_A + N_B)!}{N_A!\,N_B!}. \tag{35}$$

If N_A and N_B are sufficiently large numbers, *Stirling's theorem* can be applied as

$$\ln \frac{(N_A + N_B)!}{N_A!\,N_B!} = (N_A + N_B)\ln(N_A + N_B) - N_A \ln N_A - N_B \ln N_B$$

$$= -N_A \ln X_A - N_B \ln X_B,$$

where, respectively, X_A and X_B are the mole fractions of A and B in the mixed crystal.

Thus, the change in entropy, $\Delta S'^M$, due to mixing, is

$$\Delta S'^M = k \ln(N_A \ln X_A + N_B \ln X_B),$$

and, if $N_A + N_B = N_0$ (Avogadro's number) then the molar entropy of mixing is

* The equivalence between this definition of entropy and the definition in terms of heat flow (§1.1) is demonstrated in general terms in many texts; a particularly clear treatment is provided in ch. 2 of FAST's book (see bibliography).

References: p. 469.

$$\Delta S^M = -R\left(X_A \ln X_A + X_B \ln X_B\right). \tag{36}$$

This increase in entropy is caused by the increase in the number of spatial configurations made available to the system as a result of the mixing process and, hence, is *configurational* in origin. If there is no change in enthalpy on mixing, the Gibbs free energy change due to the mixing process is given by

$$\Delta G^M = -T\Delta S^M = RT\left(X_A \ln X_A + X_B \ln X_B\right). \tag{37}$$

Alternatively, consider the following. Consider that p_A^0 and p_B^0 are the saturated vapor pressures of pure A and pure B at temperature T and that p_A and p_B are the partial pressures of A and B exerted by the mixed crystal (or solid solution) of composition X_A at temperature T. Consider that one mole of A is isothermally evaporated from pure solid A to form A vapor at the pressure p_A^0, that the mole of A vapor is isothermally expanded to the pressure p_A and is then isothermally condensed into a large quantity of the solid solution. As the evaporation and condensation processes are conducted at equilibrium, they do not involve any change in Gibbs free energy and hence the change in Gibbs free energy for the three-step process is simply that caused by the change in pressure from p_A^0 to p_A, i.e.,

$$\Delta G = \overline{G}_{A(\text{in the solution})} - G^0_{A(\text{pure})} = RT \ln\left(p_A / p_A^0\right).$$

Similarly, for the corresponding three-step process for B,

$$\Delta G = \overline{G}_{B(\text{in the solution})} - G^0_{B(\text{pure})} = RT \ln\left(p_B / p_B^0\right). \tag{38}$$

Thus, for the mixing of n_A moles of A and n_B moles of B:

$$\begin{aligned}\Delta G' &= G'(\text{solution}) - G'(\text{unmixed A and B}) \\ &= \left(n_A \overline{G}_A + n_B \overline{G}_B\right) - \left(n_A G_A^0 + n_B G_B^0\right) \\ &= n_A\left(\overline{G}_A - G_A^0\right) + n_B\left(\overline{G}_B - G_B^0\right),\end{aligned}$$

which, from eqs. (37) and (38), can be written for one mole of solution as

$$\Delta G^M = RT\left[X_A \ln\left(p_A / p_A^0\right) + X_B \ln\left(p_B / p_B^0\right)\right]. \tag{39}$$

Comparison of eqs. (37) and (39) indicates that, if the mixing process does not involve a change in enthalpy,

$$p_A = X_A p_A^0 \quad \textit{and} \quad p_B = X_B p_B^0. \tag{40}$$

Equation (40) is an expression of *Raoult's Law* and a solution conforming with this behavior is said to exhibit Raoultian ideal behavior. If the energies of the pure states and the solution are considered to be the sums of the pair-wise bond energies between neighboring atoms, Raoultian ideal mixing requires that:

$$E_{AB} = (E_{AA} + E_{BB})/2, \tag{41}$$

where E_{AB}, E_{AA} and E_{BB} are the pair-wise bond energies of A–B, A–A and B–B pairs, respectively. If the condition given by eq. (41) is not met, the isothermal mixing process is accompanied by the evolution or absorption of heat, which, for mixing at constant pressure, represents a change in the enthalpy of the system. In such a situation random mixing of A and B atoms does not occur and hence the entropy of mixing is no longer given by eq. (36).

Any change in the enthalpy on mixing arises from a redistribution of the atoms among their quantized energy levels and this gives rise to a change in the *thermal* (as distinct from the configurational) component of the entropy of the system. Boltzmann's equation can be written as

$$S'_{total} = S'_{conf} + S'_{thermal} = k \ln (W_{conf} W_{thermal}),$$

where W_{conf} is the number of distinguishable ways in which the atoms can be distributed on the available sites and $W_{thermal}$ is the number of ways in which the energy of the system can be distributed among the particles. Thus, for the mixing process,

$$\Delta S' = k \ln \frac{W_{conf(2)} W_{thermal(2)}}{W_{conf(1)} W_{thermal(1)}},$$

and hence $\Delta S'$ is only given by eq. (35) if $W_{thermal(1)} = W_{thermal(2)}$, i.e., if no redistribution of the energy occurs, and hence no change in enthalpy occurs. This condition is required for Raoultian ideal mixing. If

$$|E_{AB}| > |(E_{AA} + E_{BB})/2|,$$

the solution exhibits a tendency towards *ordering*, i.e., towards maximizing the number of A–B contacts, and if

$$|E_{AB}| < |(E_{AA} + E_{BB})/2|,$$

the solution exhibits a tendency towards *clustering* or phase separation, i.e., towards minimizing the number of A–B contacts.

Configurational entropy is responsible for the occurrence of vacancies in metals. Consider a perfect single crystal containing N atoms on N lattice sites. If a single atom is removed from a lattice position within the crystal and is placed on the surface of the crystal, random placement of the vacancy on $N+1$ sites gives rise to a configurational entropy of

$$S = k \ln \frac{(N+1)!}{N!}.$$

This process involves an enthalpy change ΔH_v and, as the vibration frequencies of the nearest-neighbor atoms to the vacancy are altered, a change occurs in the thermal entropy, ΔS_{th}. Thus, for the formation of N_v vacancies,

$$\Delta G' = \Delta H' - T\Delta S'$$

$$= N_v \Delta H_v - N_v \Delta S_{th} T + kT \ln \frac{(N + N_v)!}{N! N_v!}$$

$$= N_v (\Delta H_v - N_v \Delta S_{th}) + kT \left[N \ln \frac{N}{N + N_v} + N_v \ln \frac{N_v}{N + N_v} \right]. \quad (42)$$

The formation of vacancies in an initially perfect crystal is thus a spontaneous process which proceeds until, thereby, the Gibbs free energy of the crystal is minimized, in which state

$$\frac{\partial \Delta G'}{\partial N_v} = 0.$$

From eq. (42), this condition occurs when

$$\frac{N_v}{N + N_v} = \exp\left(\frac{-\Delta H_v}{kT}\right) \exp\left(\frac{\Delta S_{th}}{k}\right).$$

The fraction of vacant sites in a crystal can be determined from simultaneous measurement of the thermal expansion of a sample, $\Delta l/l$, and the change in the lattice parameter, $\Delta a_0/a_0$, as measured by X-ray diffraction (see ch. 18, §2.2.2.2). As the former is influenced by both the increase in the average spacing between lattice planes and the creation of vacancies, and the latter is a measure only of the average spacing between planes, the increase in the fraction of vacant lattice sites is proportional to the difference between $\Delta l/l$ and $\Delta a_0/a_0$. Measurements of this type on aluminum give:

$$\frac{N_v}{N + N_v} = 11 \exp\left(\frac{-8820}{T}\right),$$

from which $\Delta H_v = 73.3$ kJ/mole and $\Delta S_v = 20$ J/K mole. At the melting temperature of 660°C this gives the fraction of vacant sites as 9×10^{-4}.

The thermodynamic properties of solutions which do not exhibit Raoultian ideal behavior are dealt with by introducing the concept of activity. The *activity*, a_i, of the component i in a solution is defined as:

$$a_i = p_i / p_i^0 \quad (43)$$

and, from eq. (40), is equal to the mole fraction, X_i, in a Raoultian ideal solution. Thus, the molar free energy of formation of a binary A–B solution, ΔG^M, is given by

$$\Delta G^M = RT(X_A \ln a_A + X_B \ln a_B). \quad (44)$$

The free energy of formation of n moles of a solution, $\Delta G'^M$, can be written in terms of the partial molar free energies of mixing of the components as:

$$\Delta G'^{M} = n_A \Delta \overline{G}_A^M + n_B \Delta \overline{G}_B^M$$

or, the molar free energy, ΔG^M, as:

$$\Delta G^M = X_A \Delta \overline{G}_A^M + X_B \Delta \overline{G}_B^M, \tag{45}$$

where $\Delta G_i^M = \overline{G}_i - G_i^0$ (the difference between the molar free energy of i in the solution and the molar free energy of pure i) is termed the *partial molar free energy of mixing* of i. The partial molar free energy of mixing of i and the molar free energy of formation of the solution are related as:

$$\Delta \overline{G}_i^M = \Delta G^M + (1 - X_i)\left(\frac{\partial \Delta G^M}{\partial X_i}\right)_{T,P}. \tag{46}$$

Comparison of eqs. (39) and (45) shows that in a Raoultian ideal solution

$$\Delta \overline{G}_i^M = RT \ln X_i,$$

and comparison of eqs. (39) and (44) shows that, generally,

$$\Delta \overline{G}_i^M = RT \ln a_i. \tag{47}$$

A typical ideal variation of ΔG^M with composition is shown in fig. 8. In this figure the tangent drawn to the free energy curve at any composition intercepts the $X_A = 1$ axis at $\Delta \overline{G}_A^M$ and intercepts the $X_B = 1$ axis at $\Delta \overline{G}_B^M$. This construction is a geometric representation of eq. (46). Also, as $X_i \to 0$, $a_i \to 0$ and hence, from eq. (47), $\Delta \overline{G}_i^M \to -\infty$, i.e., the vertical axes are tangents to the curve at its extremities. The relationship between the variations of the tangential intercepts with composition is given by the *Gibbs–Duhem equation*:

$$X_A \mathrm{d} \ln a_A + X_B \mathrm{d} \ln a_B = 0. \tag{48}$$

Usually, the activity of only one component of a solution is amenable to experimental measurement, and the activity of the other component, and hence ΔG^M, are obtained from integration of the Gibbs–Duhem equation.

The *activity coefficient*, γ_i, is defined as $\gamma_i = a_i / X_i$ and hence eq. (44) can be written as:

$$\Delta G^M = RT(X_A \ln X_A + X_B \ln X_B) + RT(X_A \ln \gamma_A + X_B \ln \gamma_B). \tag{49}$$

The first term on the right-hand side of eq. (49) is the molar free energy of formation of a Raoultian ideal solution, $\Delta G^{M,id}$, and the second term, being the difference between the actual molar free energy of solution and the ideal value, is called the *excess molar free energy of mixing*, G^{xs}.

6.2. Regular solution behavior

A *regular solution* is one which has an ideal entropy of mixing and a nonzero enthalpy of mixing. The properties of such a solution are best examined by means of a

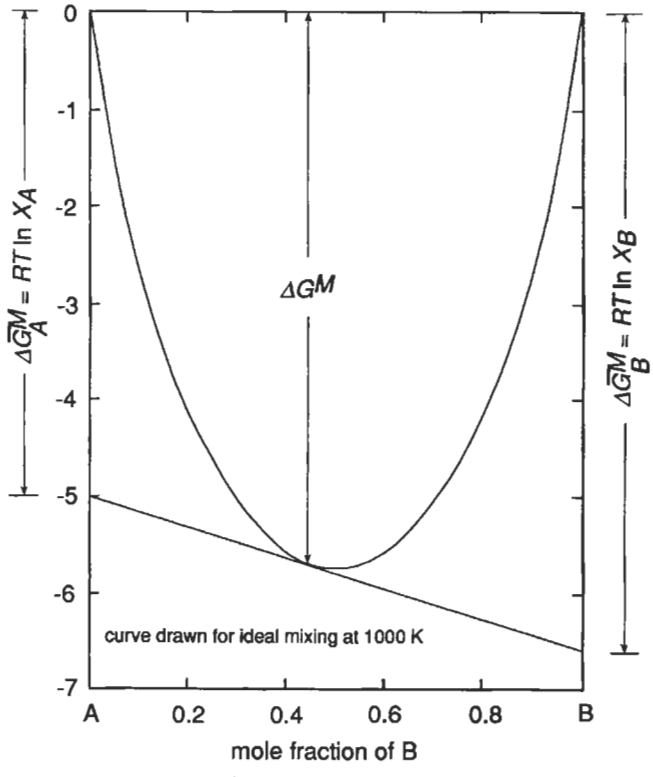

Fig. 8. The variation of ΔG^M with composition in an ideal system at 1000 K.

simple statistical model of the mixing of N_A atoms of A and N_B atoms of B. If the internal energy, U', of the solution can be taken as the sum of the pair-wise bond energies then

$$U' = P_{AB}E_{AB} + P_{AA}E_{AA} + P_{BB}E_{BB}, \tag{50}$$

where P_{ij} is the number of i–j pairwise bonds and E_{ij} is the energy of the bond relative to i and j at infinite separation. If the coordination number of an atom is z, the number of bonds involving A atoms, $N_A z$, is given by $2P_{AA} + P_{AB}$ and, similarly, the number of bonds involving B atoms, $N_B z$, is given by $2P_{BB} + P_{AB}$. Thus:

$$P_{AA} = \tfrac{1}{2} N_A z - \tfrac{1}{2} P_{AB} \text{ and } P_{BB} = \tfrac{1}{2} N_B z - \tfrac{1}{2} P_{AB},$$

substitution of which into eq. (50) gives:

$$U' = \tfrac{1}{2} N_A z E_{AA} + \tfrac{1}{2} N_B z E_{BB} + P_{AB}\left[E_{AB} - \left(E_{AA} + E_{BB}\right)/2\right].$$

The first two terms on the right-hand side represent the internal energies of N_A atoms of A and N_B atoms of B before mixing and hence, for the mixing process:

$$\Delta U' = P_{AB}\left[E_{AB} - \left(E_{AA} + E_{BB}\right)/2\right]. \tag{51}$$

If the mixing process, conducted at constant pressure, does not involve a change in volume, then, as $P\Delta V' = 0$, $\Delta H' = \Delta U'$ and eq. (51) is the expression for the enthalpy of mixing. As random mixing of the atoms is assumed, the number of A–B bonds is calculated as the product of the probability of occurrence of an A–B pair and the number of pairs of atoms. The former is given by:

$$2\frac{N_A}{N_A + N_B}\frac{N_B}{N_A + N_B},$$

and the latter is $\frac{1}{2}(N_A + N_B)z$, and hence:

$$\Delta H' = \frac{N_A N_B}{N_A + N_B} z\left[E_{AB} - \left(E_{AA} + E_{BB}\right)/2\right]. \tag{52}$$

For the mixing of n_A moles of A ($= n_A N_0$ atoms of A) and n_B moles of B ($= n_B N_0$ atoms of B), eq. (52) becomes:

$$\Delta H' = \frac{n_A n_B}{n_A + n_B} N_0 z\left[E_{AB} - \left(E_{AA} + E_{BB}\right)/2\right].$$

or, per mole of solution:

$$\Delta H^M = X_A X_B N_0 z\left[E_{AB} - \left(E_{AA} + E_{BB}\right)/2\right].$$

If $|E_{AA}| > |(E_{AA} + E_{BB}/2|$, ΔH^M is negative, which leads to exothermic mixing, and if $|E_{AA}| < |(E_{AA} + E_{BB}/2|$, ΔH^M is positive, which leads to endothermic mixing. On the other hand, if E_{AB} is the average of E_{AA} and E_{BB}, ΔH^M is zero and Raoultian ideal mixing occurs. For any given system,

$$\Omega = N_0 z\left[E_{AB} - \left(E_{AA} + E_{BB}\right)/2\right]$$

is a constant, and hence, in a regular solution, ΔH^M is a parabolic function of composition, given by:

$$\Delta H^M = \Omega X_A X_B, \tag{53}$$

and $$\Delta S^M = -R\left(X_A \ln X_A + X_B \ln X_B\right). \tag{36}$$

For any extensive thermodynamic property Q, the relationship between $\Delta\overline{Q}_i^M$ and ΔQ^M in a binary system is given by:

$$\Delta\overline{Q}_i^M = \Delta Q^M + \left(1 - X_i\right)\left(\frac{\partial \Delta Q^M}{\partial X_i}\right),$$

and thus, in a regular solution, from eq. (53):

$$\Delta\overline{H}_i^M = \Omega(1 - X_i)^2,$$

and from eq. (36):

$$\Delta\overline{S}_i^M = -R \ln X_i.$$

The partial molar free energy of mixing of i can be expressed variously as

$$\Delta\overline{G}_i^M = \Delta\overline{H}_i^M - T\Delta\overline{S}_i^M = \Delta\overline{G}_i^{M,\text{id}} + \overline{G}_i^{\text{xs}} = RT \ln X_i + RT \ln \gamma_i,$$

and hence, in a regular solution:

$$\overline{G}_i^{\text{xs}} = \Delta\overline{H}_i^M = RT \ln \gamma_i = \Omega(1 - X_i)^2.$$

Consequently, the limiting values of γ_i as $X_i \to 1$ and $X_i \to 0$ are unity and $\exp(\Omega/RT)$, respectively; i.e., with increasing dilution, the solvent approaches Raoultian ideal behavior and the activity coefficient of the solute approaches a constant value designated γ_i^0. The tendency of γ_i towards a constant value as $X_i \to 0$ is expressed as *Henry's Law*, i.e.:

$$\gamma_i \to \gamma_i^0 \text{ as } X_i \to 0,$$

and if γ_i is constant over some finite range of composition of dilute solution of i, component i is said to exhibit ideal Henrian behavior in this range, its activity being given by:

$$a_i = \gamma_i^0 X_i.$$

Application of the Gibbs–Duhem relation, eq. (48), shows that, over the composition range in which the solute B exhibits ideal Henrian behavior, the solvent A exhibits ideal Raoultian behavior.

The occurrence of Henrian ideal behavior gives rise to the concept of the Henrian standard state, illustrated in fig. 9 which shows the activity of B as a function of composition in the system A–B. The Raoultian standard state is pure B, located at the point R where $a_B = 1$. If, however, pure B behaved as it does in dilute solution in A, extrapolation of its activity along the Henry's Law line would give an activity of γ_B^0 in the hypothetical pure state at $X_B = 1$, relative to the Raoultian standard state. This hypothetical pure state is the Henrian standard state, located at the point H in fig. 9, and, relative to this standard state, the activity of B in any solution, h_B, is

$$h_B = f_B X_B,$$

where f_B is the *Henrian activity coefficient*. In the range of dilute solutions over which B exhibits Henrian ideal behavior, $f_B = 1$ and hence:

$$h_B = X_B.$$

If the vapor pressure of B in the Raoultian standard state is p_B^0, then the vapor pressure of B in the Henrian standard state is $\gamma_B^0 p_B^0$, and hence the change of standard state,

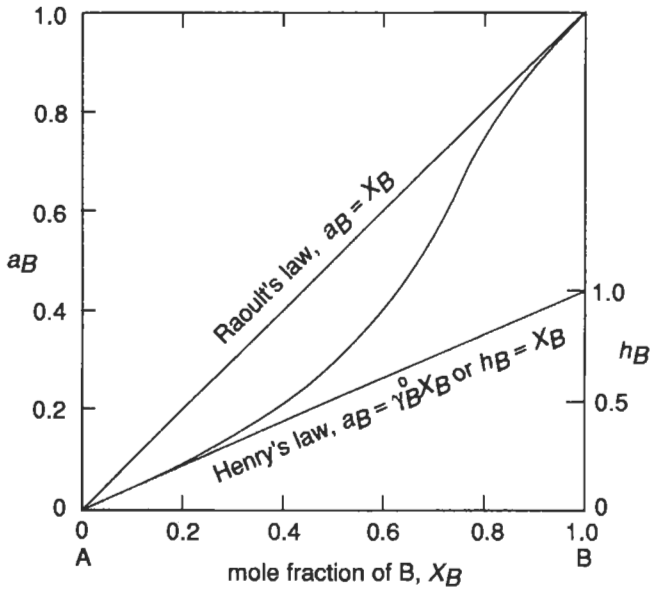

Fig. 9. Illustration of the Raoultian and Henrian standard states.

$$B_{(\text{Raoultian standard state})} \rightarrow B_{(\text{Henrian standard state})},$$

corresponds to

$$B_{\left(\text{vapor at pressure } p_B^0\right)} \rightarrow B_{\left(\text{vapor at pressure } \gamma_B^0 p_B^0\right)},$$

with a free energy change of

$$\Delta G_B(R \rightarrow H) = RT \ln \gamma_B^0.$$

7. *The thermodynamic origin of phase diagrams*

In the definition of activity, given by eq. (43), p_i^0 is the vapor pressure of pure i at the temperature of interest. However, depending on the convenience of the situation, either pure solid i or pure liquid i can be chosen as the standard state. At temperatures below the triple point, $p_{i(\text{solid})}^0 < p_{i(\text{liquid})}^0$, and so the activity of i in a solution, relative to pure solid i as the standard state, is larger than the activity relative to pure liquid i as the standard state. Conversely, at temperatures higher than the triple point temperature the reverse is the case. The activities on the two activity scales are related as

$$\frac{a_{i(\text{relative to solid standard state})}}{a_{i(\text{relative to liquid standard state})}} = \frac{p_{i(\text{liquid})}^0}{p_{i(\text{solid})}^0} = \exp\left(\Delta G_{m,i}^0/RT\right).$$

References: p. 469.

Consider the molar free energies of mixing in the system A–B, the phase diagram for which is shown in fig. 10a. For simplicity of discussion it will be assumed that both the solid and liquid solutions exhibit ideal Raoultian behavior. The molar free energies, at temperature T, are shown in fig. 10b. Pure liquid A and pure solid B are chosen as the reference states and are located at points **a** and **b** respectively. $G^0_{A(s)}$ is located at **c**, where $G^0_{A(s)} - G^0_{A(l)} = -\Delta G^0_{m,A}$ at temperature T, and $G^0_{B(l)}$ is located at **d** where $G^0_{B(l)} - G^0_{B(s)} = \Delta G^0_{m,B}$ at temperature T. Thus, relative to unmixed pure liquid A and pure solid B as the reference state, the molar free energy of the unmixed pure liquids (given by line **ad**) is $X_B \Delta G^0_{m,B}$ and the corresponding free energy of the unmixed pure solids (given by line **cb**) is $-X_A \Delta G^0_{m,A}$. Upon mixing to form Raoultian ideal solutions, the molar free energies decrease by $|RT(X_A \ln X_A + X_B \ln X_B|$ and hence, relative to the chosen reference state:

$$\Delta G^M(\text{solid solutions}) = -X_A \Delta G^0_{m,A} + RT\left(X_A \ln X_A + X_B \ln X_B\right),$$

and

$$\Delta G^M(\text{liquid solutions}) = X_B \Delta G^0_{m,B} + RT\left(X_A \ln X_A + X_B \ln X_B\right).$$

The double tangent drawn to the two free energy curves touches the curve for the solid solutions at **g** and the curve for the liquid solutions at **f**, with the intercepts at $X_A = 1$ and $X_B = 1$ being **e** and **h** respectively. As the equilibrium state is that of minimum free energy, points **f** and **g** divide the composition range into three regions. At compositions between **a** and **f** the homogeneous liquid solution has the lowest possible free energy and at compositions between **g** and **b** the homogeneous solid solution has the lowest possible free energy. However, at compositions between **f** and **g**, a two-phase mixture of liquid solution of composition **f** and solid solution of composition **g**, the free energy of which lies on line **fg**, has a lower free energy than both the homogeneous solid solution and the homogeneous liquid solution. Thus point **f** is the limit of solution of B in liquid A and **g** is the limit of solution of A in solid B, and so points **f** and **g** are, respectively, the liquidus and solidus compositions at temperature T.

Furthermore, for phase equilibrium:

$$\overline{G}_A(\text{in liquid solution } \mathbf{f}) = \overline{G}_A(\text{in solid solution } \mathbf{g}),$$

and:

$$\overline{G}_B(\text{in liquid solution } \mathbf{f}) = \overline{G}_B(\text{in solid solution } \mathbf{g})$$

or $$\Delta\overline{G}^M_A(\text{in liquid } \mathbf{f}) = \Delta\overline{G}^M_A(\text{in solid } \mathbf{g}),$$

and:

$$\Delta\overline{G}^M_B(\text{in liquid } \mathbf{f}) = \Delta\overline{G}^M_B(\text{in solid } \mathbf{g}).$$

These requirements state that, for phase equilibrium, the tangent to the molar free energy curve for the liquid solutions at the liquidus composition **f** is also the tangent to the molar free energy curve for the solid solutions at the solidus composition **g**. Geometrically, this condition is such that, simultaneously,